Partitioning of Limonene into Phospholipid Vesicle Dispersions

By

ANN-DORIE WEBLEY
DISSERTATION

Submitted in partial satisfaction of the requirements for the degree of

DOCTOR OF PHILOSOPHY

in

Food Science and Technology

in the

OFFICE OF GRADUATE STUDIES

of the

UNIVERSITY OF CALIFORNIA

DAVIS

Approved:

Stephanie R. Dungan, Co-Chair

Susan E. Ebeler, Co-Chair

Nitin Nitin

Committee in Charge

2024

Table of Contents

List of Figures

List of Tables

Abstract

The solubilization and retention of aromas in foods can be improved using phospholipid vesicle dispersions which protect these aromas from evaporation, degradation, and chemical reactions. In this work, a quantification method was developed for the solubilization and retention of volatile aromas in phosphatidylcholine vesicles, with headspace solid phase microextraction (HS–SPME) combined with gas chromatography and mass spectrometry (GC/MS). This method allows us to selectively sample volatile compounds in the vapor phase using a sorbent fiber. HS–SPME is fast, accurate and non-invasive and allows for *in situ* measurements of partition coefficients for local regions within food products. With this approach, limonene partition coefficients were determined both between vapor and water and between vesicle bilayers and water. The unilamellar, nearly monodisperse vesicles were very effective at solubilizing limonene molecules, with large bilayer–water partition coefficients of ~10^4 M^{-1}. These values are 3–8 times larger than those observed for short chain phospholipid micelles, which have smaller core volumes. In addition, vesicles can solubilize limonene up to very high mole fractions $x_{lim} \leq 0.8$, where x_{lim} is the moles of limonene relative to moles of limonene + phospholipid in the bilayers. This maximum solubilization is much greater than that measured for short chain phospholipid micelles ($x_{lim} \leq 0.5$). The bilayer–water partitioning behavior of limonene was investigated as a function of phospholipid composition and vesicle size, using lecithin enriched in phosphatidylcholine and pure dimyristoylphosphatidylcholine (DMPC). There was no significant difference in extent of solubilization whether vesicles were made using DMPC or lecithin, despite the fact that DMPC has saturated 14-carbon fatty acid tails, while lecithin is predominantly unsaturated with 18-carbon fatty acid tails. With an increase in vesicle diameter from ~100 to 200 nm, there was a marginal increase in solubilization for DMPC and a marginal decrease in solubilization for lecithin.

The vapor phase concentration of limonene was used to analyze the mixing thermodynamics through calculations of chemical potentials. For a wide range of limonene–lipid mole ratios, constant partition coefficient values could quantitatively capture solubilization in the bilayer, as predicted by ideal–dilute mixing theory for the solute. At high limonene–lipid mole ratios, however, we saw evidence of non-ideal behavior with higher measured lipid–water partition coefficients. Using regular solution theory with an interaction parameter ($\chi_{PL,L}$) of ~1 predicted this partitioning behavior quite well, suggesting that preferential solute–solute interactions may enhance solubilization at higher limonene concentrations.

With saturated phospholipids, high mole fractions of limonene in the bilayer lowered the gel–to–fluid lipid phase transition temperature through entropic contributions that could be predicted quite well with freezing point depression theory. Gel, gel/fluid coexistence, and fluid regions were observed over small to large limonene–lipid mole ratios. In the gel/fluid coexistence region, we observed constant vapor phase concentrations of limonene. At low mole fractions of limonene, formation of the gel phase decreased partition coefficients at least two-fold in comparison to the fluid phase. Above the phase transition temperature, decreases in temperature also lowered the partition coefficients, but to a much lower extent. Gel phase partition coefficients were used to modify the freezing point depression model and predict the solubilization behavior of limonene at all compositions at 15 and 20ºC. At these temperatures, experimental data agreed with the theory very well for low total limonene concentrations.

Acknowledgements

This dissertation was completed with the guidance and encouragement of a support system that I am grateful to have accumulated over the years. Firstly, I thank my committee, Dr. Stephanie Dungan, Dr. Susan Ebeler, and Dr. Nitin Nitin for the guidance that they have provided throughout my graduate school journey. Their patience and faith in my abilities have helped me to evolve into a better scientist. I extend my sincere gratitude to Dr. Dungan for teaching me how to apply thermodynamic concepts to our research and for helping me to practice writing and presenting scientific work. I am grateful for our weekly meetings and her tireless efforts as an editor. I thank Dr. Ebeler for her teachings on analytical methods and her help in troubleshooting recurring instrument problems. I am also grateful for her support in broadening my analytical chemistry skills and experience with instruments. I am thankful to Dr. Nitin for his feedback and insights that have greatly improved how I design experiments. His suggestions on approaches to try have always helped to resolve my problems.

I would like to thank members of the Dungan and Ebeler groups: Andrew Karman, Jennifer Staton, Nathan Alexander, Yiyi Li, Abhi Singh, Jesse Skratt, and Jeff McCord. I am grateful for the support and discussions during lab meetings. Special thanks to Andrew and Jen for teaching me the research methods I needed to start my project. I thank Dr. Larry Lerno for teaching me how to maintain, repair and use our analytical instruments. I also appreciate the members of my cohort and the Food Science Graduate Student Association for friendship and support in adjusting to graduate school.

Thanks to Irvine Peck's Agaya, Rashana Lydner, Toluwanimi Odemuyiwa and other close friends for their love and support, and for always being my cheerleaders. Finally, I thank my siblings, Kady-Ann, AnJE, Marrio and my parents, Claudia and Richard Webley for inspiring me to become a scientist, believing in me, and always providing encouragement.

Chapter 1

Introduction

1.1 Background

The solubilization by nanoparticles of hydrophobic compounds, such as flavors, aromas, and nutrients, can improve their bioavailability or release, lengthen their shelf life, and decrease deterioration and chemical reactions. As such, nanoparticles with the ability to host these compounds have been the focus of intense research.[1,2] In product matrices, hydrophobic compounds are usually found in non-polar regions such as vapor or lipid phases, due to low water solubility. Furthermore, their chemical and physical stability and their release or delivery are affected by other components of the product, so quantifying and controlling their distribution among multiple phases is crucial. Their local distribution and delivery or release has applications in areas of food production,[3–5] drug delivery,[6,7] and agrochemicals.[8,9] In foods, nanoparticles can enhance bioavailability without adversely affecting sensory properties of products such as taste and mouthfeel. These particles are also usually smaller than the wavelengths of visible light, resulting in transparent dispersions or solutions which are desirable in beverages.[1,10]

In this work, we focus on the solubilization and retention of flavor or aroma molecules. Flavor is an important aspect of foods, aiding in consumer appeal and satisfaction. Flavors or off-flavors are also indicators of food quality.[11] Flavor perception is multisensory, involving senses such as taste, smell, and touch.[12] While eating, flavor compounds are released from food matrices into the vapor phase, and perceived through retronasal olfaction. The pattern of flavor release is important as it can be a characteristic feature of foods. Flavor encapsulation systems must therefore be designed to optimize both flavor retention and release, while providing protection from unfavorable interactions.[11]

Microencapsulation approaches for flavors such as spray drying, extrusion, and fluidization bed coating have been extensively studied,[11,13] particularly for powder applications. Nanostructures, however, provide higher encapsulation efficiencies, increased bioavailability, and improved controlled release, while being more compatible with liquid applications.[14] To improve food quality, we need more methods to quantify the solubilization of flavors within nanoparticles and to study the effects of nanostructures on flavor distribution. Measurements of local partition coefficients are key to determining the effectiveness of these structures in enhancing solubilization, but currently these measurements are usually done with indirect or lengthy methods. Partitioning between the complex food material and the vapor phase has been investigated using methods such as equilibrium dialysis, spectrofluorometry and headspace analysis coupled to GC/MS.[15] Characterization parameters include binding or retention percentages, which reflect the amount of flavor retained when nanostructures are added, and for liquid systems, vapor–liquid partition coefficients or Henry's constants.[15] Several authors have pointed out the need for local partition coefficients between nanostructures and water, to obtain more direct information about the interactions of flavor molecules with compounds in the product matrix,[15] or the effects of structure on the solute's partitioning properties.[16] In oil-based emulsions, phase equilibrium can be used to predict the distribution between water and oil, using previously determined partition coefficients for the flavor between both vapor and liquid and vapor and bulk oil.[15]

In this dissertation, we build upon these approaches by applying headspace solid phase microextraction (HS–SPME), combined with gas chromatography and mass spectrometry (GC/MS). This allows us to study aqueous systems *in situ* and examine partitioning between the nanostructures and their aqueous environments. SPME is a quick and accurate method for concentrating and extracting volatile compounds in the vapor phase, and the measurements can be directly related to equilibrium concentrations with few prior experiments or parameters.

This approach provides information about the effects of nanoparticle structure on solubilization and release, and helps us to determine how flavor partitioning is affected by food processing methods.

1.2 Flavor Solubilization Using Phospholipid Nanostructures

Nanostructures for food applications are made with various amphiphilic compounds such as Tween surfactants, saponins, phospholipids, and milk proteins.[1,10] In this work, we focus on nanostructures made using phospholipids, which feature a phosphate headgroup, a glycerol backbone and one or more fatty acid tails. The headgroup is generally found in the *sn-3* position. Phospholipids are generally classified based on the structure of the headgroups. For our experiments we use phosphatidylcholine (PC), which has a choline group attached to the phosphate, making it zwitterionic. The general structure of a phosphatidylcholine molecule is shown in Figure 1.1. Phospholipids are usually surfactants, due to their hydrophilic headgroups and hydrophobic fatty acid tails. They are found naturally in plant and animal sources, and some have GRAS (generally recognized as safe) status.[17] As discussed by Assadpour et al. in their recent book chapter, phospholipid nanostructures, including vesicles and nanoemulsions, have been the focus of many studies dedicated to understanding and utilizing their abilities to host hydrophobic molecules in their core/bilayer.[18]

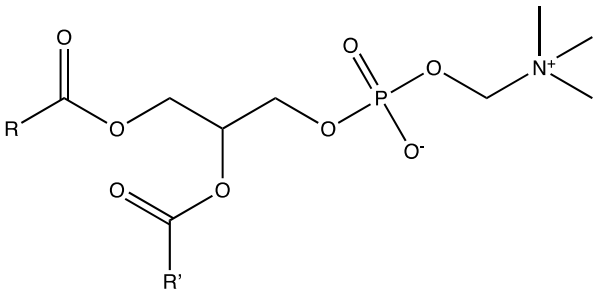

Figure 1.1: Chemical structure of a phosphatidylcholine molecule. R and R' represent fatty acid tails.

Phospholipids are particularly suited to flavor encapsulation and delivery, as lipids naturally serve as carriers of flavors in nature. The partitioning of flavors into the different phases of foods influences flavor storage, release, and ultimately quality.[16] Fat as a lipid phase serves as a reservoir for flavors with a delayed release that is dependent on lipid concentrations. Fats are also more effective at solubilizing flavor than protein or carbohydrates as a result of favorable van der Waals interactions,[19] as well as a better ability to shield non-polar solutes from contact with water. Low or fat free foods thus have a changed aroma profile and often overly quick flavor release. With nanostructures, release becomes more complex with more factors affecting partitioning than in a bulk phase. For example, the rate of flavor release may change with the size of these nanostructures due to their surface area.[16,19]

In foods, lecithins, which are mixtures of phospholipids from natural sources with varying fatty acid tails and headgroups, are commonly used as natural emulsifiers. Common sources include soy, eggs (particularly egg yolks) and sunflowers. Lecithin is obtained from plant sources because of the degumming process during oil refinement, which purifies the triglycerides. This is done by removing lipids with phosphate groups, which are polar, by adding water to hydrate those groups and lower their solubility in the oil.[20] Although the composition of lecithin is dependent on factors such as source and weather conditions,[20] it can be modified after extraction. Methods to modify lecithin include de-oiling, enriching with PCs, and hydrolyzing to produce lyso-lecithin, which has one fatty acid tail and a de-esterified hydroxyl group.[21] The lecithin product used throughout this dissertation research, Sunlipon™ 90, is produced by Perimondo and contains sunflower lecithin with 90% phosphatidylcholine. This PC–enrichment makes lecithin more comparable to the pure phospholipids typically used to create nanostructures, and enhances its amphiphilic character. Unmodified lecithin has about 40% phospholipid content, with ~16% being PC along with other lipids such as triglycerides and fatty acids.[20]

In living systems, phospholipids, particularly those with long fatty acid tails, are usually a part of bilayers such as the cell membrane. Short-chain phospholipids, however, which are soluble in water at low concentrations, can form micelles. These micelles are nanosized spherical aggregates that form spontaneously in water when amphiphiles self-assemble into structures that feature a core of hydrophobic tails and a shell of hydrophilic heads. The threshold concentration needed for this spontaneous aggregation to form a single micellar phase is called the critical micelle concentration (CMC).

As the fatty acids tails become longer and the phospholipids become less soluble in water, self-assembly to form aqueous micelle solutions becomes less likely. The packing parameter is often used to predict the colloidal structures that are most stable for amphiphilic molecules. This parameter depends on the optimal surface area per headgroup, the chain volume, and the chain length. With longer tails and higher chain volume, bilayer structures are more energetically favorable than micelles, leading to the formation of vesicles dispersed in water.[22] Vesicles are spherical particles with an aqueous core surrounded by a phospholipid bilayer shell, which may have more than one bilayer with aqueous fluid between them. Vesicles are larger than micelles with diameters ranging from 20–1000 nm, as opposed to 2–20 nm in micelles. Unlike micelles, vesicles require energy to create the dispersion in water, at concentrations above the extremely low phospholipid solubility limit. This energy is provided through agitation methods such as sonication. A two-phase vesicle–water dispersion is formed as a result. Hydrophobic compounds can solubilize within the bilayer region. Due to the aqueous region in the core or between the bilayers, vesicles can also host hydrophilic molecules.

When the phospholipids used to make vesicles feature saturated fatty acids, they have a phase transition temperature, T_G, below which the tails in the bilayer are highly ordered and in

a solid-like gel phase. When the temperature is raised above T_G, the bilayer becomes less ordered and transitions into a fluid phase. This process is shown in Figure 1.2.

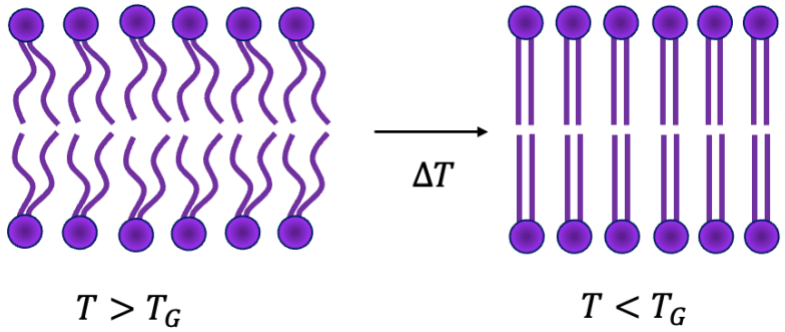

Figure 1.2: Vesicle bilayers made from saturated fatty acids reside in either the (left) fluid liquid crystal or (right) gel phase, above and below T_G, respectively.

Due to the ordered structure of the gel phase, vesicles cannot be formed below T_G as the phospholipids are not sufficiently mobile. Therefore, to form vesicles from saturated phospholipids, we need to be far enough above the phase transition temperature that all the phospholipids are fluid, since melting happens over a range of temperatures for phospholipid mixtures. This also ensures that any cooling that happens during vesicle formation does not result in a gel. Usually, ~10ºC above T_G is used for extrusion or sonication processes.[23–25] The presence of the gel phase also affects partitioning into the bilayer, with reduced ability to host solutes. As a result, processing and storage temperatures affect flavor retention and delivery from vesicles, when saturated lipids are used.

In the work presented in this dissertation, we developed solid phase microextraction as a tool to quantify the distribution of aroma compounds between vesicles and water. Using SPME, we investigated the factors that affect this distribution for the aroma molecule limonene, and the extent of the resulting changes in solubilization. The effect of phospholipid and vesicle structure on partitioning into bilayers has previously been examined for drug delivery or environmental applications,[26,27] but there is little research dedicated to flavor solubilization.[16]

By using different phospholipids, vesicle diameters, temperatures and compositions, we provided meaningful information enabling the prediction of how vesicles impact the distribution of flavors in foods.

1.3 Thermodynamics of Partitioning

In this work, we studied the partitioning of limonene into phospholipid vesicle dispersions. To measure these values accurately, we used thermodynamic principles of mixing to derive mole balances among vapor (v), aqueous solution (w), and bilayer phases. A driving force of mixing is the tendency to minimize the Gibbs free energy, G, at equilibrium. The chemical potential, μ_i, is the change in Gibbs energy with respect to moles of i, dG/dn_i, at constant temperature T, pressure and moles n_j. For a two-phase system, this requires μ_i to be equivalent in both phases (a and b), as shown below:

$$\mu_{i,a} = \mu_{i,b} \,. \tag{1.1}$$

For a solute partitioning between the water and vapor phases, the chemical potential of the solute in water is related to its concentration in water and its chemical potential $\mu_{i,w}^{\circ}$ at infinite dilution in water (ideal–dilute reference state), resulting in

$$\mu_{i,w} = \mu_{i,w}^{\circ} + kT \ln\left(\gamma_{i,w} x_{i,w}\right) . \tag{1.2}$$

Here, $x_{i,w}$ is the mole fraction of the solute in water, k is Boltzmann's constant, and $\gamma_{i,w}$ is the activity coefficient, which accounts for excess non-ideal behavior. $\gamma_{i,w} \approx 1$ for dilute solutions, which is an excellent assumption for the systems studied in this work. For the vapor phase, the chemical potential of the solute can be written as

$$\mu_{i,v} = \mu_{i,v}^{o} + kT \ln\left(\gamma_{i,v} \frac{P_i}{P_i^{o}}\right), \tag{1.3}$$

where $\mu_{i,v}^{o}$ is the chemical potential of solute vapor in equilibrium with pure liquid solute and P_i is the partial pressure of the solute above the mixture. Here, P_i^{o} is the partial pressure above

the pure solute. The mole fraction of the solute in the vapor phase, $x_{i,v}$, is equal to P_i divided by the total pressure. For an ideal gas, where the effects of enthalpic interactions are assumed to be negligible, the activity coefficient, $\gamma_{i,v}$, is 1.

$x_{i,w}$ is related to the partial pressure P_i of the solute above the equilibrated mixture. In particular, for hydrophobic solutes in water, ideal–dilute behavior is observed at low concentrations. At such concentrations, Henry's law states that the vapor pressure of the solute is dependent on its concentration in water, i.e., $P_i = H_{pc}x_{i,w}$, where H_{pc} is Henry's coefficient. This principle is commonly used to establish vapor–water partition coefficients.

For an ideal dilute solution, we can relate the constant values P_i^o, $\mu_{i,w}^{\ominus}$ and $\mu_{i,v}^o$, to these partition coefficients, recognizing that $\mu_{i,v}^o = \mu_{i,l}^o$, with $\mu_{i,l}^o$ the chemical potential of pure solute. We rewrite the chemical potentials in the vapor phase as

$$\mu_{i,v} = \mu_{i,l}^o + kT \ln \frac{P_i}{P_i^o}, \tag{1.4}$$

For a solute at equilibrium between the two phases, $\mu_{i,w} = \mu_{i,v}$, and

$$\mu_{i,w}^{\ominus} - \mu_{i,l}^o = kT \ln \frac{x_{i,v}}{x_{i,v}^o} - kT \ln x_{i,w}, \tag{1.5}$$

where $x_{i,v}^o = P_i^o / P_{atm}$, at atmospheric pressure P_{atm}. Rearrangement results in

$$x_{i,v}^o \exp\left(\frac{\mu_{i,w}^{\ominus} - \mu_{i,l}^o}{kT}\right) = \frac{x_{i,v}}{x_{i,w}}. \tag{1.6}$$

The ratio $x_{i,v}/x_{i,w}$ is a version of the partition coefficient of the solute between the vapor and water. In our experiments, this coefficient is more usefully expressed as the ratio of solute concentrations in vapor and water: $K_{vw} = C_{i,v}/C_{i,w}$. Conversion between K_{vw} and equation 1.6 can be done using molar densities.

The addition of vesicles to aqueous systems presents a separate lipid phase into which the solutes can partition. A visual representation of the equilibrium distribution is provided in Figure 1.3. To analyze and interpret our vesicle partitioning results, the solute-containing

bilayer was approximately treated as a binary, ideal–dilute mixture. The chemical potential $\mu_{i,PL}$ of the solute in the lipid was therefore represented by

$$\mu_{i,PL} \approx \mu^{\ominus}_{i,PL} + kT \ln x_{i,PL} \,. \tag{1.7}$$

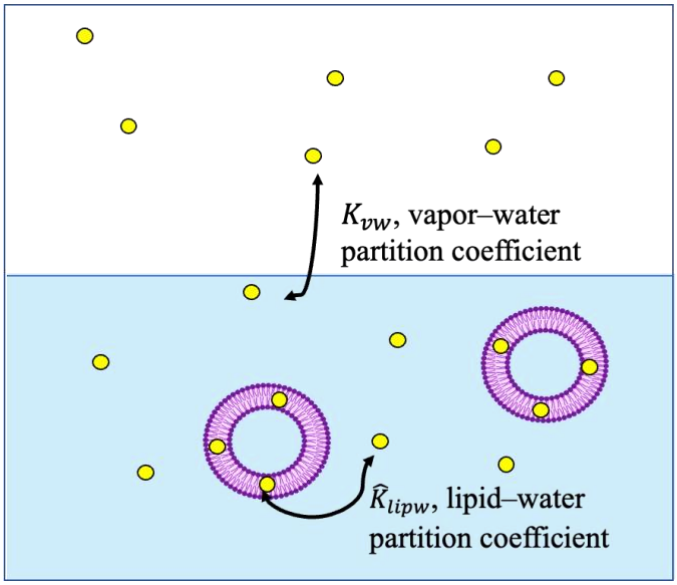

Figure 1.3: Distribution of solute between vesicle, water, and vapor phases.

Here, $\mu^{\ominus}_{i,PL}$ is the ideal dilute reference in the lipid phase and $x_{i,PL} = n_i/(n_i + n_{PL})$ is the mole fraction of solute in the lipid. As with vapor–water partitioning, $\mu_{i,w} = \mu_{i,PL}$, and

$$\mu^{\ominus}_{i,w} - \mu^{\ominus}_{i,PL} \approx kT \ln x_{i,PL} - kT \ln x_{i,w} \,. \tag{1.8}$$

Rearrangement yields

$$\frac{x_{i,PL}}{x_{i,w}} = \hat{K}_{lipw} \approx \exp\left(\frac{\mu^{\ominus}_{i,w} - \mu^{\ominus}_{i,PL}}{kT}\right), \tag{1.9}$$

where $\hat{K}_{lipw}$ is a dimensionless lipid–water partition coefficient. Using the molar volume of water, we can convert $\hat{K}_{lipw}$ to the alternative form $K_{lipw} = x_{i,PL}/C_{i,w}$.

1.4 Detecting Vapor Phase Concentration with Solid Phase Microextraction

Solid phase microextraction (SPME) is an extraction method for the analysis of volatile compounds. Fibers coated with sorbent materials are used to concentrate and extract analytes. SPME simplifies preparation of samples by reducing the need for solvent extraction and concentration steps. The coatings of SPME fibers are typically cross-linked organic polymers attached to inert rods made of materials like fused silica.[28,29] Examples of SPME fiber coatings include polydimethylsiloxane (PDMS), Carboxen® (Car) carbon adsorbent, divinylbenzene (DVB) and polyacrylate (PA). Fibers are chosen based on their compatibility with the analytes of interest. For example, PDMS can be used to extract a range of nonpolar volatile and semivolatile compounds, due to its nonpolar character. PA, on the other hand, is a more polar matrix and is typically used to extract polar, semivolatile compounds. To improve extraction of a wider range of analytes, fibers are often coated with multiple materials: for example, CAR/PDMS. Fibers also have different mechanisms for concentrating analytes. Some fibers, such as PDMS which behaves as a liquid phase, absorb analytes, while DVB adsorbs analytes onto its surface. [30]

The dimensions of SPME fibers are quite small, usually 1–2 cm long with diameters <100 μM. Due to their delicate nature, they are housed within syringe needles until extraction, and then injected into the sample with the plunger.[28,29] These fibers can be used with autosamplers to improve precision of extraction times, fiber injection depth, and automation of multiple extractions.[29] In headspace (HS) SPME, compounds are extracted from the vapor phase above the sample. This method is best suited to analytes that are volatile or semivolatile. Since SPME is also a concentration step, compounds present at low concentrations can be extracted. For analytes that are less volatile, direct immersion (DI) SPME, in which SPME fibers extract directly from a liquid phase, is a more appropriate method. However, this method can be more challenging to implement due to interference from the sample matrix and quicker deterioration

of the fiber.[30,31] For our analysis we chose to use HS–SPME due to the high volatility of limonene and because it allows us to achieve longer fiber lifetimes. Experiments performed by Lloyd et al.[32] showed very good agreement between vapor–water partition coefficients obtained using HS and DI–SPME. Figure 1.4 shows an illustration of a typical HS–SPME fiber and how it is used to extract analytes in a sample. SPME vials have airtight lids with a septum that is pierced by the needle. These vials usually have volumes of ~10 or ~20 mL.

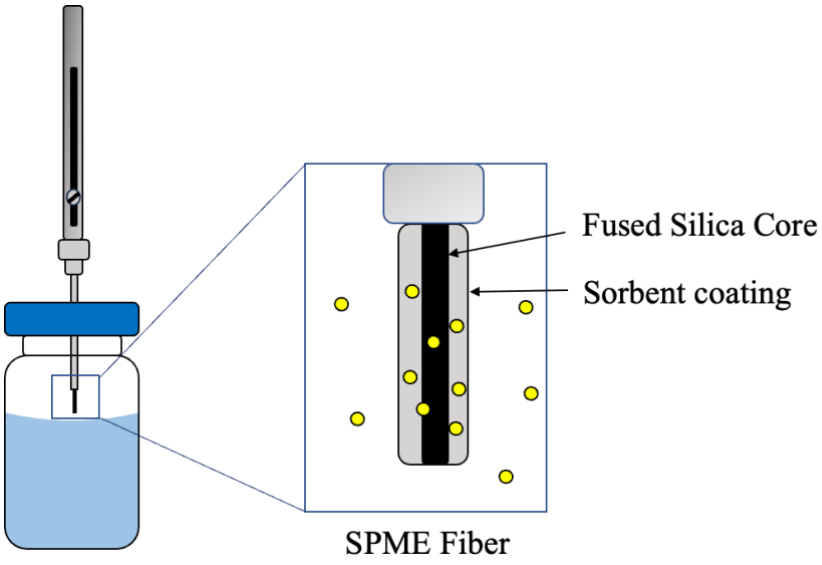

Figure 1.4: Structure of fiber used for HS–SPME analysis.

The time needed for extraction in the SPME analysis is affected by factors such as temperature, pH, and agitation. Method development usually involves determination of the optimum conditions needed to maximize the amount of analytes extracted and shorten the time taken to reach equilibration with the fiber. However, in our research, extraction times were kept short relative to that for equilibration. As a result, determining partition coefficients using HS–SPME could be done with the assumption that there is non-depletion: i.e., such small amounts of the analyte were extracted that their removal did not affect the local equilibrium established in the samples.[33] Sometimes, non-depletion is ensured by shortening the fiber to extract smaller amounts.[34] For our experiments, rather than modify the fiber itself, we used short-time

extractions, removing the fiber from the sample long before equilibration with the fiber is achieved. This method was developed by Lloyd et al.,[32] who analyzed expected mass transfer kinetics in both vapor and liquid phases to determine appropriate extraction times. Karman et al.[35] previously used short time HS–SPME to study the solubilization of limonene in short chain phospholipid micelles, showing that the micelle–water partition coefficients depend on fatty acid chain length, temperature, and limonene concentration.

SPME is often coupled to gas chromatography/mass spectrometry (GC/MS) for separation, detection, and quantification of volatile and semivolatile analytes. Non-volatile compounds can be separated with liquid chromatography (LC).[29] When using GC, solutes on SPME fibers are desorbed at the hot inlet after extraction. This step also serves as a cleaning or "bake off" step, removing analytes from the fiber prior to contacting the next sample, and thus making the method solvent-less.[28,29] After being desorbed, analytes enter the column at a low starting temperature and are moved through the column by the gas mobile phase (and by increasing oven temperature). The flow rate of the mobile phase and the affinity that the analytes have with the polymer lining the column (the stationary phase) help in determining separation. As with the fiber, the choice of column depends on the nature of the materials being separated. Other factors affecting separation include temperature profile, column length, and inlet temperature.[36] Specifics of the GC (and MS) program are outlined in Chapter 2.

After separation, analytes are detected using MS, which fragments compounds with high energy electrons, creating characteristic spectra of their mass to charge (*m/z*) ratios. A scan of a range of *m/z* ratios provides a full mass spectrum for each analyte, with characteristic intensities based on their fragmentation patterns. However, with known compounds, a scan of the *m/z* ratio associated with the highest intensity fragment, the base peak, is sufficient for identification/characterization. Chromatograms show the separated compounds and their intensity/frequency distributions over time, based on detection by the MS.[36] Integrations of

these peaks are performed for analysis of vapor phase concentrations. Quantification can be done using calibration curves for specific target compounds. Internal standards can also be used to compare peak areas for various experimental conditions. In this research project, concentrations were calculated from mole balances based on the recorded peak areas. Figure 1.5 shows the parts associated with the GC/MS instrument and the HS–SPME fiber assembly used for extraction.

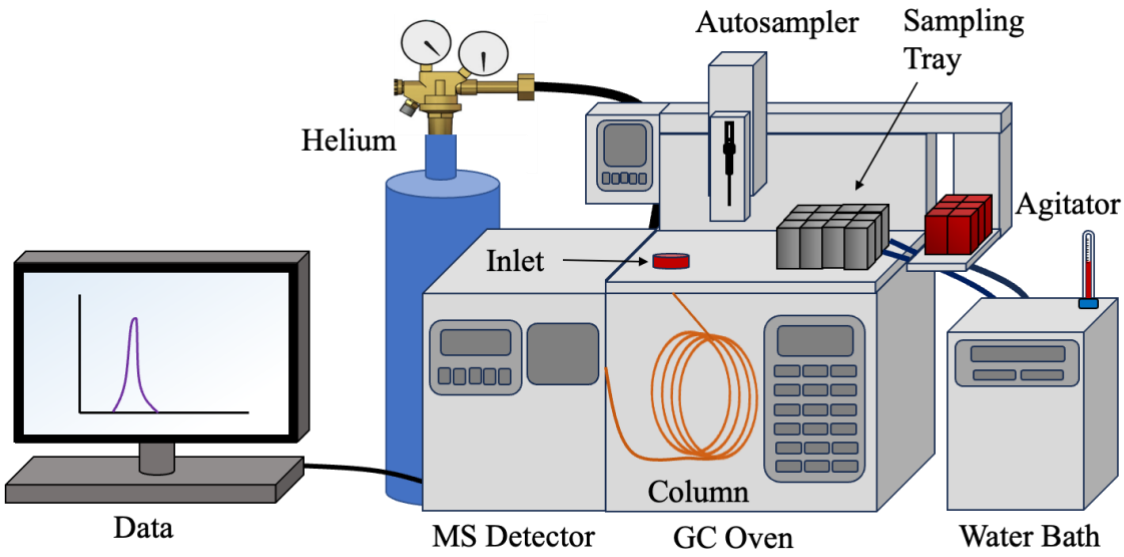

Figure 1.5: HS–SPME fiber assembly and GC/MS instrument used for partitioning experiments.

1.5 Objectives

The goal of our work was to develop HS–SPME as a non-invasive method to study the partitioning of limonene into phospholipid vesicles. By combining theory for the thermodynamics of mixing with mole balances, limonene vapor phase concentrations measured using HS–SPME were used to obtain lipid–water partition coefficients. Results for experiments performed using fixed limonene concentrations of 0.618 mM, in dispersions of Sunlipon™ 90 lecithin or dimyristoylphosphatidylcholine (DMPC) vesicles, are presented in Chapter 2. Results are compared to conventional methods described in literature to study partitioning of hydrophobic molecules into vesicles. We also compare the effectiveness of

phospholipid vesicles and short-chain phospholipid micelles as hosts for hydrophobic molecules and examine the effects of vesicle size and structure on limonene partition coefficients.

In Chapter 3, we discuss ideal and regular solution theory and use this theory to examine the partitioning behavior of limonene at low and high concentrations. Results from these experiments enabled us to evaluate whether an ideal dilute model, and thus K_{lipw} values independent of composition, are appropriate to describe partitioning into phospholipid vesicles. We examine the chemical potentials associated with solubilization in the bilayer and derive equations to describe both ideal and non-ideal behavior. Potential effects of adding solute to samples using pure limonene or dissolved binary solutions with DMSO are addressed, as well as the impact of changes in the aqueous solubility limit with temperature.

Experiments to probe the effects of temperature on the lipid–water partition coefficients are discussed in Chapter 4. These experiments were done using unsaturated as well as saturated vesicles, where for the latter there is a gel phase present at lower temperatures. Comparison of these phospholipid types allowed us to distinguish between effects of temperature on solubilization within the fluid phase, and those due to the presence of the gel phase, on solute partitioning into the bilayer. The lowering of the phase transition temperature by solutes was measured and compared to thermodynamic predictions, allowing us to examine and discuss the impact of two-phase coexistence between the gel and fluid phase during solubilization in the bilayer. The effects of hysteresis on the accuracy of measured partition coefficients are also examined.

1.6 Nomenclature

$C_{i,v}$	concentration of solute in the vapor
$C_{i,w}$	concentration of solute in the water

G	Gibb's free energy
H_{pc}	Henry's constant
k	Boltzmann's constant
K_{lipw}	lipid–water partition coefficient, $x_{i,PL}/C_{i,w}$
K_{vw}	vapor–water partition coefficient
$\widehat{K}_{lipw}$	dimensionless lipid–water partition coefficient
n_i	moles of solute
n_{PL}	moles of lipid
P_{atm}	atmospheric pressure
P_i^o	partial pressure above pure solute
P_i	partial pressure of the solute above a mixture
T_G	phase transition temperature
$x_{i,PL}$	mole fraction of solute in lipid
$x_{i,v}$	mole fraction of solute in vapor
$x_{i,w}$	mole fraction of solute in water
$\gamma_{i,v}$	activity coefficient of solute in vapor
$\gamma_{i,w}$	activity coefficient of solute in water
$\mu_{i,l}^o$	chemical potential of pure solute
$\mu_{i,PL}^{\infty}$	ideal dilute reference chemical potential of solute in the lipid phase
$\mu_{i,PL}$	chemical potential of solute in the lipid phase
$\mu_{i,v}^o$	chemical potential of solute vapor in equilibrium with pure liquid solute
$\mu_{i,v}$	chemical potential of solute in vapor
$\mu_{i,w}^{\infty}$	ideal–dilute reference chemical potential of solute in water
$\mu_{i,w}$	chemical potential of solute in water

μ_i	chemical potential of solute

Chapter 2

Local Distribution of Limonene Within Phospholipid Vesicle Dispersion

2.1 Introduction

The solubilization and retention of hydrophobic compounds such as flavors can be improved by the incorporation of vesicle dispersions into foods. Vesicles are spherical nanostructures with a lipid bilayer shell formed from amphiphiles,[37] such as phospholipids, within which hydrophobic compounds can be solubilized.[38,39] They have been applied to foods,[40,41] drug delivery systems,[42,43] and can also serve as a model for living cells, which depend on bilayers to transport metabolites and to act as a barrier in order to protect organelles.[37] Typically, phospholipids such as lecithin are generally recognized as safe (GRAS)[17] and can be readily incorporated into foods and other consumer products.

Accurate and non-destructive measurements are needed to determine the local distribution of hydrophobic compounds between vesicles, the aqueous liquid surrounding them, and the vapor phase. Current methods to study partitioning in vesicle dispersions often exclude the vapor phase completely, focusing instead on the partitioning between vesicles and the aqueous environment. These include isothermal titration calorimetry (ITC),[44,45] which requires the separate calculation of several thermodynamic properties such as the enthalpy of transfer from water to lipid. Two other methods are passive dosing[46] and equilibrium dialysis,[47] which both have long equilibration times that are on the order of days. In ITC, the vesicle dispersion is injected in aliquots into an aqueous solution of the solute, and the heat per injection used to quantify partitioning into the lipid phase. For passive dosing, partitioning between a polymer and vesicle dispersion is compared to the separate partitioning between the polymer and water. Similarly, equilibrium dialysis uses a reference without the vesicles to determine changes in solubilization. Exclusion of the vapor phase is appropriate if the analytes being studied are non-

volatile. In these cases, high performance liquid chromatography (HPLC) methods may be used to quantify analyte concentrations, for example when following passive dosing[46] or equilibrium dialysis.[47] Alternatively, vesicles can be used as the stationary phase in immobilized liposome chromatography,[48,49] where a solution including the analyte is passed through a packed column and changes in concentration are used to determine solubilization. For compounds that absorb light, spectroscopic techniques can also be used, but may require the insertion of chromophores or fluorophores to monitor changes in bilayer organization[49] if the solutes themselves cannot be measured. Spectroscopic techniques may also need the aqueous phase to be separated and analysed directly to reduce interference due to light scattered from vesicles.[50]

Non-depletion direct immersion solid phase microextraction (DI–SPME), coupled to GC/MS, was used by Escher et al.[34] to determine partition coefficients of organic acids and bases in vesicles; however, in this approach there were concerns about matrix effects and lipids binding to the fiber. Pino and coworkers[33,51,52] also used DI–SPME with long extraction times (≥120 min) to determine micelle–water partition coefficients of polycyclic aromatic hydrocarbons and phenolic compounds. Like Escher et al., they reported that some fibers may interact with the surfactants. Van der Heijan and Tonker [53] used a similar approach to predict the bioaccumulation of polycyclic aromatic compounds (PAHs), by evaluating their liposome–water partition coefficients with DI–SPME, but opting to use HPLC rather than GC for the semi-volatile solutes. In these cases, enough water/aqueous phase is used in the experiments to assume negligible partitioning into the vapor phase, and the solutes being studied were semi-volatile and therefore present at quantifiable concentrations in the aqueous phase. For very hydrophobic solutes, however, this approach may not be as sensitive.

Counts of radiolabelled solutes can be used to study distribution of volatile compounds in phospholipids *in situ*. This approach has been developed by Wishnia et al.[54] and adopted by other groups.[55,56] It uses a pre-equilibrated bottle system and monitors changes in radioactive

counts to calculate the partitioning of solutes into phospholipid bilayers. In this method, compounds are allowed to equilibrate between a vesicle dispersion, the vapor phase and the aqueous phase. Different chambers in the system have either all three phases, or only the aqueous and vapor phases. Fixed volumes from those phases are then used to calculate solute concentrations. The need for radiolabelled solutes, however, requires special handling of analytes and synthesis of those that are not commercially available.

In this work, we expand upon the SPME approach, by using short time headspace solid phase microextraction (HS–SPME) to detect solutes in the vapor rather than the aqueous phase. We determine the effect of vesicles on the local distribution of the aroma compound limonene, a monoterpene which is common in many foods and fragrances.[57,58] As explained in Chapter 1, HS–SPME uses a thin fiber coated with a sorbent film to selectively sample compounds present in the vapor phase above a sample mixture. By contacting the fiber with the sample headspace for short times, the adsorption of compounds onto the fiber does not significantly change the equilibrium of the system. This allows for accurate quantification using gas chromatography (GC) with mass spectroscopy (MS), since the measured peak areas are linearly related to the flavor's vapor phase concentration.[57] Using thermodynamic relationships together with an overall mole balance, local properties including partition coefficients and mole fractions in vesicle and water phases can be calculated. We have previously used this method to quantify limonene in water, in aqueous solutions of sodium dodecyl sulphate micelles,[57] and in short-chain phospholipid micelles.[59] Vapor–water and micelle–water partition coefficients determined with this method agreed with published literature, establishing HS–SPME as an accurate and non-invasive method to determine local partitioning properties while keeping the systems intact.

In addition, we compare the effectiveness of vesicle dispersions at limonene solubilization to that in micellar systems. As outlined in Chapter 1, vesicles and micelles are structurally

different, with vesicles having a bilayer surrounding an aqueous center, and micelles having a hydrophobic core. In addition, micelles are smaller than vesicles, and that changes the curvature, which affects the packing of the hydrophobic tails and headgroups and may alter the effectiveness of the structures at solubilizing compounds.

In this chapter we show for the first time how HS–SPME can be applied to vesicle dispersions in order to measure bilayer/water partition coefficients. We find that vesicles are much more effective at solubilizing limonene than micelles, with average partition coefficients of ~10^4 mM^{-1} as opposed to micellar partition coefficients of ~10^3 mM^{-1}. Furthermore, we examine the effects of vesicle and phospholipid structure on the solubilization of limonene in the dispersions, showing that the high lipid–water partition coefficients of limonene are largely unaffected by the changes in the acyl chains of phosphatidylcholine or the diameters of the vesicles.

2.2 Materials and Methods

2.2.1 Materials

Sunflower lecithin, Sunlipon™ 90 (90% phosphatidylcholine), with a typical composition shown in Appendix 1, was donated by Perimondo (New York, NY) and 1,2-dimyristoyl-*sn*-glycero-3-phosphatidylcholine (DMPC, >99% purity) was purchased as a 25 mg/mL solution in chloroform from Avanti Polar Lipids, Inc. (Alabaster, AL). Both lipids were used without further purification. They were stored at –18ºC to extend their shelf life and reduce oxidation. Sunlipon™ 90 samples were used for ~2 years with no significant changes to quality. Lecithin solutions were made with chloroform (HPLC grade, 99.8%) purchased from Sigma Aldrich (St. Louis, MO). Molecular Biology Reagent Water (0.1μm filtered), used for dynamic light scattering measurements, was purchased from Sigma-Aldrich, and deionized water used in HS–SPME sample preparation was obtained from a MilliQ™ water purification

system installed in the laboratory (Millipore, Bedford, MA). R-(+)-limonene (98%) was purchased from Sigma-Aldrich and dimethyl sulfoxide (DMSO, LC/MS grade) was obtained from Thermo Fischer Scientific (Waltham, MA).

2.2.2 Experimental Methods

2.2.2.1 Vesicle Preparation

To prepare vesicles, an appropriate volume of 25 mg/mL phospholipid solution in chloroform was added to a conical glass vial and placed under mild vacuum overnight to dry. DMPC solutions were purchased in concentrations of 25 mg/mL while Sunlipon™ 90 lecithin solutions were made using chloroform. After the chloroform was evaporated, the lipid cake was hydrated with 1 mL water and sonicated in a Fisher FS20 bath sonicator (Pittsburgh, PA) for 10–15 min to produce a dispersion of multilamellar vesicles. To make vesicles with average sizes >100 nm, the 1 mL dispersion was extruded 17 times with 1000 µL gas tight syringes (Hamilton, Reno, NV) through a nanosized polycarbonate membrane (100 or 200 nm) in an Avanti mini-extruder (Alabaster, AL), as shown in Figure 2.1. This extruder features steel

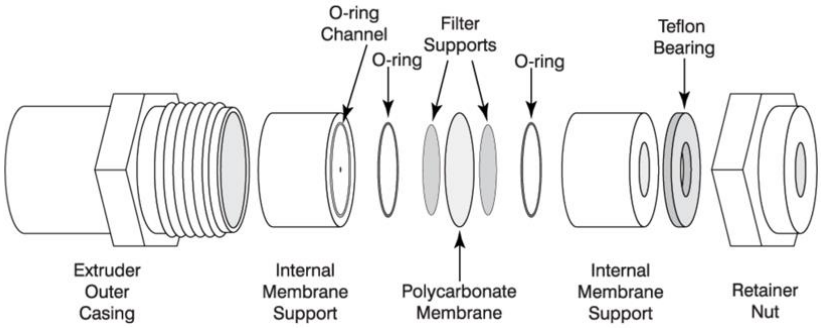

Figure 2.1. Avanti Mini Extruder used to create unilamellar vesicles (https://avantilipids.com/products/equipment/category/mini-extruder).

outer casings and polytetrafluoroethylene (PTFE) membrane supports. Whatman Nucleopore polycarbonate membranes (d. 47 mm) and 10 mm polyester drain disk supports were obtained

from Cytivia (Marlborough, MA). This membrane extrusion process created unilamellar vesicles (below 400 nm) and ensured that any larger sediments stayed on the starting side of the membrane.[60,61]

The majority of the extruded vesicle dispersion (typically 0.8 mL) was diluted to a 5 mL, 10 mM sample using Molecular Biology Regent Water. To determine average size by measuring vesicle diameter with dynamic light scattering (DLS), the remainder of the extruded dispersion was removed and further diluted to 1 mM. In cases where sample volume is limited, the DLS sample (1mM) was made from the diluted 10 mM dispersion. When more than 5 mL of the dispersion was needed, multiple extrusions were done and then combined prior to the diameter being measured. Samples remained stable with no changes in average diameter for at least one week when stored at room temperature. For DMPC samples, all mixtures and equipment were kept at temperatures >35°C to ensure that the vesicles were in the fluid phase. Temperatures of between 50 and 60ºC ensured that the temperature was still above 35ºC during the 15–20 min needed for the extrusion process. This was achieved by submerging a water-containing jar with the PTFE membrane supports, into a heated water bath; heating the water that was used in the sonicator; and placing the syringes and metal outer casings into an oven at 60ºC. DMPC vesicles with diameters <100 nm were made through successive extrusion stages. Extrusion through a membrane with 100 nm pores was followed by dilutions and then extrusions through smaller pore sizes (10 mM dispersion through 50 nm pore size, then 3 mM dispersion through 30 nm pore size). Dilutions were done to reduce the pressure in the extruder and allow the dispersion to pass through the membrane without breaking it. A sufficiently low enough pressure was not achieved with the lecithin mixture to make vesicles <100 nm.

2.2.2.2 Sample Preparation

Vesicle dispersion samples of 1mL were prepared for HS–SPME studies in 11.9±0.04 mL headspace vials (Agilent Technologies, Santa Clara, CA). The concentration of phospholipid was varied by dilution of the 10 mM stock dispersion with MilliQ water, to create concentrations from 0.01 to 5 mM. For experiments using fixed limonene concentrations, the limonene was added to the vials at amounts below its water solubility limit. This was achieved by adding pure limonene when making concentrations greater than 0.3 mmol per L of water. For lower concentrations, 0.093 mM limonene in DMSO solution was added, resulting in total concentrations of DMSO in water below 0.4%. Once limonene was added, following the protocol of Lloyd et al.,[32] the system was quickly sealed with aluminum foil (Reynolds Consumer Products, Lake Forest, Il), Teflon gaskets (19.1 mm O.D. x 14 mm I.D. x 0.13 mm thickness; Metro Industries, Inc., Grandview, MO) and 20 mm crimp caps with silicone septa (Restek, Bellefonte, PA) to minimize vapor loss. Handheld 20 mm crimpers (Perkin Elmer, Waltham, MA) were used to attach the caps to the vials.

2.2.2.3 Headspace Analysis using HS–SPME

Analysis was performed using a GC/MS instrument (Agilent Technologies 6890N GC/5975 MSD) with a DB-wax column (30 m x 0.25 mm I.D. x 0.25 μm film thickness; Agilent Technologies), an autosampler (Gerstel MPS2; Linthicum, MD) and a tray cooler (Gerstel, Linthicum, MD). A water bath (Isotemp Refrigerated Circulator Model 9100, Fisher Scientific) connected to the tray cooler was used to control sample temperature. The MS detectors were operated in the total and extracted ion mode with a 70 eV electron ionization source.[57,58]

Each sample was shaken for 3 h using the autosampler agitator to ensure local equilibrium of the solute between vesicles, water, and vapor. The preparation sequence for the

method is shown in Figure 2.2. A speed of 300 rpm (5 s on and 1 s off) was used at room temperature. The direction of mixing was reversed each time the mixer was "on". Shaking time was determined in preliminary experiments by monitoring changes in the headspace concentration. After mixing, samples were left to sit for at least 1 h in the tray cooler to ensure temperature equilibration, prior to the headspace being contacted by an 85 μm polyacrylate (PA) fiber (Restek) for 1 min. This short time allowed the solute to absorb to the fiber without disturbing the equilibrium of the system. Samples were randomized on tray, which allowed us to monitor potential time effects. There were none observed over the 13 h sampling period.

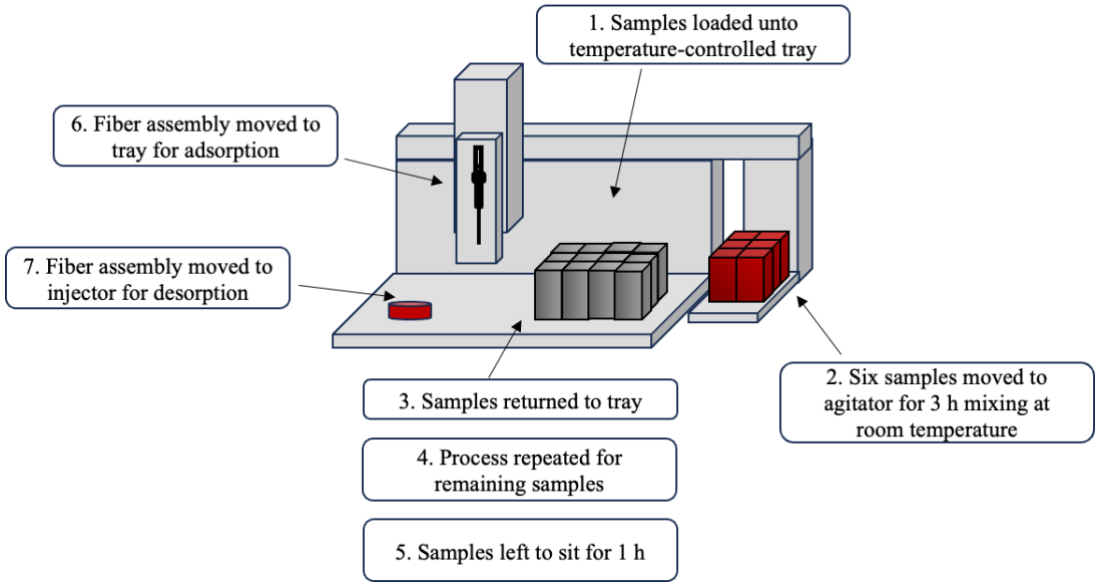

Figure 2.2. Instrument Preparatory Sequence for HS–SPME analysis.

Limonene in the SPME fibers was desorbed at the GC inlet at a temperature of 240°C for 10 min. Other GC/MS parameters are listed in Table 2.1. This desorption time also served as conditioning for successive samples. Scan or total ion mode was used to monitor changes in the limonene standards and fiber integrity over time. Limonene standards were remade roughly once per month due to oxidation and fibers were replaced after approximately 300 injections. Following manufacturer's recommendations, new fibers were preconditioned for 1 h at 260ºC.

This was followed by a series of blank injections to remove compounds adsorbed onto the fiber during manufacture and packaging. Before sampling each day, the fiber was conditioned for 10 min.

Table 2.1: GC/MS Parameters for Quantification of Limonene Vapor Concentrations above Vesicle Dispersions

Inlet Mode	Split, 50:1
Inlet Temperature (ºC)	240
Carrier Gas	Helium
Column Flow Rate (mL/min) Helium	1
GC Oven Program	40 °C, 5 °C/min to 75 °C, 40 °C/min to 240 °C
GC/MS Interface Temperature (°C)	260
MS parameters	Scan mode, *m/z* = 35 to 250 at 3.31/s; Selected ion monitoring mode, *m/z* = 68[a]

[a] Most abundant fragment

Since headspace vials can only be sampled once, each experiment was repeated three times from the same stock dispersion to produce one dispersion replicate set. One experiment was performed per day to prevent samples from sitting on the sampling tray >24h after mixing. Reference vials were used each day to normalize data. Final triplicate analysis was done using three separate dispersions of phospholipid vesicles to capture variations from extrusion. Replicates that were more than three standard deviations from the mean were considered outliers. Unless otherwise stated, standard experimental conditions were 0.618 mM of limonene at 28ºC for DMPC and 25ºC for lecithin using vesicles extruded with 200 nm membranes. Partition coefficients were determined using a Levenberg Marquardt nonlinear least-squares numerical optimization algorithm using Matlab (R2021A).

2.2.2.4 Dynamic Light Scattering

Vesicle size or diameter was determined by dynamic light scattering using a Malvern Panalytical Zetasizer Nano Range (Worcestershire, U.K.). Hydrodynamic diameters, d_H, were determined from the measured diffusion coefficient, D, using the Stokes Einstein equation,

$$d_H = \frac{kT}{3\pi\eta D}\ , \tag{2.1}$$

where k is Boltzmann's constant, T is the temperature and η is the solution viscosity. D is obtained from fits of the correlation function as a function of correlation time (Figure 2.3a).

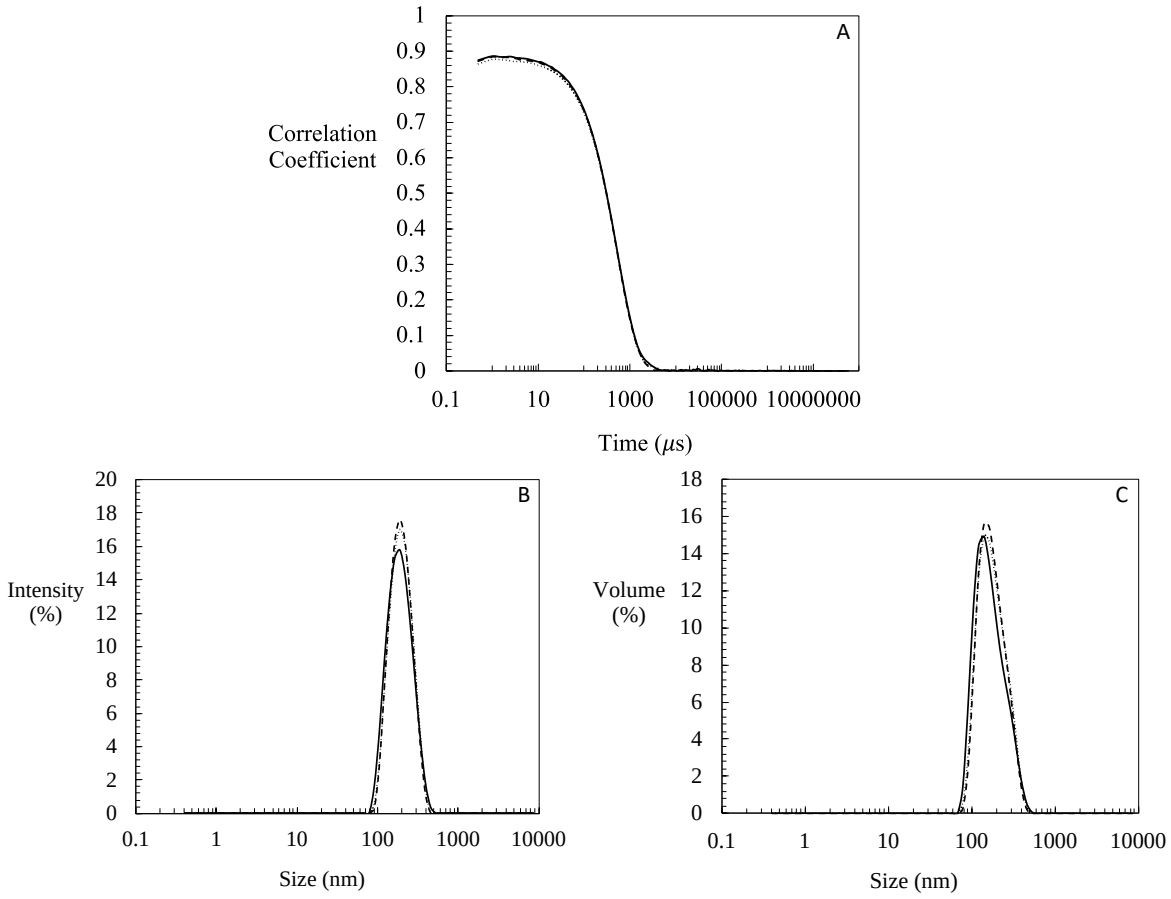

Figure 2.3. Correlation function, scattering intensity and volume distributions from DLS for typical DMPC samples. Lines (— ,– – –,⋯) represent measurement replicates.

The viscosity of the dispersant water was 0.8872 cP, and the refractive index for water and phospholipid, respectively, was 1.33 and 1.45. On average, the count rate was > 300 kcps (kilocounts of photons per seconds). Measurements were performed at a scattering angle of 90° and a temperature of 25°C. The Z-average diameter and polydispersity index (PDI) was determined using the method of cumulants. The Z-average hydrodynamic diameter ranged from 189.4±3.2 to 241.7±6.1nm with extrusion through 200nm membranes, 120.0±1.6 to

140.9±1.9 nm for 100 nm membranes and 61.8±0.618 to 66.3±0.8 nm for 30 nm membranes (Appendix 3). The PDI was generally <0.15. Figure 2.3 shows a typical result for the correlation function, scattering intensity, and volume distribution for DMPC samples. Measurements were taken using plastic disposable sizing cuvettes with 1 mL sample volume containing 1 mM dispersion.

2.3 Results and Discussion

2.3.1 HS–SPME Results for DMPC

The solubilization of limonene by DMPC vesicles was explored using HS–SPME and GC/MS. The peak areas, A, of limonene above a range of concentrations of DMPC vesicle dispersions (0.01 to 5 mM), were measured. Vesicles were extruded through a 200 nm membrane and the total limonene concentration was kept constant at 0.618 total millimoles per liter of water. The peak areas measured represent the concentrations of limonene present in the vapor phase and decrease with increasing concentrations of phospholipid, as shown in Figure 2.4A. This decrease reflects an alteration in the partitioning behavior from that of a vesicle-free water–vapor system, with the vesicles hosting some of the limonene, and shifting partitioning away from the vapor or water phases.

The peak areas above the vesicle dispersions are directly related to the vapor phase concentrations, with A/A_w being equivalent to C_v/C_v^w (Figure 2.4B). Here, C_v is the vapor phase concentration of limonene above the sample dispersion and A_w and C_v^w refer to the measured peak area and vapor phase concentration of limonene above samples without phospholipid. At very low concentrations of DMPC, from 0.01–0.5 mM, where the limonene–lipid mole ratios are very high, there was no significant difference between C_v and C_v^w. This indicates a need for higher DMPC concentrations to detectably affect the equilibrium distribution of limonene between the water and vapor phases. Initially, above 0.5 mM DMPC,

C_v/C_v^w drops steeply, then decreases more gradually as DMPC concentration increases. Overall, the vapor phase concentration of limonene is reduced 5-fold in comparison to the vesicle free solutions over the range of DMPC concentrations examined, demonstrating the large capacity that vesicles have for hosting hydrophobic molecules.

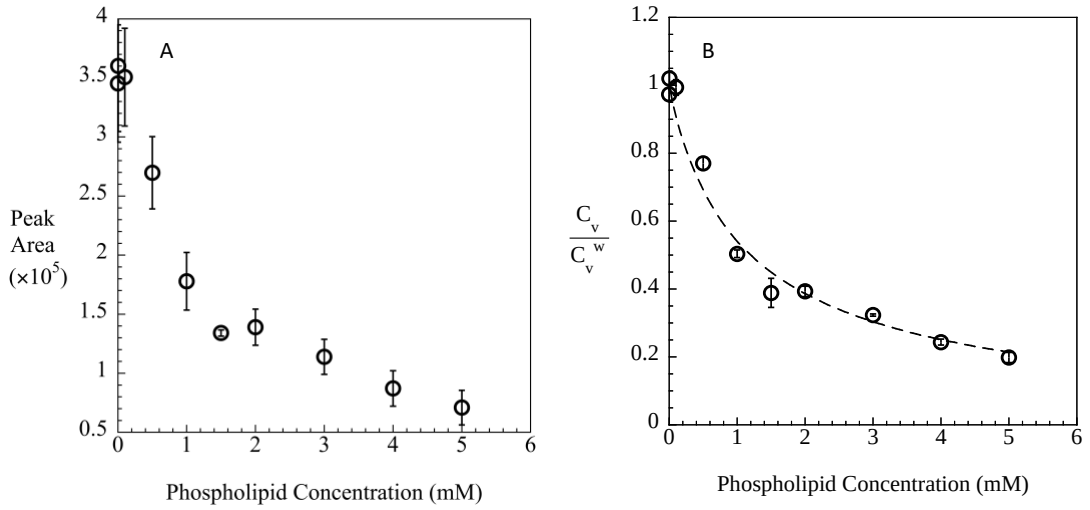

Figure 2.4: Peak area and vapor phase concentration of limonene decreases with increasing concentration of DMPC at 28ºC. Limonene concentration is fixed at 0.618 mM. Dashed line represents fit of equation 9.

2.3.2 Quantifying Lipid–Water Partitioning

At equilibrium, limonene is distributed among the vapor, water, and lipid phase (i.e. the vesicle bilayer). The total moles of limonene in the system, n_{tot}, can be related to the limonene found in the vesicle bilayers, dissolved in water, and in the vapor phase, by the mole balance below:

$$n_{tot} = n_{lim} + n_v + n_w \, . \tag{2.2}$$

Here, n_{lim}, n_v and n_w represent the moles of limonene in the lipid, vapor and water phases. This can further be expressed in terms of concentrations for the vapor and water phases (C_v and C_w) and as a mole fraction for the lipid phase:

$$n_{tot} = \frac{x_{lim} n_{PL}}{1 - x_{lim}} + C_v V_v + C_w V_w \tag{2.3}$$

Here, $x_{lim} = n_{lim}/(n_{lim} + n_{PL})$ is the mole fraction of limonene in the lipid bilayer of the vesicles, n_{PL} is the total moles of phospholipid, and V_v and V_w are the vapor and water volumes. The vapor–water (K_{vw}) and lipid–water (K_{lipw}) partition coefficients are defined as

$$K_{vw} = \frac{C_v}{C_w} \text{ and } K_{lipw} = \frac{x_{lim}}{C_w}, \tag{2.4}$$

respectively. The lipid–water partition coefficient can also be expressed in a dimensionless form as $\widehat{K}_{lipw} = x_{lim}/x_w$, where x_w is the mole fraction of limonene in water. The partition coefficients are related through

$$K_{lipw} \approx \widehat{K}_{lipw} \bar{v}_w , \tag{2.5}$$

where $\bar{v}_w$ is the molar volume of water, 0.01804 L/mol.[62] The vapor phase concentration of limonene, C_v, is related to the peak area, A, measured by GC/MS, by $A = k_p C_v$, where k_p is a proportionality constant. Using this relation and equation 2.4, we find that the area of the peak can be related to our partition coefficients by a single equation:

$$A = \frac{C_{tot} k_p K_{vw}}{1 + \frac{K_{vw} V_v}{V_w} + \frac{K_{lipw}}{1 - K_{lipw} C_w} C_{PL}} \tag{2.6}$$

where $C_{PL} = n_{PL}/V_w$ is the known concentration of phospholipid and $C_{tot} = n_{tot}/V_w$. The peak area, A_w, for the vapor phase concentration above limonene in water alone is given by

$$A_w = \frac{n_{tot} k_p K_{vw}}{V_w + V_v K_{vw}}. \tag{2.7}$$

The measured peak areas of the sample and water references are used to calculate A/A_w, which is equivalent to C_v/C_v^w. C_v^w is the vapor phase concentration for limonene above water without phospholipid.

K_{vw} has been previously determined by Karman et al.[35,63] to be 1.231±0.062 at 22ºC through "phase volume ratio" experiments in which the volumes of water and vapor were

varied. With K_{vw}, the unknown lipid–water partition coefficient K_{lipw} can then be determined by using the equation

$$\frac{C_v}{C_v^w} = \tilde{C}_v = \frac{\rho}{\rho + \dfrac{K_{lipw}\, C_{tot}}{1 + \dfrac{K_{vw}V_v}{V_w} - K_{lipw}C_{tot}\tilde{C}_v}}, \tag{2.8}$$

where ρ is the total mole ratio of limonene to lipid (n_{tot}/n_{PL} or C_{tot}/C_{PL}). Rearranging equation 2.8 leads to a quadratic solution:

$$\tilde{C}_v = \frac{1}{2}\left(\left(\nu + 1 + \frac{1}{\rho}\right) - \sqrt{\left(\nu + 1 + \frac{1}{\rho}\right)^2 - 4\nu}\right), \tag{2.9}$$

where

$$\nu = \frac{K_{vw}V_v + V_w}{V_w K_{lipw} C_{tot}}. \tag{2.10}$$

We fit equation 2.9 to measured values of $\tilde{C}_v$ over a range of ρ, adjusting only K_{lipw}, to quantify the bilayer–water partitioning.

When limonene concentrations are low, the mole fraction solubilized by the vesicles can be small compared to 1, i.e., $1 - x_{lim} \approx 1$. This allows us to express n_{lim} in equation 2.1 as $x_{lim}n_{PL}$, resulting in a simpler approximate equation for $\tilde{C}_v$:

$$\tilde{C}_v = \frac{1 + \dfrac{V_v K_{vw}}{V_w}}{K_{lipw}C_{PL} + \dfrac{V_v K_{vw}}{V_w} + 1}. \tag{2.11}$$

This approximation can be applied for $C_{tot} < 0.1$ mM, where the maximum mole fractions due to solubilization are less than 0.05. For consistency and accuracy, we used equation 2.9 to analyze all our experiments in this chapter.

DMPC has saturated fatty acid tails with 14 carbons. Since saturated acyl chains are typically solid at room temperature, their phase transition temperatures (T_G) are important for our experiments. T_G is the lipid chain melting temperature above which bilayers are in a fluid

state. Below T_G, the lipid chains become immobile but the polar headgroups retain fluidity, resulting in a so-called gel state.[22] Reduced solute distribution in the gel phase, compared to that in the fluid phase, would impact storage and delivery at lower temperatures. For DMPC vesicles, T_G is 23.3ºC[64]. To maintain fluidity, experiments were conducted at 28ºC. With a change in temperature, the properties of the system change. The vapor–water partition coefficient, K_{vw}, increases as the higher entropy vapor phase becomes more favored. A version of the van 't Hoff equation was used to calculate the change in K_{vw} for different temperatures, following the procedure outlined by Karman et al.:[59]

$$\frac{d\ln(RTK_{vw})}{d\left(\frac{1}{T}\right)} = \frac{d\ln\bar{v}_w}{d\left(\frac{1}{T}\right)} - \frac{\Delta\bar{H}_{vol}}{RT}. \tag{2.12}$$

Here, R is the gas constant (8.314 J mol^{-1}K^{-1}), T is the temperature (K) and $\Delta\bar{H}_{vol}$ is the enthalpy of volatilization (KJ/mol). $\Delta\bar{H}_{vol}$ was determined through previous experiments in our group to be 34.9 KJ/mol.[59] With a measured value for Henry's constant at 22ºC of 1.231,[59] changes in equilibrium with temperature can be determined by integrating equation 2.13 below

$$\ln\left(\frac{H_{pc2}}{H_{pc1}}\right) = \frac{-\Delta\bar{H}_{vol}}{R}\left(\frac{1}{T_2} - \frac{1}{T_1}\right), \tag{2.13}$$

yielding the resulting K_{vw} value at 28°C of 1.597. Parameters used for analysis are shown in Table 2.2. In obtaining this result we neglected the first term in equation 2.12 as there is only a small change in water's molar volume with temperature.

The normalized concentration, C_v/C_v^w, was found by comparison to reference water samples with the same limonene concentration (0.618 mM). In a water/vapor system without phospholipid, this results in a concentration of limonene in the water, C_w^w, of 3.79×10^{-5}M. The experimental C_v/C_v^w values were fit with equation 2.9, as shown in Figure 2.4B. A C_v/C_v^w ratio of 1 indicates that the vapor phase concentration in both systems are equivalent. Fitting

equation 2.9 to the data using non-linear regression yields a single constant vesicle–water partition coefficient of 13.187±0.913 mM^{-1} at 28ºC, as shown in Table 2.3.

Table 2.2: Parameters for Analysis of Limonene Partitioning in Vesicle Dispersions

Parameters	Values
$\Delta\bar{H}_{vol}$ (kJ/mol)	34.9[a]
C_w^{sat} (mM) at 25ºC	0.104[a]
V_w (L)	0.001
V_v (L)	0.0109
$\bar{v}_w$ (L/mol)	0.018044375[b]
C_{tot} (mM)	0.618
Temperature (ºC)	K_{vw} values
15	0.896
20	1.126
22	1.231[a]
25	1.404
28	1.597

[a]Karman et al.[59]
[b]CRC Handbook of Chemistry and Physics[62]

Table 2.3: Lipid–Water Partition Coefficients (K_{lipw}) of Limonene in PC Colloidal Particles

Phospholipid	Colloid	Size (nm)	T (°C)	C_{tot} (mM)*	K_{lipw}(mM^{-1})	K_{lipw}^{x} (mM^{-1})+
diC_6PC		–	23±1	4.65×10^{-5}	1.42±0.18[a]	
diC_7PC	Micelle	–	23±1	4.65×10^{-5}	3.31±0.33[a]	
					13.187±0.913	14.49±1.00 to
		200.6±5.7	28±0.1	0.618		16.93±1.17
					11.165±0.551	12.21±0.60 to
		138.1±2.3	28±0.1	0.618		15.94±0.79
		~100	30	0.3		10.87[b]
DMPC	Vesicle	~100	37	0.3		10.9[c]

*C_{tot} = limonene concentration
+$K_{lipw}^{x}=K_{lipw}/x_{PL}$
[a]Karman et al., 2021
[b]Witzke et al., 2010
[c]Dueland et al., 2012

Since regression analysis assumes there is homoscedasticity, or equal variance in all the data points, applying it to our data sets can result in errors from data points that are highly variable, particularly those with high limonene–lipid mole ratio that show little significant partitioning. To reduce the dependence of the fit on values with high variance, the data is weighted by the inverse of the variance, σ^2:

$$w = \frac{1}{\sigma^2}. \tag{2.14}$$

An alternate approach is to exclude values below 0.5 mM phospholipid where there is little to no partitioning. This produces similar values to weighting the data. However, in instances where the high variance comes from a point above 0.5 mM, this approach is insufficient. In addition, when the relative standard deviations of the points are in similar ranges, weights were not applied, as the conditions for homoscedasticity were met and weights did not affect the partition coefficient. Final K_{lipw} values were obtained as a weighted average of the three fits to the replicate data using

$$< K_{lipw} > = \frac{\sum_i w_i K_{lipw_i}}{\sum_i w_i}. \tag{2.15}$$

Here $< K_{lipw} >$ represents the weighted average, K_{lipw_i} is the replicate partition coefficient and w_i is the weight associated with K_{lipw_i} , calculated using equation 2.14. The 95% error for K_{lipw_i} is used as σ. The final error was also a weighted average calculated with

$$< w_i > = \frac{1}{\sum_i w_i}. \tag{2.16}$$

This method was chosen rather than fitting the complete triplicate data set to have a more accurate representation of the true mean and standard deviation by having independent averages that reflect different vesicle dispersions. Appendix 2 shows a comparison with fits where the averaged triplicate data is used instead. In general, the difference between K_{lipw}

values were less than 10%. In figures, error bars represent standard error of the mean between replicates.

2.3.3 Comparison of Literature Values for K_{lipw}

Our lipid–water partition coefficient measured for limonene in DMPC vesicles is comparable to published literature values. Isothermal titration calorimetry was used by Witzke et al.[65] to determine a partition coefficient, K_{lipw}^{x}, of limonene in DMPC vesicles at 30°C to be 10.87 mM^{-1}, and Duelund et al.[66] found K_{lipw}^{x} at 35ºC to be 10.9 mM^{-1} for 0.3 mM limonene, as shown in Table 2.3. These authors assumed that this partition coefficient, defined as $K_{lipw}^{x} = C_{lim}/C_w C_{PL}$, is constant, which should hold true when x_{lim} is small. K_{lipw}^{x} is related to our partition coefficient through the phospholipid mole fraction $x_{PL} = 1 - x_{lim}$ in the bilayer as

$$K_{lipw}^{x} = \frac{K_{lipw}}{x_{PL}}. \tag{2.17}$$

Since we measured K_{lipw} over a range of x_{PL} values, we can use equation 2.17 to convert our partition coefficient values to K_{lipw}^{x} for easy comparisons. Both values obtained by ITC at 30 and 35˚C are near the lower end of our range of measured values at 28ºC. When using ~200nm vesicles, we find K_{lipw}^{x}=14.49 to 16.93 mM^{-1}, and when using ~100 nm vesicles, K_{lipw}^{x}= 12.21 to 15.94 mM^{-1}. The vesicles used in Ref. 65 and 66 were extruded through 100 nm membranes. This good agreement with literature supports the accuracy of HS–SPME as a method to measure local partition coefficients in vesicles. There are several differences between the experimental set up for ITC and ours using HS–SPME. While we used water for our dispersions, the DMPC dispersion for ITC was created in a sodium phosphate buffer with a pH of 7.5. Measurements of the heat per injection were taken when the phospholipid dispersion was added to the limonene solution, and contributions from the vapor phase were excluded

from calculations. These authors also used a broader range of phospholipid concentrations, from 1–20 mM, compared to 0.01–5 mM for our experiments.

Compared to ITC, HS–SPME is a simple and fast method that needs fewer external parameters to calculate K_{lipw}. Furthermore, as limonene is volatile, the concentrations in the vapor phase are not negligible. This is of interest to us for food applications, given that we perceive flavors through retronasal olfaction. Hexane partitioning experiments by De Young and Dill[56] used radiolabeled counts of ^{2}H to determine K_{lipw} values. These authors reported a value of 6.228 mM^{-1} with DMPC vesicles at 25°C. As hexane is less hydrophobic than limonene (octanol–water partition coefficient $\log K_{ow}$ of 3.90 vs 4.57 for limonene), it should have less solute in the bilayer, leading to a lower K_{lipw}. Overall, for DMPC bilayers, the typical values observed for volatile hydrophobic compounds are on the order of 10^4 mM^{-1}.[56,65,66]

The partition coefficients obtained for limonene in vesicle systems are much higher than those obtained for the short-chain phospholipid micellar systems studied by Karman et al.[59] They found lipid–water partition coefficients for limonene with dihexanoyl phosphatidylcholine (diC$_6$PC) and diheptanoyl phosphatidylcholine (diC$_7$PC) micelles to be 1.42±0.18 mM^{-1} and 3.31±0.33 mM^{-1}, respectively[59] (Table 2.3). The vesicles' higher K_{lipw} value likely results from its larger hydrophobic core environment. While the structural differences in vesicles, where solute is incorporated into a bilayer with lower curvature, might explain the enhanced solubilization compared to micelles, contributions due to the longer chain lengths of DMPC are perhaps more significant. The increase in chain length from six to seven also lowers the CMC from 14.07±0.37 mM to 1.88±0.10 mM, as the added length increases the phospholipid hydrophobicity and allows for self-aggregation at lower concentrations. The increase in K_{lipw} in vesicles vs micelles is in line with experiments done by Keller et al,[67] which showed enhanced solubilization of the surfactant molecule, octyl glucoside, in DMPC vesicles

in comparison to octyl glucoside micelles. The K_{lipw} value in DMPC vesicles was 75 M^{-1}, which is about twice as large as the value for partitioning into octyl glucoside micelles, 38 M^{-1}.

For limonene in plant cuticles in mature trees, which are comprised primarily of waxes, K_{lipw} values between 361–433 M^{-1} were obtained using radiolabeled counts of ^{14}C.[68] As waxes are solid, partitioning is expected to be lower in comparison to fluid vesicles.

2.3.4 Effects of Phospholipid Structure on Partitioning

To determine whether phospholipid structure and composition significantly affected the partitioning properties of limonene, Sunlipon™ 90, a sunflower lecithin product with 90% phosphatidylcholine, was compared to DMPC. Unlike DMPC, which is a single structure, Sunlipon™ 90 is made up of a mixture of fatty acid tails, with >85% being unsaturated, and >89% having acyl tails that are 18 carbons long. DMPC has shorter acyl chains that are 14 carbons in length. In addition, Sunlipon™ 90 contains small amounts of lysophosphatidylcholine (2.5%) and moisture (1%) as shown in Appendix 1, while DMPC is obtained as a 99% pure material.

Results for the partitioning of limonene into lecithin vesicles, in comparison to DMPC, are shown in Figure 2.5A. Both experiments were performed at 28ºC with a limonene concentration of 0.618 mM. The partitioning behavior of limonene in Sunlipon™ 90 lecithin vesicles is the same as for DMPC, with a maximum 5-fold drop in the vapor phase concentration of limonene in comparison to the vesicle-free references, in the most concentrated dispersion. The calculated K_{lipw} value for limonene in Sunlipon™ 90 lecithin vesicles, 11.252±0.45 mM^{-1}, is not significantly different than the value for DMPC vesicles, 13.187±0.913 mM^{-1}. The final K_{lipw} values are dependent on the method used to fit the data, as shown in Figure 2.5B. When averaging separate replicates of fits, K_{lipw} for DMPC is ~14% higher than when the average of all the data is fit (Appendix 2). Most of the data points shown

in Figure 2.5, however, are overlapping. Therefore, for our experiments, the capacity of these DMPC and lecithin vesicle dispersions appear to be the same.

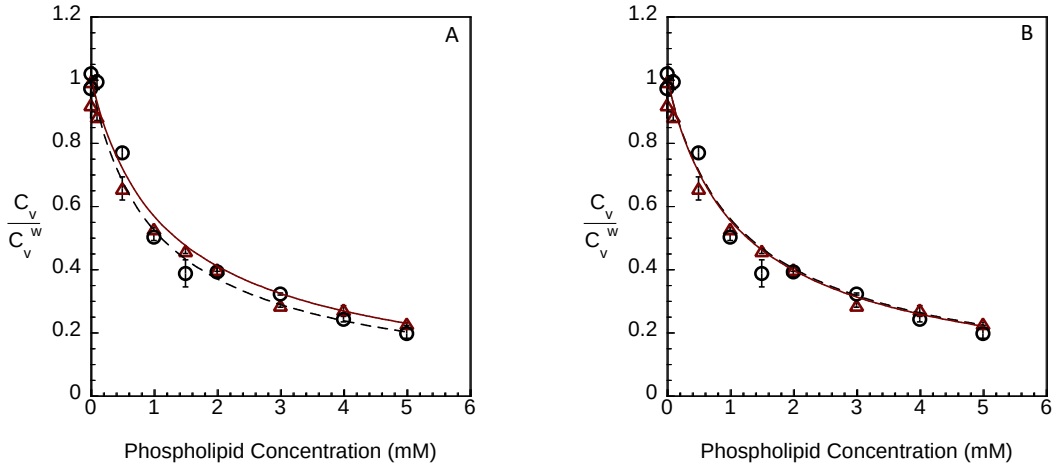

Figure 2.5: Vapor phase concentration of limonene above dispersions of Sunlipon™ 90 (sunflower lecithin) (△) and DMPC (○) vesicles at 28ºC and 0.618 mM limonene. Curved lines (—,– – –) represent nonlinear regression fits of K_{lipw} for Sunlipon™ 90 and DMPC respectively, done by (A) fitting three separate replicates and averaging K_{lipw}, and (B) fitting the average of all the data.

As limonene partitions into the phospholipid particles, it mixes with the fatty acid tails, due to the favourable entropy of mixing, but with the degree of mixing possibly being limited by the strength of limonene–limonene as well as lipid–lipid interactions.[69] Thus, changes in the fatty acid tails can impact solubilization. Partitioning into the bilayer is also heavily driven by the hydrophobic effect, with the nonpolar molecules interacting with each other and excluding water. In our discussion above of limonene partitioning into shorter chain phospholipid micelles (Section 2.3.3), increases in chain length were associated with increased partition coefficients stemming from the larger hydrophobic volume of the core. As longer alkyl chains also have lower CMCs, this effect is further enhanced as more of the longer chain phospholipids were found in micelles rather than as dissolved monomers.[70] There is also a decrease in curvature for longer fatty acid tails from an increase in packing parameter which causes

headgroups to be closer together. This curvature decrease reduces the interactions that the hydrophobic core may have with water and may have some impact on partitioning.

For the short chain phospholipid micelles, a one carbon increase in acyl chain length, from diC$_6$PC to diC$_7$PC, led to a two-fold increase in K_{lipw}. However, the magnitude of this change is not as drastic as we move from diC$_7$PC micelles to the much longer acyl tails of DMPC vesicles. We see a four-fold increase in K_{lipw} in relation to diC$_7$PC micelles, for a seven-carbon increase in chain length. It appears that the increased volume of the vesicle bilayer is not as effective at increasing partitioning as we observed in the micelles.

Besides a difference in chain length, there is also a difference in saturation between the lecithin and DMPC phospholipids. The more polar double bonds in the unsaturated fatty acid may reduce the amount of solute that partitions into the bilayer. The unchanged K_{lipw} values between DMPC and Sunlipon™ 90 lecithin vesicles may be a result of the combination of chain length and saturation. While the longer acyl tails in lecithin should enhance partitioning into the bilayer, they are also unsaturated, therefore differences are not easily observed. Work done by Keller et al.[67] show similar results for the partitioning of a surfactant molecule, octyl glucoside between water and DMPC or soybean phosphatidylcholine vesicles. At 27ºC, there was no significant difference between K_{lipw} values, although they were both about twice as large as the K_{lipw} value for octyl glucoside micelles.[67] Kwon and coworkers[26], who analyzed the solubilization of endocrine disrupters in various phospholipids, showed similar partitioning behavior for these compounds into bilayers of DMPC or the more unsaturated palmitoyloleoylphosphatidylcholine (POPC,16:0,18:1) and dioleoylphosphatidylcholine (DOPC,18:1).

It may be that enhancements due to the larger phospholipid tails are compensated by some disadvantage presented by the bilayers compared to micelles. Dulfer and Covers[27] studied the partitioning of polychlorinated biphenyl solutes into saturated phospholipid vesicles and

saw an increase in solubilization between chain lengths of 14–16 carbons for all the solutes studied. However, we saw no effect of larger tail lengths in lecithin relative to DMPC, for limonene partitioning. On the other hand, using cholesterol as the solute, Niu et al.[71] observed lower K_{lipw} values for bilayers with unsaturated fatty acid tails. There was a 40% decrease when one double bond was introduced to a saturated acyl chain and a further 45% for a second double bond. This observation was attributed to the double bonds weakening chain–cholesterol interactions, which are likely due to the rigid cholesterol molecule overlapping with the first 9–10 carbons of the chain.[71]

The effects of saturation or chain length can also be obscured by the effect of temperature on the membranes. Kwon and coworkers[26], who also studied the partitioning of endocrine disrupters into a saturated dipalmitoylphosphatidylcholine (DPPC,16:0) reported lower K_{lipw} values than those seen for POPC or DOPC, which both have at least one unsaturated fatty acid tail. However, all experiments were performed below the phase transition temperature, T_G, of DPPC, making the effect not simply one of saturation, but also of the phase transition from fluid to gel. Dulfer and coworkers[27] also noted that in their experiments, the fluidity of the bilayer membranes had a bigger impact on K_{lipw} than the length of the fatty acid tails, with chain lengths of 18–20 having lower partition coefficients than those at 14–20. Effects on partitioning of lipid phase behavior within the bilayer will be explored for our systems in Chapter 4.

2.3.5 Effects of Vesicle Structure on Partitioning

Limonene partitioning into vesicles of varying sizes was also studied. Polycarbonate membranes were used to change the diameter of Sunlipon™ 90 lecithin and DMPC vesicles. For both phospholipids, vesicles of ~200 and ~100 nm were made. Solubilization into DMPC vesicles of 63.5±2.8 nm was also compared to results with larger vesicles. These differences in

diameter result in changes to the curvature, which has the potential to affect partitioning. Figure 2.6 shows the partitioning of limonene into DMPC and Sunlipon™ 90 lecithin vesicles of varying sizes, with results that are very similar for all the vesicle dispersions. In Figure 2.7 we compare the K_{lipw} values and see a small difference between vesicles ~200 and ~100 nm for both DMPC and Sunlipon™ 90 lecithin. For DMPC, there is a marginal decrease with size, while for Sunlipon™ 90 lecithin, there is a small increase. Between DMPC vesicles with sizes of ~100 and ~60 nm, however, there is no significant difference in K_{lipw}. Values for the partition coefficients are also given in Tables 2.4 and 2.5. Takegami and coworkers,[72] also observed that varying the size of egg lecithin vesicles between 20–600 nm did not affect the partition coefficient of cholesterol. In addition, they found that the methods of vesicle preparation, including sonication and extrusion, did not affect the partition coefficients.[72] These literature results are in line with our findings.

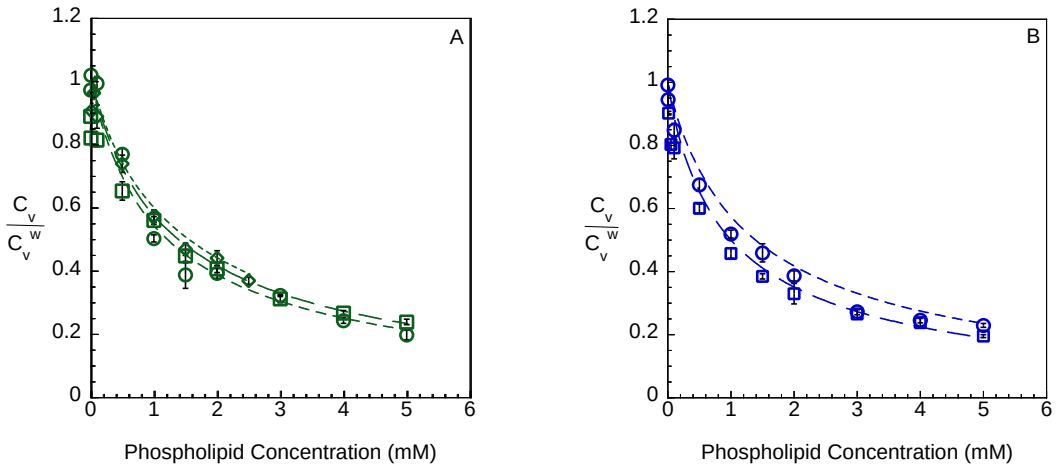

Figure 2.6: Vapor phase concentration of limonene above vesicle dispersions with diameters of ~200 (○), ~100 (□) and ~60 (◇) nm for (A) DMPC at 28ºC and (B) Sunlipon™ 90 lecithin vesicles at 25ºC. Curved lines represent nonlinear regression fits for K_{lipw}.

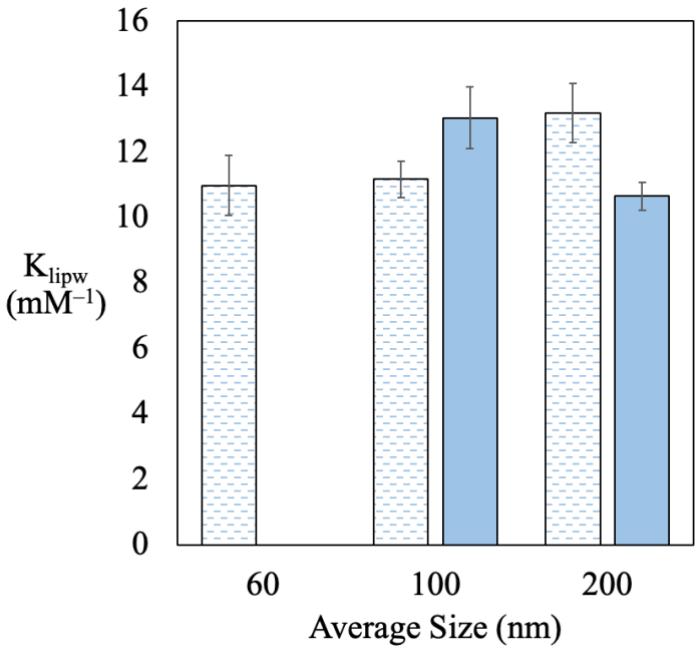

Figure 2.7: Partition coefficients for DMPC vesicles at 28ºC (blue dashes) and Sunlipon™ 90 lecithin vesicles at 25ºC (solid blue) with various average diameters.

Table 2.4: Partition Coefficients (K_{lipw}) of 0.618 mM Limonene in DMPC Vesicles at 28±0.1ºC

Size (nm)	<Size> (nm)[a]	K_{lipw} (mM^{-1})[b]	R^2	$<K_{lipw}>$ (mM^{-1})	$<\widehat{K}_{lipw}>$ ($\times 10^5$)[c]
207.7±3.6		12.675±2.952	0.9588		
189.4±3.2	200.6±5.7	13.923±1.125	0.9868	13.187±0.913	7.308±0.606
204.8±4.4		11.408±1.845	0.9735		
138.0±0.2		10.76±0.904	0.8967		
140.2±0.1	138.1±2.3	11.141±0.935	0.9717	11.165±0.551	6.188±0.305
136.2±1.7		11.726±1.037	0.9586		
66.3±0.8		10.024±2.009	0.9137		
62.3±0.5	63.5±2.8	12.048±1.456	0.963	10.979±0.919	6.084±0.509
61.8±0.6		10.403±1.468	0.9422		

[a]Errors are standard error of the mean

[b]Nonlinear regression weighted by $1/\sigma^2$, where σ represents the standard deviation of the replicates

[c]$<\widehat{K}_{lipw}>$ values are of order 10^5

Table 2.5: Partition Coefficients (K_{lipw}) of 0.618 mM Limonene in Sunlipon™ 90 Lecithin Vesicles

Size (nm)	<Size> (nm)[a]	T (°C)	K_{lipw} (mM^{-1})[b]	R^2	<K_{lipw}> (mM^{-1})	<$\widehat{K}_{lipw}$> ($\times 10^5$)[c]
229.5±2.3			10.548±0.533	0.9834		
221.9±2.4	231± 5.8	25±0.1	10.286±0.856	0.9839	10.656±0.425	5.905±0.236
241.7±6.1			12.007±1.235	0.9901		
120.0±1.6			12.773±1.735	0.9644		
143.2±1.1	134.0±7.4	25±0.1	13.277±1.776	0.9548	13.044±0.944	7.229±0.523
140.9±1.9			13.077±1.454	0.9572		
231.9±4.4			11.146±0.996	0.9787		
238.7±5.5	234.3±2.2	28±0.1	10.821±0.543	0.9767	11.252±0.45	6.236±0.249
232.3±1.8			14.115±1.352	0.9399		

[a]Errors are standard error of the mean
[b]Nonlinear regression weighted by $1/\sigma^2$, where σ represents the standard deviation of the replicates
[c]<$\widehat{K}_{lipw}$> values are of order 10^5

2.4 Conclusion

We have established HS–SPME as an accurate and non-invasive method to determine the lipid–water partition coefficient of hydrophobic molecules in phospholipid vesicle dispersions. Compared to other methods often used to study partitioning into vesicles, this method is fast, simple and requires few thermodynamic parameters for calculations. It also involves the vapor, water, and lipid phases, allowing us to model the behavior of hydrophobic molecules *in situ*. Phospholipid vesicles are very effective at solubilizing limonene, with K_{lipw} values on the order of 10^4 M^{-1}. These K_{lipw} values, obtained for limonene in DMPC and lecithin vesicles using HS–SPME, are similar to published literature values using ITC. Phospholipid vesicles have higher K_{lipw} values than short-chain phospholipid micelles, which have K_{lipw} values on the order of 10^3 M^{-1}, reflecting the larger hydrophobic core volumes of the former. Structural differences between phospholipids do not affect the partitioning of limonene into the bilayer. There were no differences in partitioning between DMPC which has 14-carbon, saturated fatty acid tails and Sunlipon™ 90 lecithin, which has mostly unsaturated,

18-carbon fatty acid tails. There is a marginal effect of size between vesicles with diameters between ~100 to 200 nm.

2.5 Nomenclature

A	detected peak area of limonene in the vapor phase
A_w	detected peak area for limonene in water reference
C_{PL}	concentration of the phospholipid in water
C_v^w	vapor phase concentration of limonene in water reference
C_v	concentration of limonene in the vapor phase
C_w^{sat}	solubility limit of limonene in water
C_w	concentration of limonene in the water
$\hat{C}_{PL}$	$\frac{C_{PL}}{C_w^{sat}}$
$\hat{C}_{tot}$	$\frac{C_{tot}}{C_w^{sat}}$
$\tilde{C}_v$	$\frac{C_v}{C_v^w}$
$\hat{C}_v$	$\frac{C_v}{C_v^o}$
H_{pc}	Henry's constant
$\Delta\overline{H}_{vol}$	enthalpy of volatilization
K_{lipw}	lipid–water partition coefficient
$\widehat{K}_{lipw}$	Dimensionless lipid–water partition coefficient
k_p	limonene proportionality constant for GC/MS
K_{vw}	vapor–water partition coefficient
$\widehat{K}$	$K_{lipw}C_w^{sat}$

n_{lim}	moles of limonene in the vesicle bilayer
n_{PL}	moles of phospholipid
n_v	moles of limonene in the vapor phase
n_w	moles of limonene in the water phase
n_{tot}	total moles of limonene in the system
R	gas constant
T	temperature
T_G	phase transition temperature
V_v	vapor volume
V_w	water volume
$\hat{V}$	$\frac{K_{vw}V_v}{V_w} + 1$
w	weights for experimental data
x_{lim}	mole fraction of limonene in the vesicle bilayer
x_{PL}	mole fraction of phospholipid in the vesicle bilayer
x_w	mole fraction of limonene in the water phase
ν	$\frac{K_{vw}V_v + V_w}{V_w K_{lipw} C_{tot}}$
$\bar{v}_w$	molar volume of water
ρ	limonene–lipid mole ratio, n_{tot}/n_{PL}
σ	standard deviation

Chapter 3

Effects of Composition on Partitioning of Limonene into Phosphatidylcholine Vesicles

3.1 Introduction

Partitioning of hydrophobic solutes into nanostructures is often analyzed with ideal mixing theory,[15,73–75] which assigns effects of intermolecular interactions that partly drive solubilization to different infinitely dilute reference potentials in water and bilayer. In this way, composition dependent contributions to the chemical potentials due to mixing enthalpy are assumed to be negligible. The two "solutions" involved in the distribution are considered ideal–dilute solutions. Using ideal mixing, the lipid–water partition coefficient, K_{lipw}, remains constant with solute concentration, and only depends on temperature. In Chapter 2, results were analyzed with this assumption of ideal mixing in both the lipid bilayer phase and the outside aqueous phase. Determinations of constant K_{lipw} values by Lloyd et al.[32] and Karman et al.[35] also used ideal mixing theory for limonene partitioning in lipid micellar systems. With this assumption, for both micelles and vesicles, much of the solute distribution behavior was quantitatively captured.

When there are significant differences between solute–solute and solute–solvent interactions in the system, however, K_{lipw} will be affected by the mole fraction of the solute, particularly in the lipid phase. To account for these interactions, in this chapter we apply regular solution theory, which introduces the interaction parameter, χ, to describe how solute–solute, solvent–solvent, and solute–solvent interactions impact mixing. In the case of mixture components that have stronger solute–solute or solvent–solvent attraction, the interaction parameter will be positive,[69] from components' preference to associate with "like" molecules rather than forming solute–solvent neighbors. When there are stronger solute–solvent attractive

interactions, $\chi < 0$; $\chi = 0$ reflects ideal behavior. Figure 3.1 shows the mole fractions of limonene in the water, vapor, and lipid phases at equilibrium. For lipid–water partitioning, limonene and phospholipid in the bilayer are treated as a pseudobinary mixture (true binary for DMPC and limonene), with the phospholipid being the lipid solvent.

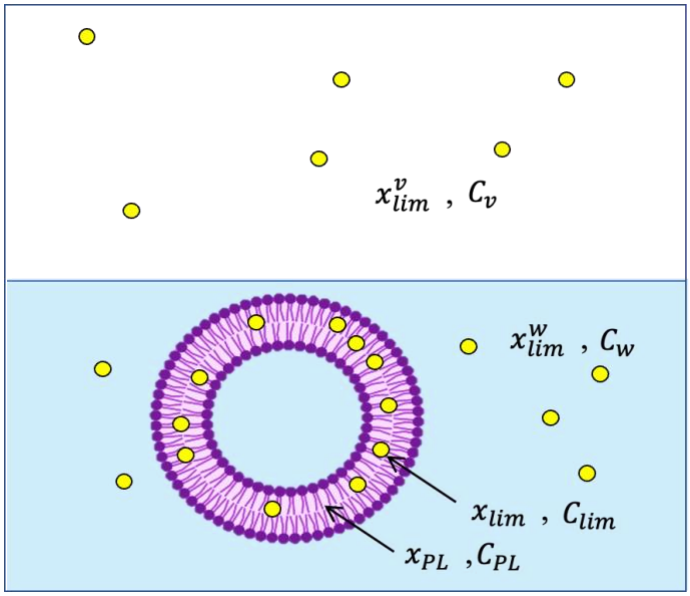

Fig 3.1: Regions for defined concentrations and mole fractions of limonene and phospholipid for limonene in equilibrium between the vapor, water, and lipid phases.

Regular solution theory has been successfully applied to several lipid solvents with hydrophobic solutes. Hawker[76] showed that the partition coefficients of chlorinated compounds between the bulk solvent triolein and water reflect non-ideal behavior and that regular solution theory could be used to predict the solubilities of these compounds in lipids. For some detergents partitioning into lipid bilayers, regular solution theory has been found to be more adequate than ideal mixing theory, due to the dependence of K_{lipw} on the mole fractions of detergent in the bilayer.[67,75] The ionic surfactants, sodium alkyl sulfate and alkyl trimethyl ammonium bromide, were found to deviate from ideal mixing when partitioning into phosphatidylcholine vesicles, with non-zero interaction energies.[77]

In food products and other consumer packaged goods, there is a wide range of aroma or flavor concentrations added. When using colloidal systems to host these molecules, their distribution and release will be dependent on the partition coefficients, making it important to understand how aromas mix with solvents to alter partitioning. In this chapter, we use experimental data to determine the extent to which limonene follows ideal mixing theory when partitioning into phospholipid bilayers. Using headspace–solid phase microextraction (HS–SPME), we determined the vapor phase concentration of limonene, which was used to calculate lipid–water partition coefficients over various ranges of bilayer mole fractions. Furthermore, by fixing phospholipid concentrations and varying solute, we found the maximum amount of limonene that can be solubilized by phospholipid vesicles, a property that is important to the design of new consumer products. We also conducted phase volume ratio experiments to determine the impact of the solvent DMSO on the vapor–water partition coefficient, and to analyze how the solubility limit of limonene, C_w^{sat}, changes with temperature. These parameters are important as they impact any calculations done using pure limonene as a reference.

3.2 Materials and Methods

3.2.1 Materials

Partially purified lecithin from sunflower seeds, Sunlipon™ 90 (90% phosphatidylcholine) was donated by Perimondo (New York, NY); this ingredient is designated "lecithin" throughout the text. 1,2-dimyristoyl-*sn*-glycero-3-phosphatidylcholine (DMPC, >99% purity) was purchased as a 25 mg/mL solution in chloroform from Avanti Polar Lipids, Inc. (Alabaster, AL). Both phospholipids were used without further purification. Lecithin solutions were made with chloroform (HPLC grade, 99.8%) purchased from Sigma Aldrich (St. Louis, MO). The Molecular Biology Reagent Water (0.1μm filtered) used for dynamic light scattering measurements was purchased from Sigma-Aldrich (St. Louis, MO)

and the deionized water used for HS–SPME sample preparation was obtained from a MilliQ™ water purification system installed in the laboratory (Millipore, Bedford, MA, resistivity of 18 MΩ·cm). R-(+)-limonene (98%) and dimethyl sulfoxide (DMSO) were purchased from Sigma-Aldrich.

3.2.2 Experimental Methods

3.2.2.1 Sample Preparation

The vesicle preparation protocol is outlined in Section 2.2.2.1. Briefly, a solution of phospholipid in chloroform is dried under vacuum and hydrated with water to form multilamellar vesicles after sonication. Unilamellar vesicles were subsequently formed via extrusion and diluted with water for HS–SPME experiments and for size determination through dynamic light scattering (DLS) (Malvern Panalytical Zetasizer Nano Range, Worcestershire, U.K.).[60,61] To measure K_{lipw} with fixed limonene concentrations, samples of 1 mL were prepared for HS–SPME by adding fixed volumes of limonene to a range of phospholipid concentrations (from 0.01 to 5 mM). For experiments using fixed phospholipid concentrations, various volumes of pure limonene were added to 1 mL of 1 or 3 mM phospholipid samples. All samples were prepared in 20 mL vials with liquid volumes of 2 and 17 mL. Limonene amounts added to these vials ranged from 200 to 1800 nanomoles.

3.2.2.2 Headspace Analysis using HS–SPME

Analysis was done following the procedure outlined in Section 2.2.2.3. The GC/MS instrument used was equipped with an Agilent DB-wax column, and was connected to an autosampler and a tray cooler. The MS detector was operated in the total and extracted ion mode with a 70 eV electron ionization source.[57,58] Samples were shaken for 3 h in the autosampler agitator at a speed of 300 rpm at room temperature prior to SPME sampling. After

sitting for at least 1 h to ensure temperature equilibration, the headspace was sampled using an 85 μm polyacrylate (PA) fiber (Restek) for 1 min and desorbed in the GC inlet at 240°C for 10 min. GC/MS parameters are listed in Table 2.1. Sample *replicates* were done using the same stock dispersion and *triplicate* analysis was done on averaged replicates from three separate dispersions of phospholipid vesicles (cf. Section 2.2.2.3). Replicates that were more than three standard deviations from the mean were considered outliers.

K_{lipw} values were determined using a Levenberg-Marquardt nonlinear least-squares numerical optimization algorithm using Matlab (R2021A). Weighted averages for K_{lipw} were calculated using equations 2.14 to 2.16. The slopes used to calculate K_{vw} values were determined with Microsoft Excel (Redmond, WA) using linear regression with zero intercepts for the slopes and ANOVA for their standard errors. Errors in K_{vw} were determined using error propagation developed by Lloyd et al.[132] and weighted averages of the slope ratios calculated as explained in Section 2.3.2. In figures, error bars represent the standard error of the mean between replicates.

3.3 Results and Discussion

3.3.1 Quantifying Lipid–Water Partitioning

The mole balance for limonene at equilibrium between water, lipid and vapor phase is derived in Section 2.3.2. From this mole balance, the vapor phase concentration ratio $\tilde{C}_v$ satisfies

$$\frac{C_v}{C_v^w} = \tilde{C}_v = \frac{\rho}{\rho + \dfrac{K_{lipw}\, C_{tot}}{1 + \dfrac{K_{vw} V_v}{V_w} - K_{lipw} C_{tot} \tilde{C}_v}}. \tag{2.8}$$

In this equation, C_v is the vapor phase concentration of limonene in the headspace of a vial containing vesicle dispersion, C_v^w is the concentration of limonene above water, ρ is the mole

ratio of total limonene to lipid in the sample vials, and C_{tot} is the total moles of limonene per liter of water in the sample. V_v and V_w are the vapor and water volumes. Parameters used for data analysis are given in Table 2.2. Equation 2.8 (Section 2.3.2) is solved for $\tilde{C}_v$ as

$$\tilde{C}_v = \frac{1}{2}\left(\left(\nu + 1 + \frac{1}{\rho}\right) - \sqrt{\left(\nu + 1 + \frac{1}{\rho}\right)^2 - 4\nu}\right), \tag{2.9}$$

where

$$\nu = \frac{K_{vw}V_v + V_w}{V_w K_{lipw} C_{tot}} = \frac{\hat{V}}{K_{lipw} C_{tot}} \tag{2.10}$$

with $\hat{V} = 1 + K_{vw}V_v/V_w$. Equations 2.9 and 2.10 were used to analyze sample sets prepared at constant C_{tot}.

In this chapter, we also feature experiments where the phospholipid concentration was kept constant and the concentration of limonene varied over a wide range. As limonene concentrations in the water phase approach the solubility limit $C_w^{sat} = 1.04 \times 10^{-4}$ mM for limonene in water alone for several of these experiments, it is more appropriate to use vapor phase concentrations above pure limonene, rather than above limonene in water, as a reference. This situation corresponds to values $C_{tot} > 0.9$ mM. For these experiments, a ratio of $A/A° = C_v/C_v^o$ was determined from our HS–SPME measurements, with $A°$ and C_v^o representing the limonene peak area and vapor phase concentration, respectively, above a pure solute reference. C_v^o and $A°$ can be related to the aqueous solubility C_w^{sat} of limonene in water alone using Henry's law:

$$C_v^o = \frac{A^o}{k_p} = C_w^{sat} K_{vw}\,, \tag{3.1}$$

and equation 3.1 can be used to renormalize the vapor phase prediction (2.9) according to

$$\hat{C}_v = \frac{C_v^w}{C_v^o}\tilde{C}_v = \frac{1}{\hat{V}}\frac{C_{tot}}{C_w^{sat}}\,\tilde{C}_v\,. \tag{3.2}$$

Multiplying equation 2.9 above by C_v^w/C_v^o therefore yields

$$\hat{C}_v = \frac{C_{tot}}{2\hat{V}C_w^{sat}}\left(\left(\nu + 1 + \frac{1}{\rho}\right) - \sqrt{\left(\nu + 1 + \frac{1}{\rho}\right)^2 - 4\nu}\right). \tag{3.3}$$

For experiments where C_{tot} is varied at constant phospholipid concentration C_{PL}, the parameter ν in equation 3.1 is no longer constant, and $\hat{C}_v$ in equation 3.3 is not solely a function of ρ. However, by rewriting the latter equation using $C_{tot} = C_{PL}\rho$, $\hat{C}_v$ can alternatively be expressed as

$$\hat{C}_v = \frac{1}{2}\left(b - \sqrt{b^2 - 4\frac{\hat{C}_{PL}\rho}{\hat{K}\hat{V}}}\right). \tag{3.4}$$

In equation 3.4,

$$b = \frac{\hat{C}_{PL}}{\hat{V}}(1 + \rho) + \frac{1}{\hat{K}} \tag{3.5}$$

and

$$\hat{K} = K_{lipw}C_w^{sat}\,; \qquad \hat{C}_{PL} = \frac{C_{PL}}{C_w^{sat}}. \tag{3.6}$$

A summary of the equations and the relevant experimental conditions under which they were applied are provided in Table 3.1.

Table 3.1: Equations Used to Find K_{lipw} and Corresponding Conditions

	Experimental conditions	
	C_{tot} fixed	C_{PL} fixed
$\tilde{C}_v$	$\frac{1}{2}\left(\left(\nu + 1 + \frac{1}{\rho}\right) - \sqrt{\left(\nu + 1 + \frac{1}{\rho}\right)^2 - 4\nu}\right)$ [a,b]	
$\hat{C}_v$	$\frac{C_{tot}}{2\hat{V}C_w^{sat}}\left(\left(\nu + 1 + \frac{1}{\rho}\right) - \sqrt{\left(\nu + 1 + \frac{1}{\rho}\right)^2 - 4\nu}\right)$ [b,c]	$\frac{1}{2}\left(b - \sqrt{b^2 - 4\frac{\hat{C}_{PL}}{\hat{K}\hat{V}}\rho}\right)$ [d,e]

[a] Equation 2.9
[b] $\nu = \frac{\hat{V}}{K_{lipw}C_{tot}}$
[c] Equation 3.3
[d] Equation 3.4
[e] $b = \frac{\hat{C}_{PL}}{\hat{V}}(\rho + 1) + \frac{1}{\hat{K}}$

3.3.2 Effects of Composition on Partitioning

The distribution of limonene in systems with fixed limonene and varying phospholipid concentrations was compared to mixtures where the limonene concentration was varied, while the concentration of phospholipid remained fixed. In the latter experiments, rather than keeping C_{tot} well below the aqueous solubility limit, the limonene concentration was increased until the vesicles solubilized their maximum mole fractions. Consequently, in these experiments, the concentration of limonene in water becomes equivalent to C_w^{sat} at sufficiently high mole ratios of limonene to phospholipid. Fits of equation 3.4 to vapor phase data for 1 mM and 3 mM lecithin, with various limonene amounts, are shown in Figure 3.2, with obtained K_{lipw} values given in Table 3.2. The vapor phase concentration of limonene above the samples are seen in the figure to monotonically increase with added limonene, reaching a plateau at solute saturation. At 20ºC, the K_{lipw} results for these two lecithin concentrations are the same within error, as seen in Table 3.2. For these experiments, the partitioning behavior is unchanged by the different overall mixture composition of phospholipid, limonene, and water.

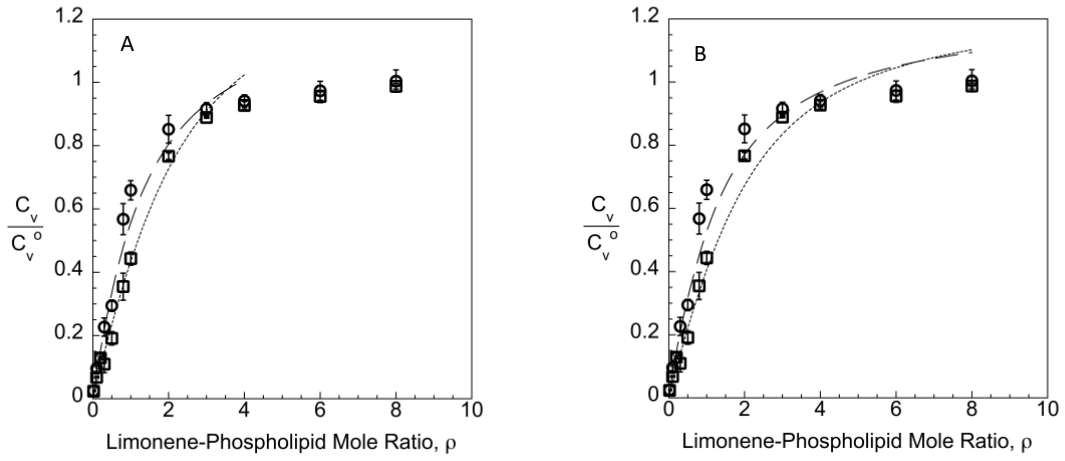

Figure 3.2: Vapor phase concentration of limonene above 1 (○) and 3 mM (□) lecithin at 20ºC. Dashed lines represent nonlinear regression fits of data for (A) $\rho \leq 4$ or (B) $\rho \leq 8$ to obtain K_{lipw}.

Table 3.2: Partition Coefficients (K_{lipw}) of Limonene in Sunlipon™ 90 Lecithin Vesicles

$\hat{C}_v$ range	Size (nm)	<Size> (nm)[a]	C_{PL} (mM)*	K_{lipw} (mM^{-1})	R^2	<K_{lipw}> (mM^{-1})[b]	<$\widehat{K}_{lipw}$> ($\times 10^5$)[c]
$\rho \leq 4$	197.4±4.7	203.8 ±9	1	7.047±0.585	0.983	7.055 ±0.321	3.910 ±0.178
	192.4±1.9			7.192±0.632	0.9867		
	221.6±12.7			6.98±0.484	0.9879		
all ρ	197.4±4.7	203.8 ±9	1	7.766±0.582	0.9739	7.795 ±0.324	4.32 ±0.18
	192.4±1.9			7.916±0.561	0.9722		
	221.6±12.7			7.706±0.544	0.9765		
$\rho \leq 4$	217.8±3.2	199.4 ±9.3	3	7.632±0.375	0.9882	7.455 ±0.283	4.131 ±0.157
	187.8±2.9			7.126±0.612	0.9684		
	192.6±0.8			7.314±0.609	0.9701		
all ρ	217.8±3.2	199.4 ±9.3	3	8.388±0.343	0.9837	7.993 ±0.253	4.43 ±0.14
	187.8±2.9			6.971±0.744	0.9720		
	192.6±0.8			7.707±0.434	0.9907		

*C_{PL} = Lecithin concentration
[a]Errors are standard error of the mean
[b]Nonlinear regression weighted by $1/\sigma^2$, where σ represents the standard deviation of the replicates
[c]<$\widehat{K}_{lipw}$> values are of order 10^5

The data in Figure 3.2 also provides us with the maximum mole ratios, ρ^{sat}, at which solubilization of limonene reaches saturation, as well as the corresponding maximum solute mole fractions, x_{lim}^{sat}. The value of ρ is set by the total moles of added limonene and phospholipid in the sample, whereas the mole fraction refers to the binary composition within the bilayer only. The mole fraction can be calculated from $\hat{C}_v$, by first using the latter to determine the concentration of limonene present in the vapor phase:

$$C_v = \hat{C}_v C_w^{sat} K_{vw} . \tag{3.7}$$

The moles of limonene in the lipid phase, n_{lim}, is then determined by subtracting the moles of limonene present in the vapor and water phases according to

$$n_{lim} = n_{tot} - C_v \left(V_v + \frac{V_w}{K_{vw}} \right) . \tag{3.8}$$

Since the moles of phospholipid in the system was fixed at $n_{PL} = C_{PL}V_w$, the mole fractions for each experimental point, $x_{lim} = n_{lim}/(n_{lim} + n_{PL})$, can then be determined.

Overall, limonene mole ratios for these experiments ranged from 0.02 to 8, which correspond on average to mole fractions in the vesicle of 0.009 to 0.88. For lecithin at 20ºC, the bilayer solubilized limonene up to an estimated maximum mole ratio of $\rho^{sat} = 4.2 \pm 1$, or a bilayer mole fraction of $x_{lim}^{sat} = 0.79$, which can be seen from the plateau in Figure 3.2. ρ^{sat} is determined from the intersection of the fit using equation 3.4 and $\hat{C}_v = 1$ using data for 1 and 3 mM lecithin. The data in Figure 3.2 suggests that ρ^{sat} could be even higher, at 6–8. The mole fraction, x_{lim}, is calculated as discussed above using equations 3.7 and 3.8. Thus, we find that the vesicles can host a sizable amount of limonene in the bilayer before the system becomes saturated. On a volume basis, x_{lim}^{sat} corresponds to a limonene volume fraction of 45% in the bilayer. For comparison, short chain phosphatidylcholine micelles, comprised of diC_6PC or diC_7PC, host maximum limonene mole fractions of 0.25 and 0.51 at 23ºC, respectively.[35] These differences between solubility limits in micelles and vesicles are consistent with the higher partition coefficients measured by us within the vesicle dispersions.

Equation 3.4 with a single constant value for the partition coefficient K_{lipw} could successfully fit $\hat{C}_v$ data at both fixed phospholipid concentrations in Figure 3.2, across a range of mole ratios or mole fractions. In Figure 3.2A, we show the fits obtained for the condition $\rho \leq 4$, whereas for Figure 3.2B, the entire range of ρ values are used. This comparison was made because it can be difficult to determine exactly where the system becomes saturated with limonene and where the fit range should end. The values for the fits, however, are not statistically different, as shown in Table 3.2. We therefore used K_{lipw} values obtained by fitting the whole range of ρ for analysis.

When the phospholipid concentration C_{PL} was varied as in the experiments shown in Figure 3.3, the partition coefficient appears to change with the concentration of limonene being

used. For these experiments, the data was fit with equation 2.9 to find K_{lipw}. With lecithin dispersions at 25ºC, a steeper drop in $\tilde{C}_v$ with C_{PL} was observed for systems with 0.618 mM limonene, than for those with 0.093 mM (Figure 3.3A). This dependence on C_{tot} was also

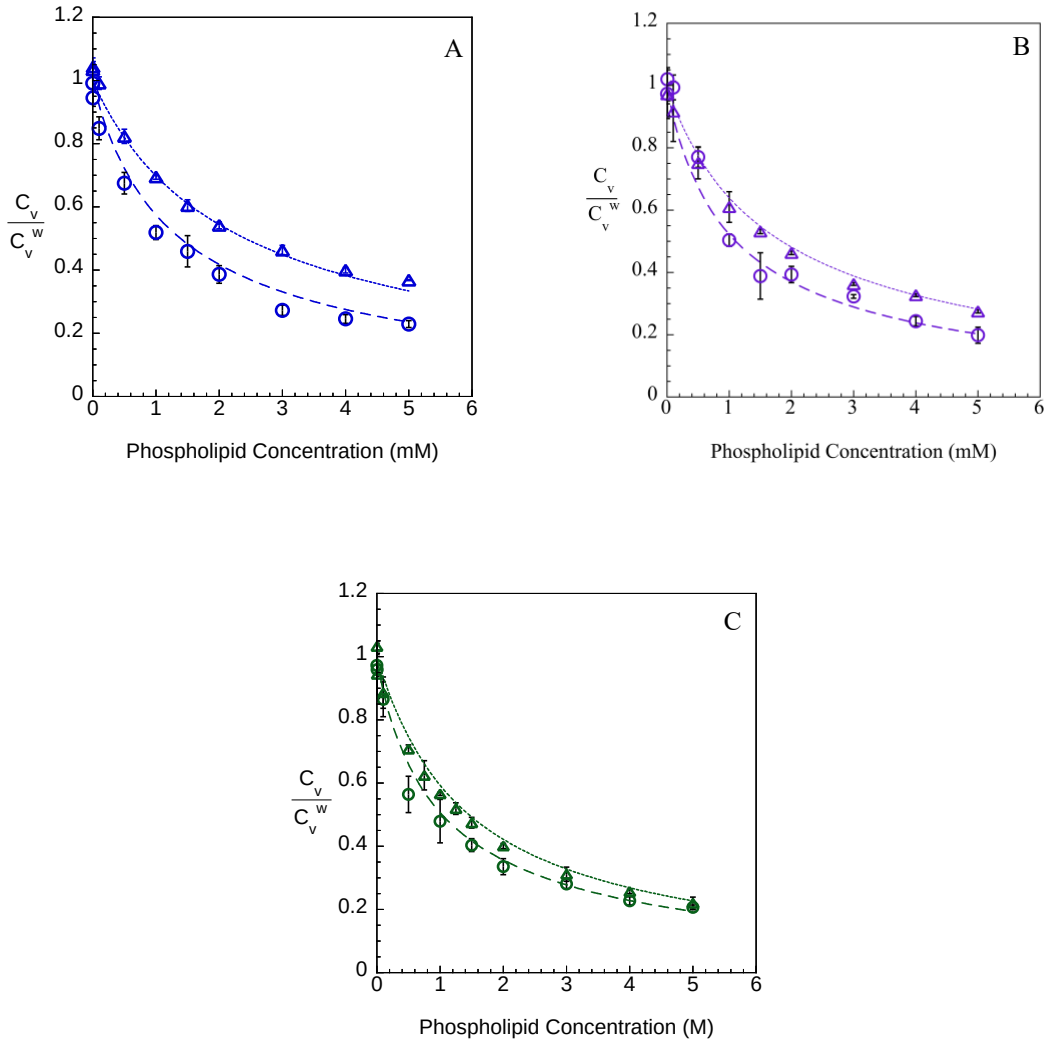

Figure 3.3: Vapor phase concentrations at fixed totals of 0.093 mM (△) and 0.618 mM (○) limonene, above dispersed vesicles of (A) Sunlipon™ 90 lecithin at 25ºC, (B) DMPC at 28ºC, and (C) Sunlipon™ 90 lecithin at 20ºC. Curved lines (⋯, - - -) represent nonlinear regression fits for K_{lipw} of 0.093 and 0.618 mM limonene respectively.

observed with DMPC vesicles at 28ºC (Figure 3.3B). Most notably, at lower concentrations of limonene (0.093 mM), obtained values for K_{lipw} were 42% lower at 25ºC in lecithin dispersions (Table 3.3) and 38% lower in DMPC dispersions at 28ºC (Table 3.4) than for experiments with

C_{tot} = 0.618 mM. For lecithin dispersions at 20ºC, there was no difference in partitioning between 0.093 and 0.618 mM (Figure 3.3C). However, as can be seen in Figure 3.4, the partition coefficients at 20ºC are not the same for all C_{tot} values: for example, with 0.297 and 0.803 mM limonene, the partition coefficients are higher than those with 0.093 mM.

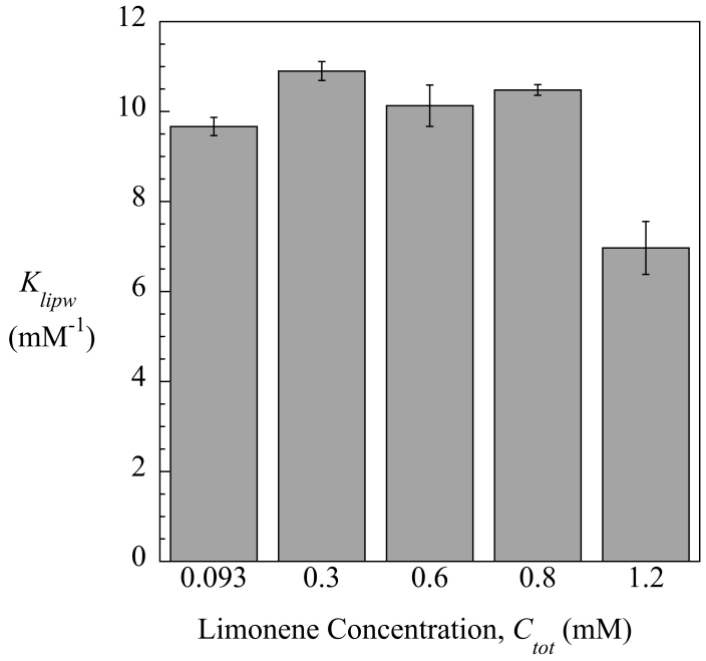

Figure 3.4: Variation in limonene K_{lipw} values with total limonene concentration in Sunlipon™ 90 lecithin vesicles at 20ºC.

A shift in partitioning behavior with total limonene was previously observed by Lloyd et al.[57] and Karman et al.[35] for limonene in micelle solutions. They observed larger K_{lipw} values for systems where lipid concentrations were fixed and limonene concentrations were high. Lloyd et al.[57] suggested that these observations may be due to structural changes in the micelles with the addition of high mole fractions of limonene, which could enhance partitioning. These variations in K_{lipw} with composition suggest that limonene solubilization by colloidal systems may be non-ideal and that there may be significant contributions from solute–solute interactions at higher concentrations.

Table 3.3: Partition Coefficients (K_{lipw}) of Varying Concentrations of Limonene in Sunlipon™ 90 Lecithin Dispersions

Size (nm)	<Size> (nm)[a]	T (°C)	C_{tot} (mM)*	K_{lipw} (mM^{-1})	R^2	<K_{lipw}> (mM^{-1})[b]	<$\widehat{K}_{lipw}$> ($\times 10^5$)[c]
225.6±2.6	230.3 ±4.6	25±0.1	0.093	7.393±0.851	0.9864	5.484 ±0.11	3.039 ±0.062
225.9±4.5				5.773±0.146	0.9290		
239.4±2.1				4.965±0.179	0.9632		
229.5±2.3	231 ±5.8	25±0.1	0.618	10.55±0.53	0.9834	10.66 ±0.43	5.905 ±0.326
221.9±2.4				10.29±0.86	0.9839		
241.7±6.1				12.01±1.24	0.9901		
202.4±3.0	205.8 ±2.7	20±0.1	0.093	8.303±0.591	0.9961	9.668 ±0.201	5.369 ±0.111
211.1±2.2				10.56±0.36	0.9948		
203.8±2.1				9.492±0.266	0.9968		
192.5±3.4	208 ±9.3	20±0.1	0.297	10.36±0.29	0.9965	10.90 ±0.21	6.038 ±0.122
224.6±3.6				12.00±0.53	0.9949		
206.8±1.1				11.41±0.45	0.9960		
234.0±1.7	231.7 ±2.6	20±0.1	0.618	11.34±0.76	0.9749	10.13 ±0.46	5.614 ±0.254
234.6±1.1				8.076±0.882	0.9688		
226.4±2.6				10.45±0.761	0.9745		
199.6±5.4	210.9 ±10.3	20±0.1	0.803	11.44±0.606	0.9874	10.48 ±0.12	5.808 ±0.066
201.6±1.8				10.34±0.13	0.9898		
231.4±2.9				11.81±0.45	0.9648		
178.9±9.0	207.9 ±15.3	20±0.1	1.24	7.393±0.783	0.9817	6.969 ±0.589	3.861 ±0.326
231.0±4.6				6.025±2.791	0.8918		
213.8±3.4				6.461±0.943	0.9429		

*C_{tot} = limonene concentration
[a]Errors are standard error of the mean
[b]Nonlinear regression weighted by $1/\sigma^2$, where σ represents the standard deviation of the replicates
[c]<$\widehat{K}_{lipw}$> values are of order 10^5

Table 3.3 also presents results for constant K_{lipw} values, fit to the 20˚C lecithin data shown in Figures 3.3C and Appendix 3. For vesicles at 20ºC, the K_{lipw} values range from 6.969 to 10.90 mM^{-1} as seen in Figure 3.4. For several higher mole fractions, K_{lipw} is above the maximum possible value, $1/C_w^{sat} = 9.6\ mM^{-1}$, where $x_{lim} = 1$ is the mole fraction of pure limonene. In practice, a mole fraction of one is inaccessible for limonene as a solute within a bilayer. Non-ideal interactions may instead increase K_{lipw} at high limonene concentrations and

could explain why we obtained $K_{lipw} \geq 9.6\ \mathrm{mM}^{-1}$ with assuming constant partition coefficients.

To further assess the variation in K_{lipw} values at different compositions, all of the lecithin vapor concentration data at 20ºC (presented in Figures 3.2, 3.3C, and in Appendix 3) were plotted together as a function of the overall limonene–to–phospholipid mole ratio, ρ (Figure 3.5). Note that here some vapor data was renormalized using equation 3.2 to convert

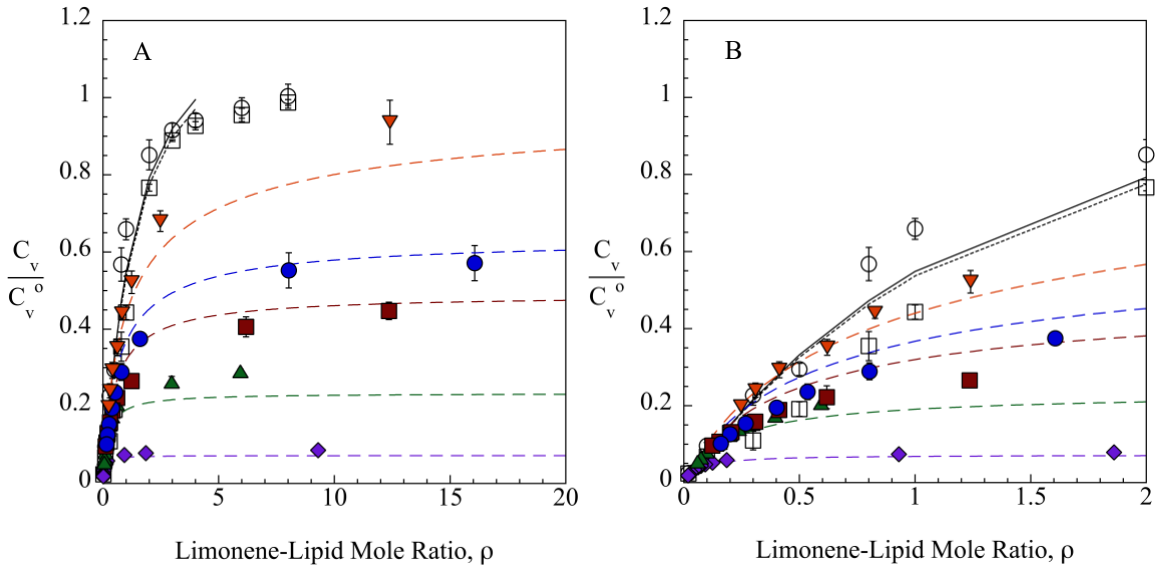

Figure 3.5: Equation 3.3 predictions, with $K_{lipw} = 7.993\ \mathrm{mM}^{-1}$, of vapor phase concentrations of limonene as a function of ρ above lecithin dispersions at 20˚C, for various fixed C_{tot} (----) or C_{PL} (—) values. Points represent experimental data for 3 mM (○) and 1 mM lecithin (□), with varying total limonene; and 0.093 mM (◆), 0.297 mM (▲), 0.618 mM (■), 0.803 mM (●), and 1.24 mM (▼) limonene, with varying lecithin. Range of mole ratios is (A) 0–20 or (B) 0–2.

$\tilde{C}_v$ to $\hat{C}_v$. Dashed lines are predictions from equation 3.3, all made using a partition coefficient of 7.993 mM^{-1}. This value was obtained from the 3 mM lecithin experiments shown in Figure 3.2 (open circles in Figure 3.5). The curves with this single value of K_{lipw} do a quite adequate job of predicting $\hat{C}_v$ over the entire ρ range, for different concentrations C_{tot}.

In general, $\hat{C}_v$ increased as ρ increased, approaching a maximum of one only when the concentration of limonene in water, C_w, was equivalent or greater than the solubility limit, C_w^{sat}. We can see from Figure 3.5 that samples with $C_{tot} = 1.2$ mM limonene produced aqueous solution concentrations very close to C_w^{sat}. A lower K_{lipw} value obtained for this concentration (Figure 3.4) may be a result of changed partitioning behavior at or near saturation. In addition, Figure 3.5 shows that there was much overlap in the range of ρ values applied in the experiments performed at 20ºC. Determinations of K_{lipw} were not achieved from samples that feature distinct ranges for x_{lim}, which would allow one to distinguish easily between dilute and semidilute bilayer partitioning behavior. This fact may obscure differences in partitioning due to the size of the mole fraction of limonene in the bilayer. In Figure 3.5A, the data most visible are for high limonene–lipid mole ratios where there should be little to no solubilization, hence the plateau in $\hat{C}_v$. In Figure 3.5B, we see that for the lower mole ratios, the predictions made using $K_{lipw} = 7.993$ mM^{-1} work better for 0.093 and 0.297 mM limonene, but give higher $\hat{C}_v$ values than the experimental data for 0.618 and 0.803 mM limonene.

The measured vapor phase concentrations presented in Figure 3.5 provide information on the limonene chemical potential, μ_{lim}^v, since for an ideal gas

$$\mu_{lim}^v = \mu_{lim}^{o,v} + kT \ln \frac{C_v}{C_v^o} \tag{3.9}$$

where $\mu_{lim}^{o,v}$ is the chemical potential of limonene vapor above pure limonene. Thus,

$$\ln \hat{C}_v = \frac{\mu_{lim}^v - \mu_{lim}^{o,v}}{kT} \tag{3.10}$$

determines the difference in chemical potential of the aroma compared to that above the pure liquid, due to effects of the vesicle dispersion. The chemical potential in the vapor is directly related to that of limonene dissolved in aqueous solution at concentration C_w, which in turn is set by the extent of partitioning into the vesicle bilayers. Therefore, by knowing the overall

composition ρ, either C_{tot} or C_{PL}, and the value K_{lipw}, equation 3.3 or 3.4 can be used to predict C_w, using

$$C_w = \hat{C}_v C_w^{sat} . \tag{3.11}$$

Measured values for $(\mu_{lim}^{v} - \mu_{\text{lim}}^{o,v})/kT$ from equation 3.10 are plotted versus predictions for C_w from $\hat{C}_v$ calculated from equation 3.3 or 3.4, using $K_{lipw} = 7.993$ mM^{-1}. Data for different mixture compositions and various experimental replicate sets collapse in this figure to a single curve, representing the relationship between chemical potential (measured) and C_w (predicted using a single K_{lipw}). As vesicles were able to solubilize more limonene, the solute chemical potential decreased, lowering the limonene activity. In the other limit, as μ_{lim} approached μ_{lim}^{o}, the vesicles' capacity for limonene was reached and additional limonene must phase separate.

Assuming ideal mixing, the chemical potential of limonene in the water, μ_{lim}^{w}, is defined in equation 1.4. To a very good approximation, x_{lim}^{w} can be expressed as the product of the molar concentration of limonene in water, C_w, and the molar volume of water, $\bar{v}_w$. Equation 1.4 can thus be rewritten as

$$\frac{\mu_{lim}^{w} - \mu_{lim}^{\ominus,w}}{kT} = \ln C_w + \ln \bar{v}_w . \tag{3.12}$$

Since pure limonene references were being used for $\hat{C}_v$ measurements, equation 3.12 is modified with addition of the term $(\mu_{lim}^{\ominus,w} - \mu_{lim}^{o})/kT$, where μ_{lim}^{o} is the chemical potential of pure limonene, resulting in

$$\frac{\mu_{lim}^{w} - \mu_{lim}^{o}}{kT} = \frac{\mu_{lim}^{\ominus,w} - \mu_{lim}^{o}}{kT} + ln C_w + ln \bar{v}_w . \tag{3.13}$$

Here, using equation 3.10, $(\mu_{lim}^{w} - \mu_{lim}^{o})/kT$ is also equivalent to $\ln \hat{C}_v$, and $(\mu_{lim}^{\ominus,w} - \mu_{lim}^{o})/kT$ represents the transfer of one molecule of limonene from pure solute into water. An estimate for $(\mu_{lim}^{\ominus,w} - \mu_{lim}^{o})/kT$ of 13.08 was calculated using the most dilute experimental point and

equation 3.13. This value is very close to the value of 13.31 obtained by Karman et al.[35] The data in Figure 3.6 nearly collapse along a single curve, showing again the substantial effectiveness of the ideal–dilute theory. A plot of $\ln \hat{C}_v$ vs $\ln C_w$ should be linear for an ideal mixture. In Figure 3.7, the same data from Figure 3.6 is given on a semi-log plot, with data collapsing to a straight line with slope close to unity, consistent with expectations.

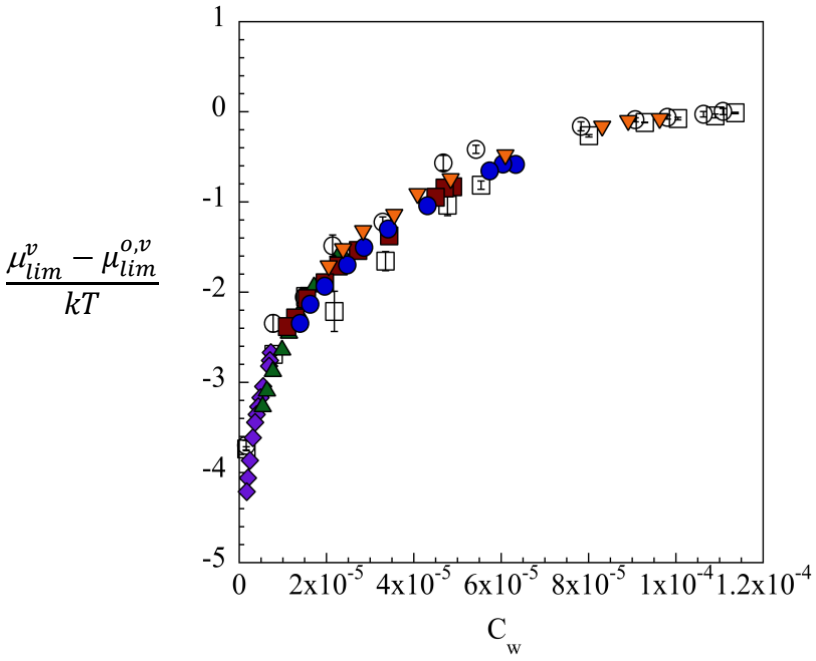

Figure 3.6: Chemical potentials of varying mole fractions of limonene in water with predictions for C_w made using equations 3.4 and 3.11, with $K_{lipw} = 7.993\ \text{mM}^{-1}$. Experimental points are for total limonene concentrations of 0.093 mM (◆), 0.297 mM (▲), 0.618 mM (■), 0.803 mM (●), and 1.24 mM (▼) in 0.01–5 mM lecithin dispersions, as well as fixed 3 mM (○) and 1 mM (□) lecithin concentrations with 0.2–0.8 mole ratios of limonene–to–lipid. Experiments were carried out at 20ºC.

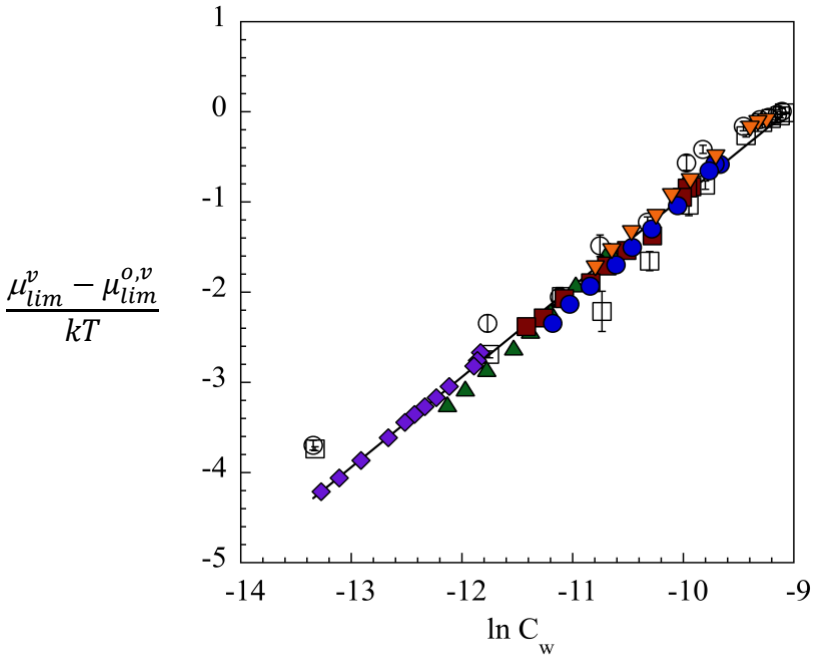

Figure 3.7: Chemical potentials of varying mole fractions of limonene with predictions for ln C_w. Experimental points are for total limonene concentrations of 0.093 mM (◆), 0.297 mM (▲), 0.618 mM (■), 0.803 mM (●), and 1.24 mM (▼) in 0.01–5 mM lecithin dispersions, as well as fixed 3 mM (○) and 1 mM (□) lecithin concentrations with 0.2–0.8 mole ratios of limonene–to–lipid. Experiments were carried out at 20ºC.

3.3.3 Chemical potential of limonene during mixing

We can examine the effect of limonene concentration on overall partitioning behavior by evaluating changes in the chemical potential using regular solution theory applied to the binary mixture in the bilayer. Here, we treat limonene as a solute in a phospholipid "solvent", so that the chemical potential μ_{lim}^{PL} of limonene is predicted to be

$$\mu_{lim}^{PL} = \mu_{lim}^{o} + kT \ln x_{lim} + kT\chi_{PL,L}(1 - x_{lim})^2 \,. \qquad (3.14)$$

Here, μ_{lim}^{o} is the chemical potential of pure limonene, x_{lim} is the mole fraction of limonene in a bath of phospholipid molecules and $\chi_{PL,L}$ represents the interaction parameter for phospholipid (PL) and limonene (L), so that the last term in equation 3.14 captures non-ideal behavior. By definition, $\chi_{PL,L} = z[V_{PL,L} - 1/2(V_{PL,PL} + V_{L,L})]/kT$, where z is the number of nearest neighbors, and $V_{i,j}$ is the energy of the interaction between i and j molecules. The interaction parameter compares the interactions between similar and dissimilar interactions.

Using the infinite dilution solute convention in the form described by Dill and Bromberg,[69] we obtain a new reference chemical potential:

$$\mu_{lim}^{\circ,PL} = \mu_{lim}^{o} + kT\chi_{PL,L}\,, \tag{3.15}$$

which represents the energy required to transfer one limonene molecule into pure phospholipid: i.e., the chemical potential of the solute in an infinitely dilute solution. Combined with equation 3.14, equation 3.15 becomes

$$\mu_{lim}^{PL} = \mu_{lim}^{\circ,PL} + kT\ln x_{lim} + kT\chi_{PL,L}x_{lim}(x_{lim} - 2)\,. \tag{3.16}$$

When $x_{lim} \ll 1$ or if $\left|\chi_{PL,L}\right| \ll 1$, the last term in equation 3.16 is negligible, and the chemical potential becomes the ideal–dilute result:

$$\mu_{lim}^{PL} = \mu_{lim}^{\circ,PL} + kT\ln x_{lim}\,. \tag{3.17}$$

Using the regular solution theory outlined in equation 3.16, we can examine non-ideal interactions and their connection to variations in K_{lipw}. Consider first ideal behavior in the bilayer, where the last term in equation 3.16 is negligible. As the chemical potential of the solute in lipid is equivalent to its chemical potential in water, $\mu_{lim}^{PL} = \mu_{lim}^{w}$, where $w =$ water and μ_{lim}^{w} is represented with the ideal–dilute equation

$$\mu_{lim}^{w} = \mu_{lim}^{\circ,w} + kT\ln x_{lim}^{w}\,. \tag{3.18}$$

We equate equations 3.17 and 3.18 and from this relationship, the difference in chemical potential to transfer the solute from water to the lipid phase at infinite dilution is represented by

$$\frac{\mu_{lim}^{\circ,w} - \mu_{lim}^{\circ,PL}}{kT} = \ln\left(\frac{K_{lipw}^{o}}{\bar{v}_w}\right) = \ln\left(\frac{x_{lim}}{x_{lim}^{w}}\right)\,. \tag{3.19}$$

Here, K_{lipw}^{o} is the lipid–water partition coefficient at this ideal dilute limit; K_{lipw}^{o} does not vary with composition. Figure 3.8 is a cartoon showing the chemical potentials associated with the lipid and water phases.

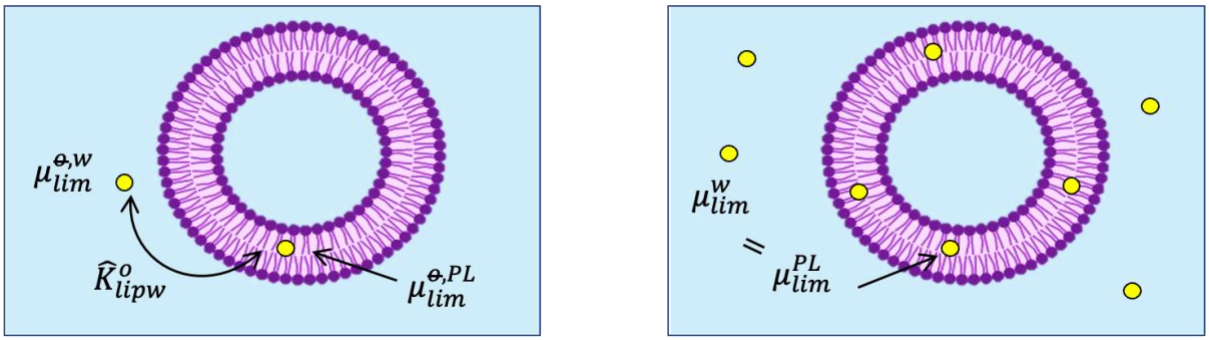

Fig 3.8: Chemical potentials, reference chemical potentials, and the ideal–dilute partition coefficient $\hat{K}_{lipw}^{o}$ for limonene in the water and lipid phases.

Next, non-ideal contributions for the lipid phase can be incorporated. By equating the chemical potential of limonene in water to μ_{lim}^{PL} in equation 3.16, we obtain

$$\mu_{lim}^{\ominus,w} + kT \ln C_w + kT \ln \bar{v}_w = \mu_{lim}^{\ominus,PL} + kT \ln x_{lim} + kT\chi_{PL,L}x_{lim}(x_{lim} - 2)\,. \tag{3.20}$$

To evaluate experiments with fixed limonene concentrations, we rearrange equation 3.20 to solve for C_w, then divide by $C_w^w = C_v^w/K_{vw}$ from the limonene in water reference (equation 2.7), resulting in

$$\frac{C_w}{C_w^w} = \tilde{C}_v = \frac{x_{lim}\hat{V}}{K_{lipw}^{o} C_{tot}} \exp\left[\chi_{PL,L}x_{lim}(x_{lim} - 2)\right], \tag{3.21}$$

with

$$C_w^w = \frac{C_{tot}}{\hat{V}}\,. \tag{3.22}$$

In equation 3.21, the reference chemical potentials in equation 3.20 are reexpressed using K_{lipw}^{o} from equation 3.19. For experiments with fixed phospholipid concentrations and much higher limonene concentrations, we divide equation C_w in 3.20 instead by C_w^{sat}, resulting in

$$\frac{C_w}{C_w^{sat}} = \hat{C}_v = \frac{x_{lim}}{K_{lipw}^{o} C_w^{sat}} \exp\left[\chi_{PL,L}x_{lim}(x_{lim} - 2)\right]. \tag{3.23}$$

Measurements of $\tilde{C}_v$ are preferred to $\hat{C}_v$ when possible, due to the dependence of equation 3.23 on C_w^{sat}. C_w^{sat} can vary with temperature, and to capture this dependence

experimental solubility values are needed, which are difficult to obtain accurately. Therefore, calculations made without C_w^{sat} may be more accurate.

For lecithin at 20ºC, we used the partition coefficient measured for 3 mM lecithin, 7.993± mM^{-1} (Table 3.2), as our estimate for K_{lipw}^{o} since it captures a wide range of x_{lim} values, starting from $x_{lim} = 0.009$. Limonene vapor phase concentrations were then predicted for the entire range of x_{lim} with equations 3.21 and 3.22. To compare these predictions to the experimental data, corresponding ρ values are calculated from x_{lim} and n_{lim}. With $n_{PL} = n_{lim}(1 - x_{lim})/(x_{lim})$, the total mole ratio ρ can be rewritten as

$$\rho = \frac{C_{tot}V_w}{n_{PL}} = \frac{C_{tot}V_w x_{lim}}{n_{lim}(1 - x_{lim})} \ . \tag{3.24}$$

Here, the moles of limonene $n_{lim} = V_w(C_{tot} - C_w\hat{V})$, found by substituting $C_v = C_w K_{vw}$ into equation 3.8 and with C_w found by multiplying equation 3.21 by 3.22. The experimental results and predictions are shown in Figure 3.9 for 0.093 and 0.618 mM limonene. A fixed K_{lipw}^{o} of 7.993 mM^{-1} and $\chi_{PL,L} = 1$ quantitatively captures the partitioning behavior for both data sets. This good agreement suggests that at 0.093 mM limonene, we may already be seeing non–ideal behavior for limonene in the bilayer at higher mole fractions.

At higher temperatures, there is a larger difference between the partition coefficients at low and high concentrations. At 25ºC, K_{lipw} values for 0.093 and 0.618 mM limonene in lecithin dispersions were evaluated as 5.484±0.11 and 10.66±0.43 mM^{-1}, respectively, from fits done with equation 2.9 (Figure 3.3C and Table 3.3). Here, the K_{lipw} value for 0.093 mM limonene, 5.484 mM^{-1}, was used as our estimate of K_{lipw}^{o}, for $\rho < 9.3$. Predictions for $\tilde{C}_v$ were made using equation 3.21 and a $\chi_{PL,L}$ value of 1.1 for limonene in lecithin dispersions at 25ºC. The comparison between theory and data is shown in Figure 3.10, and indicates that these parameters work quite well in capturing the data.

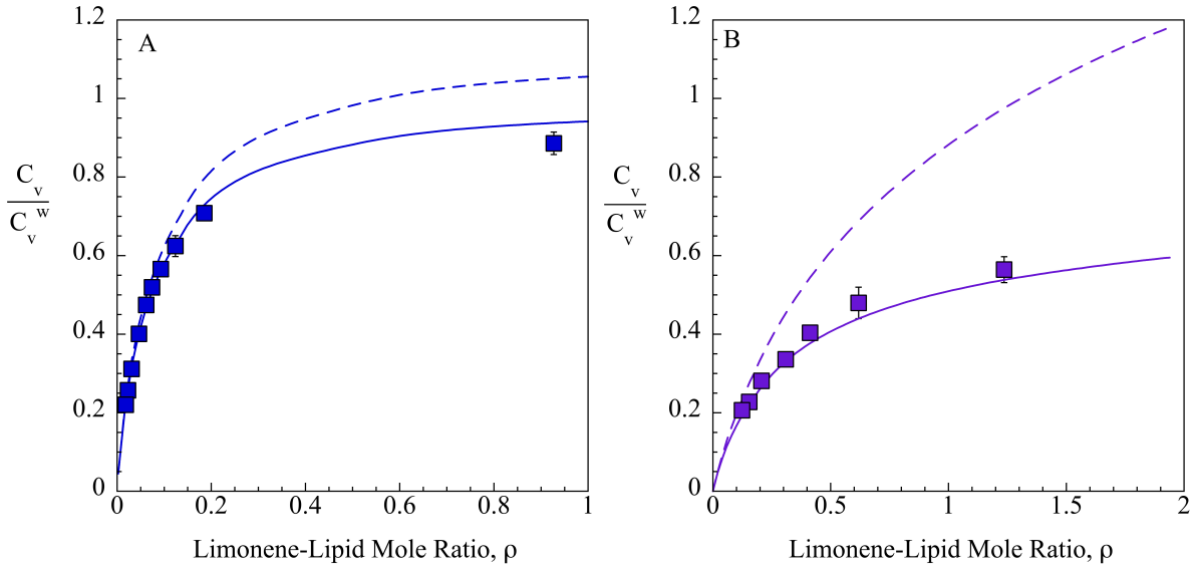

Figure 3.9: Predictions for the vapor phase concentration, $\tilde{C}_v$, using regular solution theory with $\chi_{PL,L} = 0$ (---) and $\chi_{PL,L} = 1$ (—) for (A) 0.093 mM and (B) 0.618 mM limonene in lecithin dispersions at 20ºC. Experimental points (■, ■) represent vesicles with average sizes of 200 nm.

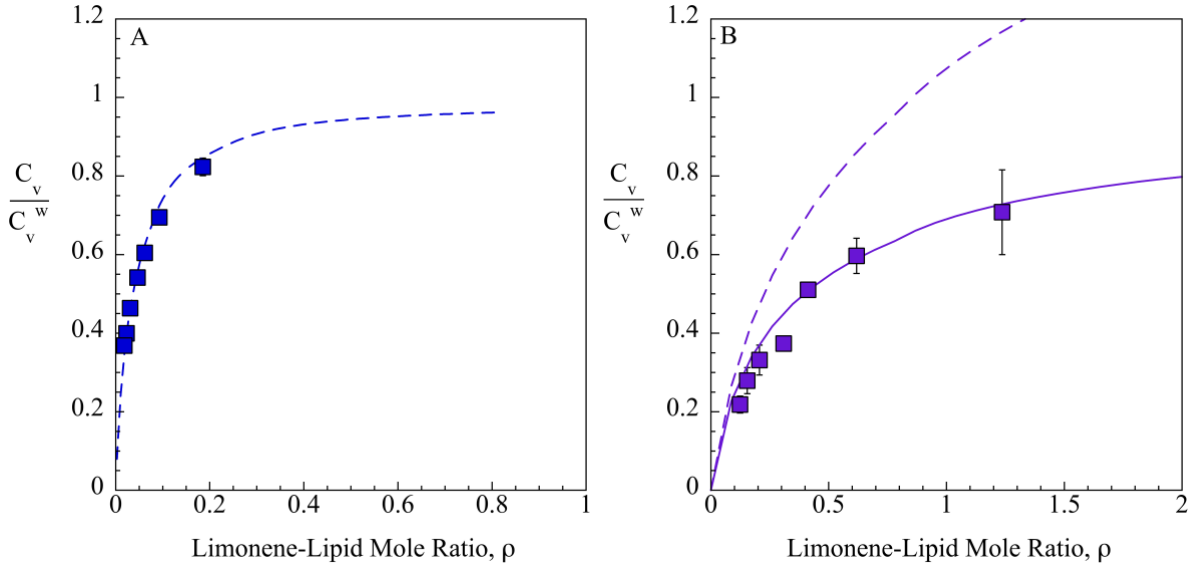

Figure 3.10: Predictions for the vapor phase concentration, $\tilde{C}_v$, using regular solution theory with $\chi_{PL,L} = 0$ (---) and $\chi_{PL,L} = 1.1$ (—) for (A) 0.093 mM and (B) 0.618 mM limonene in lecithin dispersions at 25ºC. Experimental points (■, ■) represent vesicles with average sizes of 200 nm.

For DMPC at 28ºC, we observed similar behavior. The partition coefficient obtained from fits of equation 2.9 to data for 0.093 mM limonene and $\rho < 9.3$ is $K_{lipw}^{o} = 8.396 \pm$

0.574 mM^{-1} at this temperature. This value is lower than $K_{lipw} = 13.187 \pm 0.913$ mM^{-1}, obtained by fitting data at 0.618 M limonene (Table 3.4). Using 8.396 mM^{-1} as K^{o}_{lipw}, a $\chi_{PL,L}$ value of 1 predicts the 0.618 mM data well (Figure 3.11). These positive values for $\chi_{PL,L}$ suggest that limonene may deviate from ideal behavior at higher concentrations. In Figures 3.9–3.11, curves for $\chi_{PL,L} = 0$ is shown for lecithin and DMPC. They show reasonably good agreement with the data at $\rho < 0.1$ for lecithin at 20ºC and 25ºC and DMPC at 28ºC. The enthalpic interactions captured by $\chi_{PL,L}$ would explain the higher and more variable partition coefficients observed from fitting experiments directly with equation 2.9. However, there could be other factors affecting partitioning into lipid bilayers that are not covered by regular solution theory. For example, the change in partitioning with limonene concentration is greater at 25ºC for lecithin than at 20ºC. This may be due to structural effects of the bilayer membrane itself, such as aggregation at low temperatures.

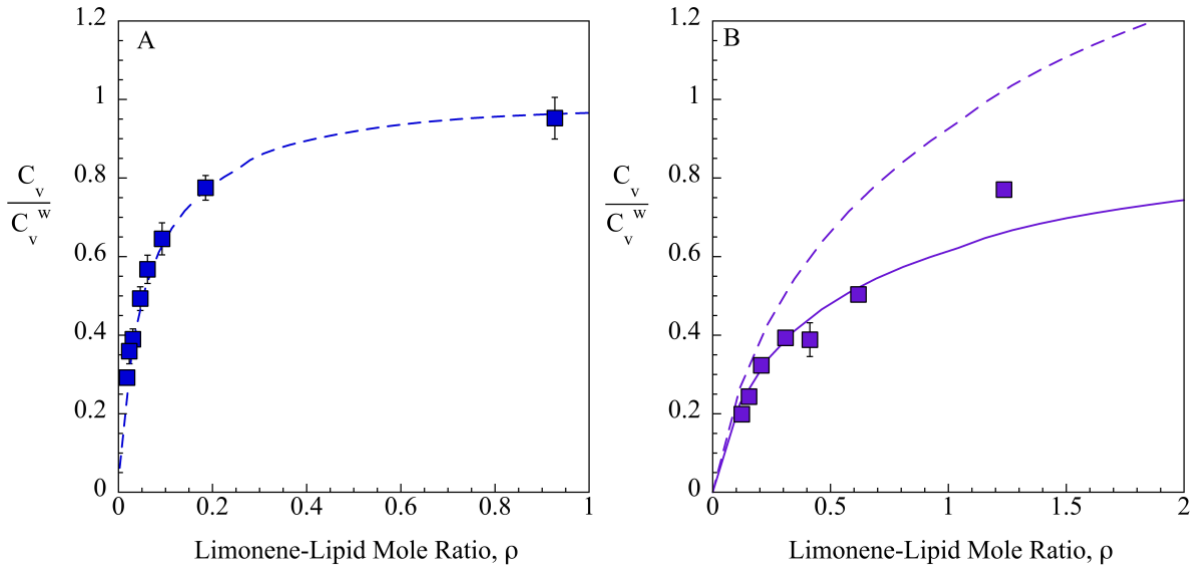

Figure 3.11 Predictions for the vapor phase concentration, $\tilde{C}_v$, using regular solution theory with $\chi_{PL,L} = 0$ (---) and $\chi_{PL,L} = 1$ (—) for (A) 0.093 mM and (B) 0.618 mM limonene in DMPC dispersions at 28ºC. Experimental points (■, ■) represent vesicles with average sizes of 200 nm.

Table 3.4: Partition Coefficients (K_{lipw}) of Limonene in DMPC Vesicles

Size (nm)	<Size> (nm)[a]	T (°C)	C_{tot} (mM)*	K_{lipw} (mM^{-1})	R^2	$<K_{lipw}>$ (mM^{-1})[b]	$<\widehat{K}_{lipw}>$ ($\times 10^5$)[c]
221.2±1.0	220.3±13.5	28	0.093	9.956±0.959	0.9926	8.396 ±0.574	4.653 ±0.318
196.5±0.9				11.17±2.132	0.9578		
243.1±3.2				7.063±0.76	0.9873		
207.7±3.6	200.6±5.7	28	0.618	12.68±2.95	0.9588	13.19 ±0.913	7.308 ±0.506
189.4±3.2				13.92±1.13	0.9868		
204.8±4.4				11.41±1.85	0.9735		

*C_{tot} = limonene concentration
[a]Errors are standard error of the mean
[b]Nonlinear regression weighted by $1/\sigma^2$, where σ represents the standard deviation of the replicates
[c]$<\widehat{K}_{lipw}>$ values are of order 10^5

3.3.4 Effects of DMSO on Vapor Water Partition Coefficient

To achieve low concentrations of limonene in some of our experiments, a solution of limonene in DMSO is added to water, rather than pure limonene. This procedure is used because we cannot accurately retain nanoliter volumes of pure limonene due to its high volatility. Experiments performed by Lloyd et al.[32] and Karman et al.[35] to determine the vapor–water partition coefficient of limonene, K_{vw}, were also performed at low limonene concentrations in water using DMSO as a carrier solvent. They found that at these low concentrations, up to 0.02 mM, the effect of DMSO is negligible. We used a combination of pure limonene and limonene in DMSO to achieve the wide range of mole ratios for experiments with fixed phospholipid concentrations. To ensure that there are no differences in the vapor phase partitioning of limonene at higher concentrations of up to 0.3 mM limonene, phase volume ratio experiments were performed following the method by Lloyd et al.[32] outlined below. Peak areas of the solute above two separate sets of vials with different water volumes were analyzed with linear regression from plots of peak area versus moles of limonene added. K_{vw} was then determined from the ratio of the slopes.

The HS–SPME peak area above limonene alone in water, $A_w = k_p C_v^w$, introduced in equation 2.7, can be reexpressed in terms of the liquid fill fraction in the vial $f = V_w/V_t$, where $V_t = V_w + V_v$ is the total volume of the vials. Equation 2.7 can thus be expressed as

$$A_w = \frac{n_{tot}\, k_p\, K_{vw}}{V_t(K_{vw}(1-f)+f)}. \tag{3.25}$$

For a series of samples where n_{tot} is varied, the slope, S, of A_w versus n_{tot} is given by

$$S = \frac{k_p K_{vw}}{V_t(K_{vw}(1-f)+f)}. \tag{3.26}$$

If there are two separate fill fractions, with the same total volumes of limonene, the ratio of slopes, S_1/S_2, is

$$\frac{S_1}{S_2} = \frac{K_{vw}\,(1-f_2)+f_2}{K_{vw}(1-f_1)+f_1}. \tag{3.27}$$

The above equation can then be rearranged to give an expression for K_{vw}:

$$K_{vw} = \frac{\mathcal{R}f_1 - f_2}{(1-f_2)-\mathcal{R}(1-f_1)}, \tag{3.28}$$

where $\mathcal{R} = S_1/S_2$.

Figure 3.12 shows measurements made at 25ºC with fill fractions of 0.0952 and 0.809. Samples were prepared by addition of pure limonene or by adding limonene in a DMSO solution. The total amounts of limonene added ranged from 200 to 1800 nanomoles. DMSO concentrations were fixed at 0.45% v/v and 0.05% v/v (volume DMSO/volume water) for low and high fill fractions respectively. For both preparations, the peak areas of limonene were proportional to the total moles of limonene added. Each data set was fit with a linear regression using a zero-intercept. The slopes and their corresponding R^2 values are presented in Table 3.5. The average slope ratio, $\mathcal{R}$, is found using the weighted average of the replicates as described in Section 2.3.2. The weights, $w = 1/\sigma_{\mathcal{R}}^2$, were calculated with the propagated error for $\mathcal{R}$, $\sigma_{\mathcal{R}}^2$,

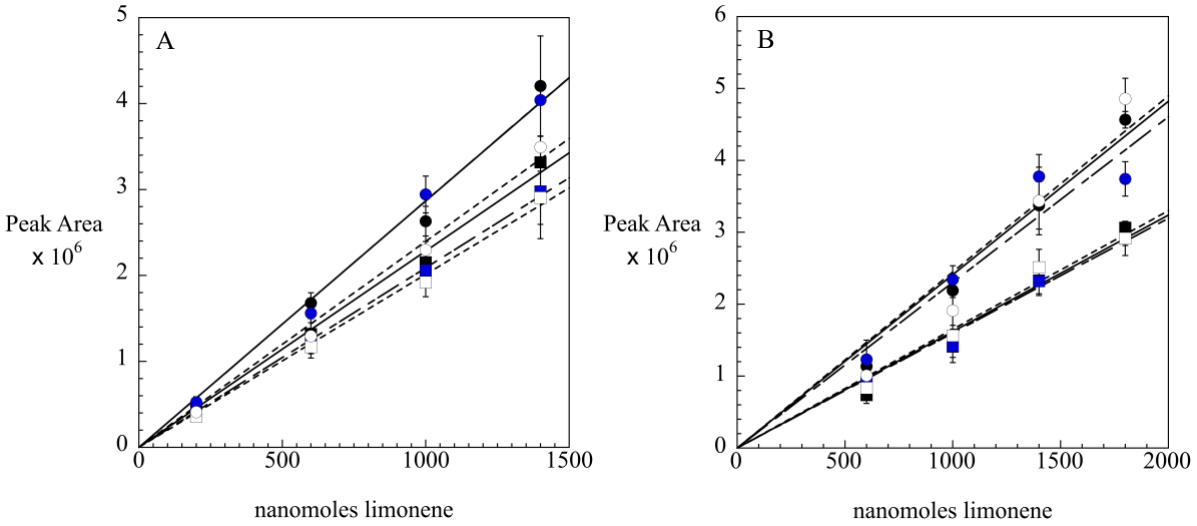

Figure 3.12: Peak areas of limonene above water for fill fractions of 0.0952 (○) and 0.809 (□) using A) limonene in DMPC solution and B) pure limonene. Different colors represent replicates.

as shown below:

$$\sigma_{\mathcal{R}}^2 = \pm\mathcal{R}\sqrt{\left(\frac{\sigma_{S_1}}{S_1}\right)^2 + \left(\frac{\sigma_{S_2}}{S_2}\right)^2}\,. \tag{3.29}$$

Here, σ_{S_1} and σ_{S_2} represent the standard error of the slopes S_1 and S_2 found with linear regression. The relative error, $\in = \pm\sigma_{\mathcal{R}}/\mathcal{R}$, is used to calculate the error in the slope ratio as $\mathcal{R}_{err} = \mathcal{R}(1+\in)$. The relative error in the partition coefficient, $\sigma_{K_{vw}} = (K_{vw,err} - K_{vw})/K_{vw}$ was then calculated using $K_{vw,err}$ as

$$K_{vw,err} = \frac{\mathcal{R}(1+\in)f_1 - f_2}{(1-f_2) - \mathcal{R}(1+\in)(1-f_1)}\,. \tag{3.30}$$

There was a bigger difference between the slopes for pure limonene than for the limonene/DMSO mixture, leading to slightly lower $\mathcal{R}$ values. As shown in Table 3.5, the K_{vw} value calculated for pure limonene is 1.563 ± 0.119, which is not statistically different from the 1.400 ± 0.085 calculated for the limonene/DMSO solution. A significantly lower K_{vw} with added DMSO could indicate a greater solubility of limonene in water with the DMSO solvent. The combination of both pure limonene and limonene/DMSO solutions for experiments should therefore have no significant impact on the analysis and interpretation of the data.

Table 3.5: Vapor–Water Partition Coefficients (K_{vw}) of Limonene

	Slope 1 ($nmol^{-1}$)	Slope 1 R^2	Slope 2 ($nmol^{-1}$)	Slope 2 R^2	R	<R>*	K_{vw}
Pure Limonene	1620.1 ±342.2	0.9708	2410.7 ±428.7	0.9912	0.719 ±0.095		
	1615.3 ±96.3	0.9922	2167.2 ±321.1	0.9536	0.745 ±0.119	0.734 ±0.065	1.563 ±0.119
	1649.9 ±101.9	0.9916	2448.9 ±377.1	0.9391	0.748 ±0.136		
Limonene in DMSO	2011.6 ±106.5	0.9729	2559.6 ±287.0	0.9938	0.786 ±0.097		
	2283.9 ±124.8	0.9981	2865 ±199.5	0.9965	0.797 ±0.071	0.790 ±0.050	1.400 ±0.085
	2089.7 ±156.9	0.9877	2674.1 ±276.9	0.9768	0.781 ±0.100		

* Weighted slope ratio using propagated error

3.3.5 Changes in Solubility Limit with Temperature

The solubility limit of limonene, C_w^{sat}, is dependent on temperature.[35,78] Our analysis using regular solution theory is sensitive to the solubility limit when the pure reference is used. As shown in Section 3.2, the water reference can be only sometimes used to avoid such issues. There is limited published data available on the change in the solubility limit of limonene with temperature.[35,78] In this section we use HS–SPME data for pure limonene and limonene in water to determine how much C_w^{sat} changes with temperature.

Rearranging the mole balance for limonene in water, equation 2.9 results in an expression for the proportionality constant, k_p:

$$k_p = \frac{A_w(V_w + V_v K_{vw})}{n_{tot} K_{vw}} \tag{3.31}$$

Equation 3.31 can be used with measured peak areas to estimate k_p at specific temperatures. Then, using Equation 3.1, C_w^{sat} can be determined using the peak area above pure limonene

samples at the same temperature, taken on the same day. Table 3.6 compiles values for C_w^{sat} measured using limonene at a variety of temperatures, using HS–SPME triplicates, with this data presented in Figure 3.13.

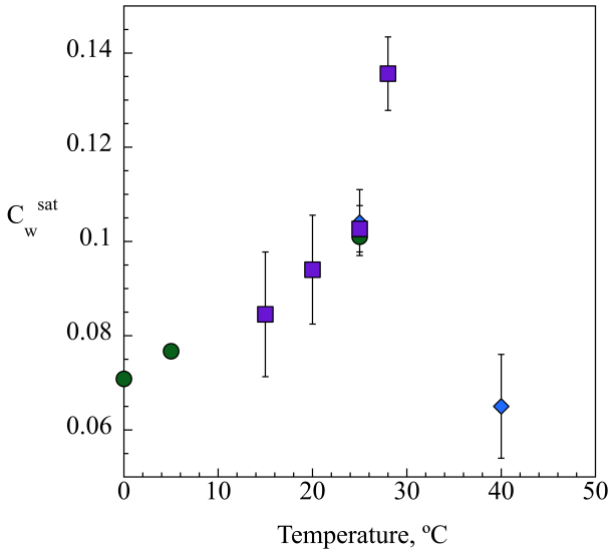

Figure 3.13: Changes in the solubility limit of limonene, C_w^{sat}, with temperature. Experimental data from this work (■), Massaldi and King[78] (●), and Karman et al[85] (◆).

At 25ºC, the value of C_w^{sat} obtained was 0.103 ± 0.005 mM. Although this method uses a single compositional point value for the proportionality constant k_p, instead of a more accurate slope estimate, the calculated C_w^{sat} is in excellent agreement with values obtained through more robust and extensive solubility limit experiments.[35,78] The measured solubility value at this temperature from Karman et al.[35] is 0.104±0.007 mM and is 0.101 mM from Massaldi and King.[78] In both the works of Massaldi and King[78] and Karman et al.,[35] increasing concentrations of limonene were added to water in vials and the peak area recorded with GC to find the threshold concentration for saturation. Massaldi and King[78] used a syringe to perform headspace analysis along with a flame ionization detector and calculated C_w^{sat} from limonene's saturated vapor pressure. Karman et al.[35] used a SPME fiber and GC/MS, along with K_{vw} values. Figure 3.13 shows a clear increase in the solubility of limonene for higher temperatures. Combining all the data between 0 and 25ºC, we find a linear increase in C_w^{sat} of

1.25×10^{-3} mM/ºC. These significant changes in solubility with temperature indicate that it is therefore essential to have accurate C_w^{sat} values in order to analyze measurements not done at 25ºC.

Table 3.6: Solubility Limit of Limonene at Various Temperatures Obtained From Reference Vial Measurements

T(ºC)	Individual Triplicate Measurements[c]	Average C_w^{sat} (mM)	Literature values (mM)
0			0.071[a]
5			0.077[a]
15	0.098 (4.9); 0.071 (4.3)	0.084 ± 0.013	
20	0.083, 0.105 (3.3C); 0.077, 0.104 (A3.1A); 0.089 (A3.1B)	0.094 ± 0.011	
25	0.098 (3.3A); 0.108 (2.4B)	0.103 ± 0.005	0.101[a] 0.104±0.007[b]
28	0.136	0.136± 0.008	
40			0.065±0.011[b]

[a]Massaldi and King, 1973
[b]Karman et al.[59]
[c]from data presented in figure number in parenthesis, each value calculated with different C_{tot}

3.4 Conclusion

Ideal and regular solution theory has been applied to analyze the partitioning behavior of limonene in phospholipid vesicles. When K_{lipw} was assumed to be a constant, independent of composition, a value of $K_{lipw} = 8$ mM^{-1} captured data reasonably well for lecithin at 20ºC, across a wide range of total limonene and lecithin concentrations. However, there was an observable variation in K_{lipw} among experiments that use different total limonene concentrations. In particular, we see higher K_{lipw} values for higher C_{tot}. At 20ºC, we could predict the vapor phase concentration of limonene for different values of C_{tot} using a constant value of $K_{lipw} = K_{lipw}^{o}$ and ideal mixing theory. However, application of an interaction parameter, $\chi_{PL,L}$, predicts the data more closely. For lecithin at 25ºC and DMPC at 25ºC, predictions made using an interaction parameter also match the data more closely than

predictions made using ideal mixing alone. Therefore, it is possible that there are non-ideal interactions that enhance partitioning for higher mole fractions of limonene in the bilayer. We have also shown that the vapor–water partition coefficient is not affected by the addition of the solute DMSO at concentrations of below 0.45% v/v in water. Finally, the solubility of limonene in water is affected by temperature. This affects some calculations that are sensitive to C_w^{sat}. We have used HS–SPME data to estimate these values and show that they increase with temperature.

3.5 Nomenclature

A	detected peak area of limonene above vesicle dispersion
A^o	detected peak area of limonene above pure reference
A_w	detected peak area of limonene above water
b	$\frac{\hat{C}_{tot}}{\hat{V}}(1+\rho)+\frac{1}{\hat{K}}$
C_{PL}	concentration of phospholipid in water
C_{tot}	total concentration of limonene in sample
C_v^o	vapor phase concentration of limonene above pure reference
C_v^w	vapor phase concentration of limonene in water reference
C_v	concentration of limonene in the vapor phase
C_w^{sat}	solubility limit of limonene in water
C_w^w	concentration of limonene in the water in samples without phospholipid
C_w	concentration of limonene in the water
$\hat{C}_{PL}$	$\frac{C_{PL}}{C_w^{sat}}$
$\tilde{C}_v$	$\frac{C_v}{C_v^w}$

$\hat{C}_v$	$\frac{C_v}{C_v^o}$
f	fill fraction, V_w/V_t
k	Boltzmann's constant
K_{lipw}^o	lipid water partition coefficient at the ideal dilute limit
K_{lipw}	lipid–water partition coefficient
k_p	proportionality constant of limonene in GC column
$K_{vw,err}$	propagated error in the partition coefficient
K_{vw}	vapor–water partition coefficient
$\widehat{K}$	$K_{lipw}C_w^{sat}$
n_{lim}	moles of limonene in the bilayer
n_{PL}	Moles of phospholipid
n_{tot}	total moles of limonene in the system
$\mathcal{R}$	slope ratio, S_1/S_2
$\mathcal{R}_{err}$	error of slope ratio
S	slope of $A\ vs\ n$ plots
$V_{i,j}$	energy of the interaction between i and j molecules
V_t	total volume of vials
V_v	vapor volume
V_w	water volume
$\widehat{V}$	$\frac{K_{vw}V_v}{V_w} + 1$
w	weights used to calculate averages
x_{lim}^{sat}	maximum mole fraction of limonene in lipid bilayer
x_{lim}^{w}	mole fraction of limonene in the water

x_{lim}	mole fraction of limonene in lipid bilayer
z	number of nearest neighbors
$\in$	relative error of slope ratio
$\mu_{lim}^{\theta,PL}$	ideal–dilute chemical potential of solute in phospholipid
$\mu_{lim}^{o,v}$	chemical potential of limonene vapor above pure limonene
μ_{lim}^{o}	chemical potential of pure solute
μ_{lim}^{PL}	chemical potential of limonene in phospholipid
μ_{lim}^{v}	chemical potential of limonene in the vapor phase
$\mu_{lim}^{\theta,w}$	ideal–dilute chemical potential of limonene in water
μ_{lim}^{w}	chemical potential of limonene in the water
ν	$\frac{K_{vw}V_v + V_w}{V_w K_{lipw} C_{tot}}$
$\bar{v}_w$	molar volume of water
ρ	limonene–lipid mole ratio
ρ^{sat}	maximum mole ratios for limonene solubilization
χ	interaction parameter between solute and solvent
$\chi_{PL,L}$	interaction parameter between limonene and phospholipid
$\sigma_{K_{vw}}$	relative error in the partition coefficient
$\sigma_{\mathcal{R}}^2$	propagated error of slope ratio
σ_S	standard error of the slope

Chapter 4

Partitioning of Limonene into Fluid and Gel Phases of DMPC Vesicles

4.1 Introduction

Vesicle bilayers are typically in a fluid or liquid crystal phase with fatty acid tails that have liquidlike character. When sufficiently cooled, vesicles made using phospholipids with saturated fatty acid tails with their high melting points feature a gel phase where the fatty acid tails are crystallized.[37] The fatty acid tails pack closely, and the stiffness of the bilayer increases.[79] The temperature below which the gel phase appears is referred to as the phase transition temperature, T_G. The phase of vesicles has an impact on the partitioning properties of solutes due to the differences in the packing of the fatty acid tails.

Typically, there is much lower solubilization in the gel phase in comparison to the fluid phase. This phenomenon is observed when comparing partitioning into vesicles made with saturated vs unsaturated phospholipids at the same temperature. For some estrogenic compounds, Yamamoto et al.[47] observed K_{lipw} values that were an order of magnitude lower when partitioning occurred into saturated vesicles in the gel phase, in comparison to unsaturated vesicles in the fluid phase. Similarly, Kwon and coworkers[26] studied the partitioning of endocrine disrupters into several phospholipid vesicles. For dipalmitoylphosphatidylcholine (DPPC) vesicles at temperatures below T_G, K_{lipw} values were also an order of magnitude lower, in comparison to unsaturated vesicles.

There are also several studies comparing the fluid and gel phase partition coefficients for the same phospholipid. van Wezel et al.[80] saw K_{lipw} values decrease by a factor of 2–6 for chlorinated benzenes in DPPC vesicle dispersions as they moved from the fluid to gel phase. Simon et al.,[55] who studied the partitioning of benzene into various lipid structures, saw K_{lipw} values decrease by a factor of three when below T_G, for DMPC, DPPC, and

distearoylphosphatidylcholine (DSPC). However, for $T > T_G$ there was no significant change in K_{lipw} with temperature. Similarly, De Young and Dill[56] observed that the partition coefficient of hexane into DMPC vesicles decreased over three-fold as lipid transitioned from the fluid to gel phase, but showed a smaller decrease when temperature was lowered in fluid phase systems. They also studied the partitioning of benzene[81] into DMPC vesicles. At very dilute benzene concentrations, K_{lipw} values decreased five-fold from the fluid to gel phase.

As refrigeration is a common food preservation method, how flavor distribution between the lipid, water and vapor phases changes with temperature is useful information to help inform lipid choice and flavor concentrations. Furthermore, vesicles are not stable on their own for prolonged periods at room temperature and systems that utilize vesicles to host solutes are often refrigerated. The temperature dependence of solubilization has implications beyond the food industry, as vesicles are often used as carriers for other hydrophobic compounds such as drug molecules, which may be heated or cooled during processing, storage, or delivery.

It can be challenging to study partitioning into the gel phase, since its ordered structure is affected by the incorporation of solutes in the bilayer. Cholesterol, in particular, has been shown to have the effect of "fluidizing" some bilayer membranes by causing the fatty acid tails to adopt a more disordered liquid crystal packing at temperatures where the pure phospholipid bilayer is typically in the gel phase.[56,82] Anesthetics and narcotics are other classes of compounds that have similar mechanisms of action in bilayer membranes, with much research dedicated to understanding this phenomenon.[80,83] There have been limited experimental reports showing that limonene can lower the phase transition temperature of DMPC vesicles.[44,84] Along with other terpenes, limonene has also been reported to act as a penetration enhancer. In the case of skin permeation, by fluidizing the stratum corneum, which is the lipid matrix of the outermost skin layer, limonene increases the membrane partition coefficients of other hydrophobic compounds such as drugs.[85]

We used headspace–solid phase microextraction (HS–SPME) to measure limonene partition coefficients as a function of temperature and to determine the effect of the bilayer phases on partitioning. Differential scanning calorimetry (DSC) allowed us to determine the phase transition temperature of DMPC vesicles with and without the addition of limonene. DSC is widely employed for measuring the phase transition temperature of phospholipids, by measuring the energy transferred to or from a sample as heat. The sample is compared to a reference, specifically one that does not experience physical or chemical changes over the range of temperatures being studied. The temperature of the sample and the reference are kept equal, and there is excess enthalpy at a phase change since more heat needs to be supplied to the sample to maintain the same temperature as the reference. There is a corresponding peak which gives us the phase transition enthalpy at the melting point or T_G.[86]

This chapter explores the differences in solubilization between gel and fluid vesicle dispersions by varying the temperature. The effects of limonene itself on the phase behavior of the bilayer are also examined through both HS–SPME and DSC experiments, with results compared with ideal mixing theory. The comparison allows us to predict the effects of limonene or other solutes on the bilayer. With this information, complex effects of composition and temperature on the limonene distributions within vesicle dispersions can be understood in terms of the mixture phase behavior. The ability of vesicles to solubilize and release flavors or bioactive compounds can then be better predicted or controlled.

4.2 Materials and Methods

4.2.1 Materials

1,2-Dimyristoyl-*sn*-glycero-3-phosphatidylcholine (DMPC, >99% purity) was purchased as a 25 mg/mL solution in chloroform and as a powder from Avanti Polar Lipids, Inc. (Alabaster, AL). They were used without further purification. Water (Molecular Biology

Reagent, 0.1μm filtered) used for dynamic light scattering measurements was purchased from Sigma-Aldrich (St. Louis, MO) and deionized water with a resistivity of 18 MΩ·cm used for HS–SPME sample preparation was obtained from a MilliQ™ water purification system installed in the laboratory (Millipore, Bedford, MA). R-(+)-limonene (98%) and dimethyl sulfoxide (DMSO) were purchased from Sigma-Aldrich.

4.2.2 Experimental Methods

4.2.2.1 Sample Preparation

Vesicles for HS–SPME experiments were prepared following the procedure previously outlined in Chapter 2. Briefly, some volume of 25 mg/mL DMPC solution in chloroform was added to a conical flask and left to dry overnight under vacuum. The resulting lipid cake was then hydrated with 1 mL water and sonicated in a Fisher FS20 bath sonicator (Pittsburgh, PA) for 10 to 15 minutes, resulting in a dispersion of multilamellar vesicles with a known molar lipid concentration. These dispersed vesicles were then extruded 17 times through a nanosized polycarbonate membrane to create unilamellar vesicles. Once extruded, the dispersion was diluted with water to a concentration of 10 mM. Some of the extruded or 10 mM dispersion was further diluted to 1 mM and used to determine the average vesicle size with DLS, as described in Section 2.2.2.4 (Malvern Panalytical Zetasizer Nano Range, Worcestershire, U.K.).[60,61] To ensure vesicles were in the fluid phase during preparation, all solutions and equipment were kept at temperatures >35ºC. Samples of 1 mL were prepared for HS–SPME by adding fixed volumes of pure limonene to set total moles of limonene per liter of water, C_{tot}, at values above 0.3 mM to a range of phospholipid concentrations (from 0.01 to 5 mM), made by diluting our 10 mM dispersion with MilliQ™ water. For $C_{tot} \leq 0.3$ mM, appropriate volumes of a 0.93 M limonene in DMSO solution were added.

To prepare vesicles for differential scanning calorimetry (DSC) experiments, 0.049 g of DMPC powder was added to a conical glass vial with 1 mL water and sonicated for 10–15 minutes to produce a dispersion of multilamellar vesicles with 240 mM DMPC. Appropriate volumes of limonene were added to 25–100 μL of these dispersions to create 0.01, 0.1, 0.2 and 1.24 limonene–lipid mole ratio samples. These were shaken at room temperature with the same autosampler agitator used for SPME (Gerstel MPS2; Linthicum, MD) at 300 rpm for 3 hours in 20.01±0.08 mL SPME vials. Liquid volumes of 1 mL or less were used.

4.2.2.2 Headspace Analysis using HS–SPME

Analysis of the vapor phase concentration of limonene in the vials was done following the procedure outlined in Chapter 2. A GC/MS instrument with a DB-wax column, an autosampler and a tray cooler was used. Temperature on the sampling tray was controlled with a water bath. The MS detectors were operated in the total and extracted ion mode with a 70 eV electron ionization source.[57,58] Each sample was shaken for 3 hours using the autosampler agitator to achieve equilibrium before sampling. Here, a speed of 300 rpm was used at room temperature. After this mixing, samples sat for at least 1 hour to equilibrate to the programmed temperature of the water bath, then the headspace was contacted by an 85 μm polyacrylate fiber (Restek) for 1 minute and desorbed into the GC inlet at 240°C for 10 minutes. Samples sat on tray for 4–13 h before being analysed by the GC. The samples were therefore randomized on the tray to determine potential effects of sampling time. Such effects were only seen in samples at 15ºC with higher concentrations of limonene (0.618 mM) as discussed in Section 4.3.4.3. The preparatory sequence is shown in Figure 4.1 and GC/MS parameters are listed in Table 2.1. Sample replicates were done using the same stock dispersion and triplicate analysis was done using three separately prepared dispersions of phospholipid vesicles. (Replicates that were more than 3 SD from mean were considered outliers). Partition coefficients were

determined using a Levenberg Marquardt nonlinear least-squares numerical optimization algorithm using Matlab (R2021A). Weighted averages for K_{lipw} were calculated using equations 2.14 to 2.16. In figures, error bars represent the standard error of the mean between replicates, except for Figure 4.15 (28ºC), where weighted errors (equation 2.16) were used to capture dissimilar variances between replicates.

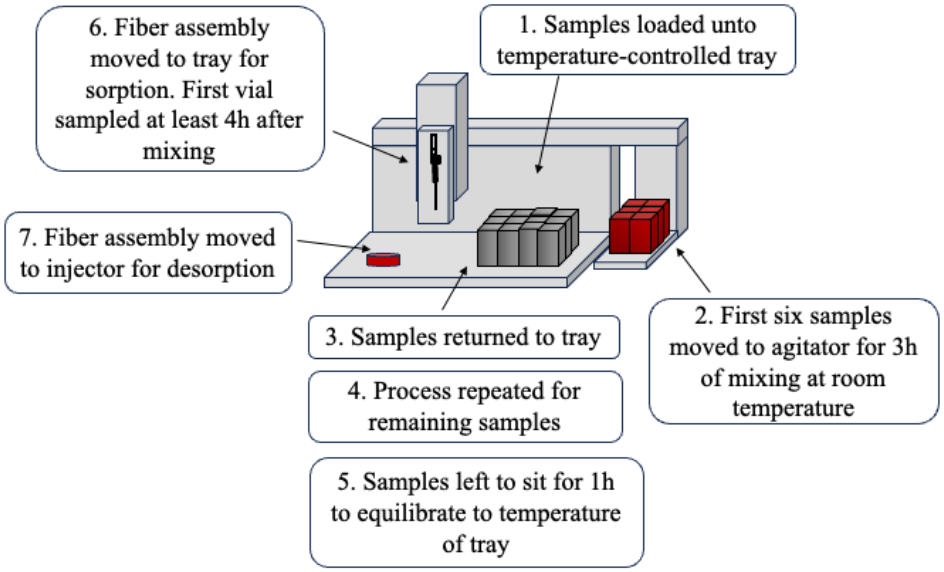

Figure 4.1: Instrument Preparatory Sequence for HS–SPME analysis.

4.2.2.3 Differential Scanning Calorimetry Measurements

Sample vials, prepared as described in Section 4.2.2.1 above, remained sealed for 20 hours maximum before DSC analysis. Calorimetry was performed at the United States Department of Agriculture (USDA) laboratory in Albany, CA, using a Perkin Elmer 8500 Differential Scanning Calorimeter instrument. Once vials were opened, at least 5 mg of the dispersion with 240 mM DMPC and various mole ratios of limonene to DMPC (0–1.2) was added to Perkin Elmer large volume capsules (Shelton, CT). These capsules feature cylindrical DSC pans and covers (2.79 mm H, 7.54 mm D, stainless steel) and an O-ring (Viton rubber, thickness 0.022”). Samples were quickly weighed out with a spatula; a pipette could not be effectively used due to the thick consistency of the samples. To prioritize closing samples

quickly to prevent loss of limonene to the environment, sample masses were not controlled. Capsules were sealed with a Perkin Elmer quick press.

The DSC instrument was equipped with nitrogen gas and an Intracooler 2P (Perkin Elmer) for cooling. An empty reference vial and a sample vial were placed in the sampling chamber and heat flow measurements taken from 10ºC to 30ºC, at a rate of 1ºC/min. At least 5 mg of sample was needed to observe a signal. Integration of the peaks obtained provided phase transition temperatures and enthalpy changes. There was a difference of ~2ºC between the programmed instrument temperature and the recorded sample temperature. For analysis, the sample temperature was used rather than the programmed temperature. Thermograms were normalized by dividing the heat flow by the mg of mass for better comparison. Three replicates were done for each limonene–lipid mole ratio studied. Each replicate was prepared individually to assess the impact of random errors and sample variance. Although the heat flow profiles appear offset in the figures below, the peak areas and phase transition temperatures are reproducible with relative standard deviations generally <10%.

4.3 Results and Discussion

4.3.1 Partitioning of Limonene into DMPC Vesicles at Different Temperatures

To probe the effect of fluidity on the partitioning properties of limonene, experiments were performed at 20 and 28ºC, which are above and below the phase transition temperature of ~25ºC for DMPC. As presented in Chapter 2, the vapor–water partition coefficient (K_{vw}) changes with temperature and can be calculated with the van 't Hoff equation (equation 2.13). Calculated K_{vw} values for limonene at different temperatures are presented in Table 2.2, along with other parameters used for these HS–SPME experiments. With an increase in temperature, there is also an increase in K_{vw}. These values enable us to convert HS–SPME data from the vapor phase to information on limonene distributions within the vesicle dispersion.

Vapor concentration (C_v) data for limonene from HS–SPME experiments at different temperatures is presented in Figure 4.2. The data was taken at various concentrations of DMPC, with a fixed amount of total limonene corresponding to $C_{tot} = 0.618$ mM. To obtain lipid–water partition coefficients, K_{lipw}, this vapor phase data, plotted as a function of the ratio $\rho/(1+\rho)$ in Figure 4.2B, is fit with the mole balance below:

$$\frac{C_v}{C_v^w} = \tilde{C}_v = \frac{1}{2}\left(\left(\nu + \frac{1+\rho}{\rho}\right) - \sqrt{\left(\nu + \frac{1+\rho}{\rho}\right)^2 - 4\nu}\right), \tag{2.9}$$

where

$$\nu = \frac{K_{vw}V_v + V_w}{V_w K_{lipw} C_{tot}}. \tag{2.10}$$

Equation 2.9 above is derived in Section 2.3.2. Here, $\tilde{C}_v$ is the ratio of C_v from the sample to C_v^w, the measured vapor phase concentration of limonene above water in the absence of phospholipid. C_{tot} represents the total moles of limonene divided by the volume of water. V_v and V_w are the vapor and water volumes (Table 2.2) and ρ is the known ratio (n_{tot}/n_{PL}) of the total moles of limonene to that of phospholipid, which is equivalent to C_{tot}/C_{PL}.

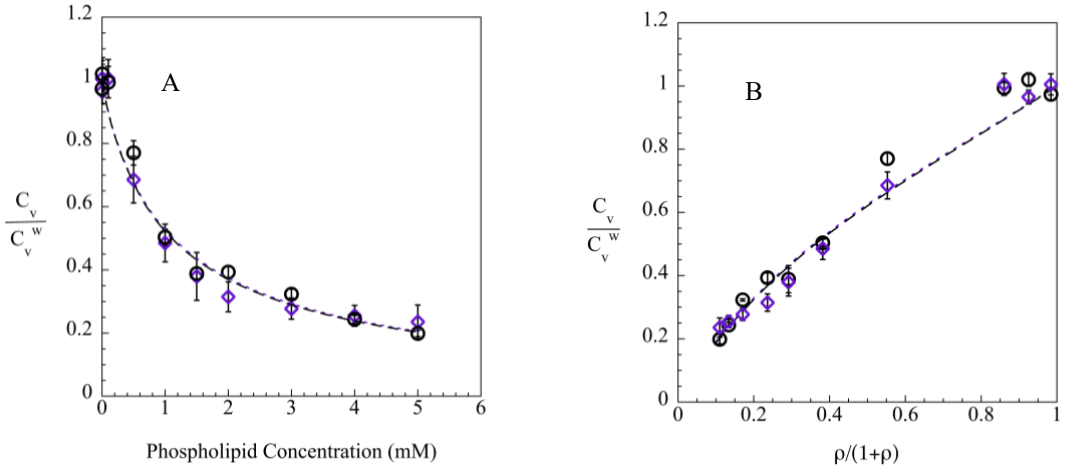

Figure 4.2: Vapor phase concentrations, $\tilde{C}_v$, versus (A) phospholipid concentration and (B) $\rho/(1+\rho)$, for samples with 0.618 mM limonene and DMPC vesicles at 28ºC (○) and 20ºC (◇). Curves represent nonlinear regression fits of K_{lipw}.

Equation 2.9 was fit to data in Figure 4.2B for DMPC vesicle dispersions of 20 and 28ºC, with K_{lipw} the only adjustable parameter. We were able to fit the data to obtain a single constant value for K_{lipw}. At both temperatures, C_v decreases 5-fold in comparison to C_v^w when $C_{PL} = 5$ mM. Results for K_{lipw} are given in Table 4.1. By using the appropriate, temperature dependent values for K_{vw}, we find that the lipid–water partition coefficient at 20ºC, 9.336±0.749 mM^{-1}, is lower than that at 28ºC, 13.19±0.913 mM^{-1} (Table 4.1). This is an interesting observation, as the 20ºC temperature is below T_G (~25ºC), yet the small decrease in K_{lipw} at this lower temperature is more consistent with temperature changes occurring *above* T_G, since the gel phase of DMPC is expected to solubilize much less limonene than does the fluid phase.[56,80] Furthermore, although the K_{lipw} values are different at the two temperatures, in Figure 4.2 we see that $\tilde{C}_v$ decreases at the same rate for 20 and 28ºC, reflecting similar partitioning behavior of limonene.

The finding that K_{lipw} does not drastically decrease below 25ºC would seem to indicate that introduction of limonene causes structural changes in the vesicles at 20ºC, since the vesicles are not behaving like they are in a gel phase. We hypothesize that limonene is fluidizing the membrane upon solubilization and decreasing the phase transition temperature of DMPC. Consequently, the 20ºC data may only be capturing temperature effects within a fluid bilayer, which, at this temperature range, should not have the same impact on partitioning as a fluid-to-gel transition.[55]

In Figure 4.3, $\tilde{C}_v$ measurements are shown versus C_{PL} (Figure 4.3A) or $\rho/(1+\rho)$ (Figure 4.3B) for $C_{tot} = 0.618$ at 15ºC. In the latter, it is evident that fits of equation 2.9 with a single value of K_{lipw} does not adequately capture the experimental results over the entire range of ρ values. In particular, for the four highest phospholipid concentrations in Figure 4.3A, $\tilde{C}_v$ remains relatively constant, instead of decreasing gradually as is observed for our results presented in Chapters 2 and 3, and as predicted from equation 2.9. Thus, capturing this

Table 4.1: Partition Coefficients (K_{lipw}) of Limonene in DMPC Vesicles

Size (nm)	<Size> (nm)[a]	T (°C)	C_{tot} (mM)	ρ	Phase[d]	K_{lipw}	R^2	$<K_{lipw}>$ (mM^{-1})[b]	$<\widehat{K}_{lipw}>$ ($\times 10^5$)[c]
202.1±0.6 183.9±4.7 182.7±1.1	189.6 ±6.3	15	0.2	0.04–20	gel	4.018±0.257 3.483±0.281 3.463±0.496	0.9713 0.9729 0.8924	3.735 ±0.177	2.07 ±0.098
186.8±2 207±0.8 192.1±0.8	195.3 ±6	15	0.618	0.12–61.8	fluid (H)	9.444±2.962 10.04±3.821	0.9162 0.845	9.668 ±2.341	5.358 ±1.297
196.5±0.9 188.6±4.8 182.7±1.1	189.3 ±4	20	0.093	0.05–0.093	gel	3.263±0.594 3.834±0.506 3.731±0.525	0.9729 0.9844 0.9772	3.642 ±0.311	2.018 ±0.172
198.4±2.2 204.7±4.7 206.9±3.2	203.3 ±2.5	20	0.618	0.12–61.8	fluid (H)	12.80±1.51 10.15±1.92 7.712±0.965	0.9567 0.9715 0.9652	9.336 ±0.749	5.174 ±0.415
198.4±2.2 204.7±4.7 206.9±3.2	203.3 ±2.5	20	0.618	0.31–61.8	fluid (H)	13.41±1.93 10.87±3.22 8.415±1.653	0.9571 0.9649 0.9737	10.57 ±1.17	6.084 ±0.509
221.2±1 196.5±0.9 243.1±3.2	220.3 ±13.5	28	0.093	0.02–9.3	fluid	9.956±0.959 11.17±2.132 7.063±0.76	0.9926 0.9578 0.9873	8.396 ±0.574	4.653 ±0.318
207.7±3.6 189.4±3.2 204.8±4.4	200.6 ±5.7	28	0.618	0.12–61.8	fluid	12.68±2.95 13.92±1.13 11.41±1.84	0.9588 0.9868 0.9735	13.19 ±0.91	7.308 ±0.506

[a]Errors are standard error of the mean

[b]Nonlinear regression weighted by $1/\sigma^2$, where σ represents the standard deviation of the replicates

[c]$<\widehat{K}_{lipw}>$ values are of order 10^5

[d](H) indicates data likely affected by hysteresis

vapor concentration data would require K_{lipw} to change with ρ. Limonene fluidizing the gel membrane at some values of ρ would explain this deviation, with some samples remaining in the gel phase at low ρ values and others being fluid as ρ increases.

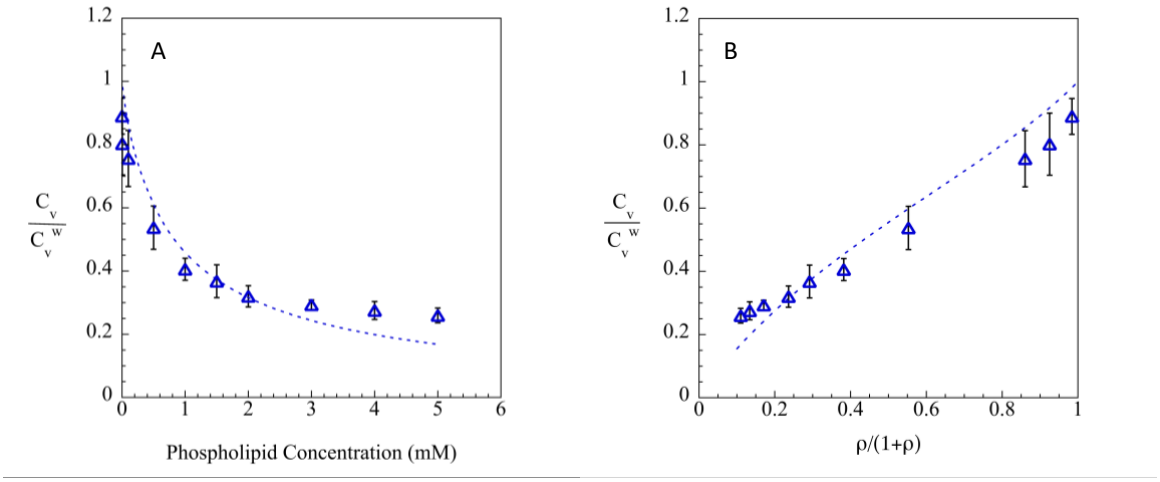

Figure 4.3: Vapor phase concentrations, $\tilde{C}_v$, versus (A) phospholipid concentration and (B) $\rho/(1+\rho)$, for samples with 0.618 mM limonene and DMPC vesicles at 15ºC. Curves represent nonlinear regression fits of K_{lipw}.

4.3.2 Decrease in Phase Transition Temperature with Limonene in the Bilayer

To evaluate the effect of limonene on membrane/bilayer fluidity, DSC was used to measure T_G of DMPC-containing vesicles with different limonene–to–phospholipid mole ratios, ρ. Here, the heat flow represents the energy being supplied to the samples as a function of time to raise their temperature at a specified, slow rate. This differential heat transfer (at constant pressure), dq_p, is equivalent to $C_p dT$, where C_p is the heat capacity at constant pressure. At a phase change, there is excess energy being transferred to the sample to reach the same temperature as the control, resulting in a peak. The change in enthalpy, ΔH, is then calculated with $\Delta H = \int_{T1}^{T2} C_p dT$ from peak areas in the thermograms (plots of heat flow or heat capacity vs temperature).[86]

In Figure 4.4A, for DMPC alone, a large peak is observed at $T = 25.29$°C (Table 4.2), with a second much smaller peak at $T = 16$ºC. DMPC vesicles without limonene were thus

found to have a T_G value of 25.29 ± 0.37°C, comparable to reported values of 23–25ºC[44,87,88] shown in Table 4.3. This peak represents the main transition of DMPC from the P_β ripple gel phase to the L_α fluid phase. There is also a pretransition from the L_β gel phase to P_β, typically observed at ~14ºC,[44,84] in good agreement with our smaller peak at 16ºC in our experiments. T_G of DMPC remained unchanged at low limonene–lipid mole ratios as observed in Figures 4.4B. However, as shown in Figures 4.4C–E, increasing those ratios to $\rho = 0.1$ and higher, and consequently raising the concentration of limonene in the bilayer, lowers T_G values until the phase transition can no longer be observed over the scanned temperatures above 10ºC (Table 4.2).

Table 4.2: Effect of Limonene on the Phase Transition Temperature (T_G) of DMPC Vesicles

ρ	x_{PL}	T_G(°C)	$\Delta H_{dispersion}$ (J/g)	$\Delta_{G\to F}\,\bar{H}_{DMPC}$ (J/mol)	$\Delta_{G\to F}\,\bar{S}_{DMPC}$ (J/mol K)
0	1	25.29±0.37	5.687±1.048	27550±5078	92.32±17.03
0.01	0.99	24.92±0.17	5.097±0.317	24690±1536	82.85±5.12
0.1	0.91	22.06±0.81	3.242±0.611	15700±2959	53.19±9.87
0.2	0.83	20.03±1.35	0.668±0.052	3238±251	11.05±0.9
1.2	0.46	<10	–	–	–

Figure 4.5 shows averaged thermograms for all mole ratios, compared in a single plot. The pre-transition behavior, associated with gel polymorphism, was not explored in our studies due to the small size of the peak. In addition, the transition was only observed if we used a low starting temperature of 5ºC, given its closeness to 10ºC. For the main transition peaks, we see broadening and a decrease in peak heights as well as differences in the enthalpy change or excess enthalpy, ΔH, associated with the phase transition.

The specific ΔH values, ΔH_m, for the transition were calculated by the DSC software using the heat flow (rate of heat addition) and the mass of the sample. Since the samples

include water as well as vesicles in the dispersion, this intensive value represents the enthalpy change per mass of the dispersion, $\Delta H_{m,dispersion}$. The mass fraction (m_f) of DMPC in water is calculated as

$$m_f = \frac{n_{PL} MW_{PL}}{m_{water} + (n_{PL} MW_{PL})}, \tag{4.1}$$

where n_{PL} is the total moles of lipid in water, m_{water} is the mass of water, and $MW_{PL} = 678$ g/mol is the molecular weight of DMPC. This mass fraction is used to reexpress ΔH_m in terms of DMPC only ($\Delta_{F\to G}\,\bar{H}_{DMPC}$), on a molar basis as $\Delta_{F\to G}\,\bar{H}_{DMPC} = \Delta H_{m,dispersion}\, MW_{PL}/m_f$. For 240 mM DMPC the mass fraction is 0.140. Table 4.2 shows the reported $\Delta H_{m,dispersion}$ values along with the calculated $\Delta_{G\to F}\,\bar{H}_{DMPC}$ and $\Delta_{G\to F}\,\bar{S}_{DMPC}$ results for various limonene–to–phospholipid mole ratios. Note that the positive enthalpy and entropy values shown in Table 4.2 represent gel→fluid transitions and $\Delta_{G\to F}\bar{H} = -\Delta_{F\to G}\bar{H}$ and $\Delta_{G\to F}\bar{S} = -\Delta_{F\to G}\bar{S}$. The change in enthalpy for DMPC without solute, $\Delta_{G\to F}\,\bar{H}^o_{DMPC}$, is 27.550±5.078 kJ/mol. An analysis by Caffery and Hogan[89] of the DMPC data available in LIPIDAT, a database for lipid thermodynamic data, concludes that $\Delta\bar{H}^o_{DMPC}$ values range from 12 to 37 kJ/mol, as obtained using a variety of methods. Our value falls within that range. Other groups who used DSC reported values similar to ours, as is shown in Table 4.3.[44,87,88] $\Delta_{G\to F}\,\bar{S}^o_{DMPC}$ is calculated using the Gibbs free energy, $\Delta G = \Delta H - T\Delta S,$ with $\Delta G = 0$ at the phase transition temperature. The molar entropy for DMPC without solute, $\Delta_{G\to F}\,\bar{S}^o_{DMPC}$, was found to be 92.32±17.03 J/molK.

Table 4.3: Comparison to Literature Values for Phase Transition Temperatures and Corresponding Enthalpy Changes for DMPC

T_G (°C)	ΔH_{DMPC} (J/mol)	Refs
25.29 ± 0.37	27550±5078	this work
24	22175	Dueland et al., 2012
23.8	25900	Di Foggia et al., 2017
23.6	27916	Bayerl et al., 1989
25.08	31280±510	Sarpietro et al., 2021

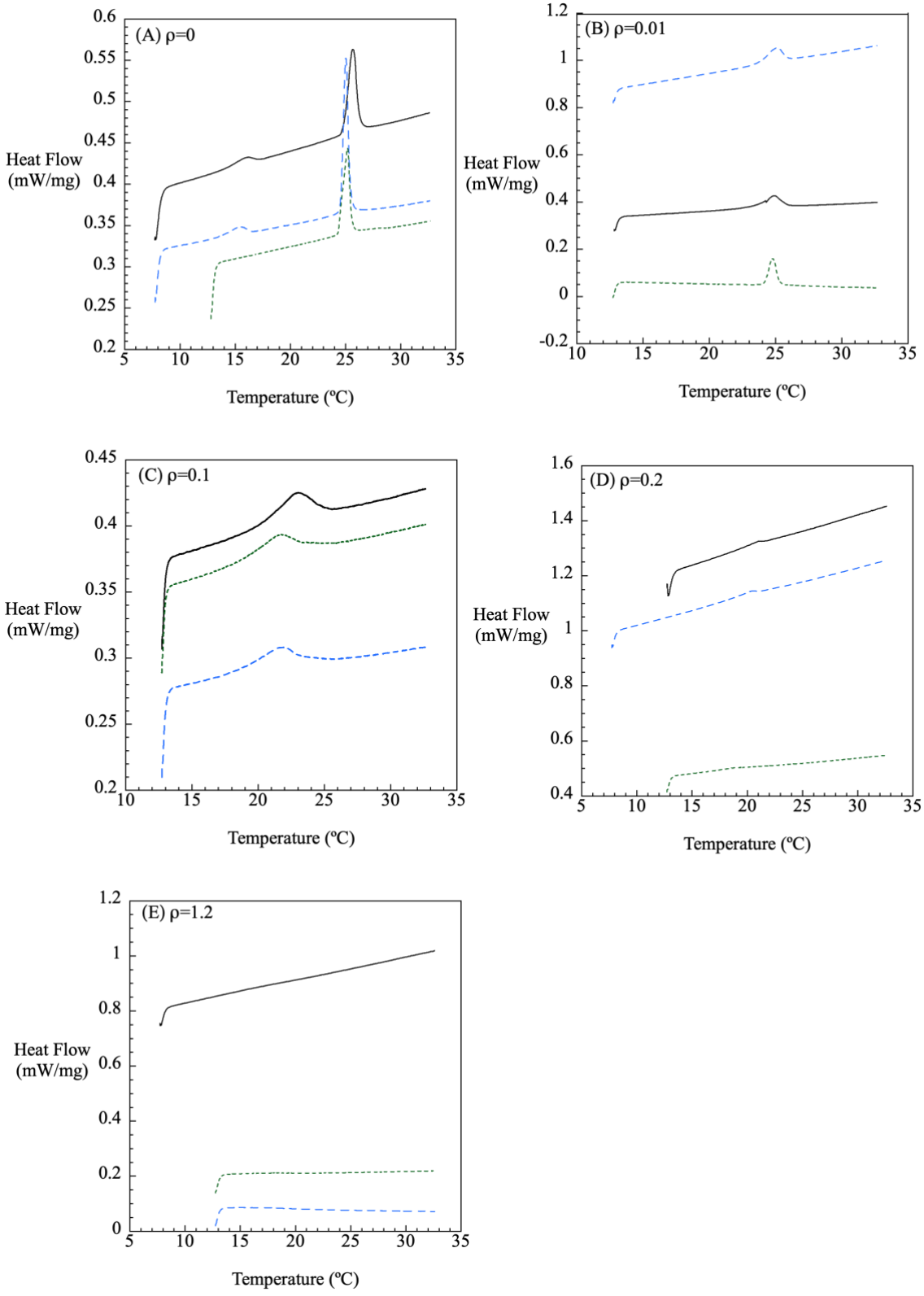

Figure 4.4: DSC sample replicates with limonene to DMPC mole ratios of (A) 0, (B) 0.01, (C) 0.1, (D) 0.2, and (E) 1.2. Each thermogram represents a separate 240 mM DMPC sample. Samples were normalized by mass.

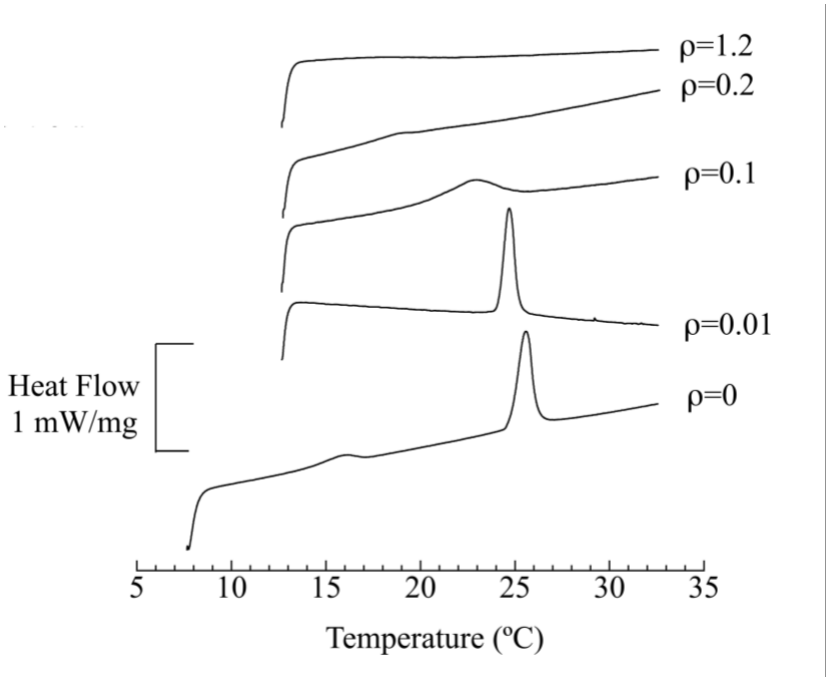

Figure 4.5: Heat flow (rate of heat added) for 1˚C/min DSC scans of 240 mM DMPC dispersions, showing change in phase transition temperature with limonene–lipid mole ratio, ρ.

From Table 4.2, we can see that the decrease in peak heights and peak broadening with increasing ρ (Figures 4.4 and 4.5) correspond to a reduction in both the enthalpy and entropy change during the phase transition. This decrease is likely due to increased disorder in the gel phase with the incorporation of limonene, thereby requiring less energy for the gel–to–fluid phase transition, and a reduced difference in the number of possible arrangements between the phases. Peak broadening is often attributed to decreased cooperativity, which is the tendency for large numbers of molecules to change phases as a group and stabilize each other in the new phase through intermolecular interactions.[90] Broader peaks are then used as a measure for cooperativity with higher concentrations of solutes reducing the number of phospholipids that experience simultaneous phase transition.[24,84,91] Consequently, higher solute concentrations would correspond to broader peaks for the phase transition. However, some researchers argue that this observation is not a measure of cooperativity but rather a result of a two-phase coexistence region between the gel and fluid phase caused by the addition of solute.[37] The presence of this region increases the temperature range over which the phase transition is

observed. A similar peak evolution phenomenon has also been observed by Duelund et al.[44] and Sarpietro et al.[84] in multilamellar DMPC vesicles. Increasing limonene mole fractions in the bilayer up to 0.15[44] or 0.12[84] respectively, led to progressively lower T_G, along with peaks that were similarly shorter and broader.

Limonene also lowers the phase transition temperature of other phospholipids, including DPPC, as shown by Mendanha et al.,[92] where limonene–lipid mole ratios above 0.618 lowered T_G by at least 8ºC. Other terpenoids, including terpineol, cineol, and nerodinol,[84,92] and hydrophobic solutes such as anesthetics have been observed to decrease T_G of phospholipids. Vanderkooi et al.[93]showed that the anesthetics ether and chloroform decrease the T_G of DMPC. These phenomena were also attributed to mixing entropy. Furthermore, the small effects on T_G by low mole fractions of limonene is consistent with other solutes. Simon et al.[55] reported that a low benzene mole fraction of 0.1 only lowered the T_G of phosphatidylcholine vesicles by about 1ºC.

4.3.3 Predicting the Phase Transition Temperature in Vesicle Bilayers

The lowering of T_G can be analysed and predicted using ideal mixing theory.[37,44,93] As limonene mixes with the fatty acid tails of the phospholipid, it lowers the latter's chemical potential through the entropy of mixing. This then leads to a lower T_G, which can be approximately calculated with theory developed for the freezing point depression, with the assumption that no solutes are present in the gel phase. This theory also allows us to determine the mole fraction of limonene that fluidizes the membrane from a gel state.

At equilibrium, the chemical potential, μ_{PL}, of the phospholipid in the fluid (F) and gel (G) phases of the bilayer are equivalent:

$$\mu_{PL}^{F} = \mu_{PL}^{G} . \tag{4.2}$$

The chemical potential of phospholipid in the bilayer at some temperature, T, can be evaluated using ideal solution theory as

$$\mu_{PL}^{F}|_{T_G} = \mu_{PL}^{Fo}|_{T_G} + kT \ln x_{PL}^{*} = \mu_{PL}^{Go}|_{T_G} . \tag{4.3}$$

Here, x_{PL}^{*} is the critical mole fraction of phospholipid inside the fluid bilayer at the phase transition, μ_{PL}^{Fo} is the chemical potential of the pure phospholipid in the bilayer fluid phase, $T = T_G$ is the gel transition temperature in the presence of limonene, and k is Boltzmann's constant. In equation 4.3, $\mu_{PL}^{G}|_{T_G} = \mu_{PL}^{Go}|_{T_G}$ since partitioning into the gel is neglected. For $T_G < T_G^o$, where T_G^o is the gel transition temperature of the phospholipid bilayers without limonene, equation 4.3 can be rewritten as

$$\ln x_{PL}^{*} = \frac{\Delta_{F\to G}\bar{H}^o}{kT_G}\bigg|_{T_G} - \frac{\Delta_{F\to G}\bar{S}^o}{k}\bigg|_{T_G} . \tag{4.4}$$

Here, $\Delta_{F\to G}\bar{H}^o$ and $\Delta_{F\to G}\bar{S}^o$ are the enthalpy and entropy change, respectively, per molecule at the phase transition of the pure DMPC bilayer at T_G. If we assume $\Delta_{F\to G}\bar{H}^o|_{T_G} \approx \Delta_{F\to G}\bar{H}^o|_{T_G^o}$, and $\Delta_{F\to G}\bar{S}^o|_{T_G} \approx \Delta_{F\to G}\bar{S}^o|_{T_G^o}$, then

$$\ln x_{PL}^{*} \approx \frac{\Delta_{F\to G}\bar{H}^o}{kT_G}\bigg|_{T_G^o} - \frac{\Delta_{F\to G}\bar{S}^o}{k}\bigg|_{T_G^o} . \tag{4.5}$$

During the phase change at T_g°, $\Delta_{F\to G}\bar{G}^o|_{T_G^o} = \Delta_{F\to G}\bar{H}^o|_{T_G^o} - T_G^o\Delta_{F\to G}\bar{S}^o|_{T_G^o} = 0$, so that

$$\Delta_{F\to G}\bar{S}^o|_{T_G^o} = \frac{\Delta_{F\to G}\bar{H}^o}{T_G^o}\bigg|_{T_G^o} . \tag{4.6}$$

Thus, equation 4.5 becomes

$$\ln x_{PL}^{*} \approx \frac{\Delta_{F\to G}\bar{H}^o|_{T_G^o}}{k}\left(\frac{1}{T_G} - \frac{1}{T_G^o}\right). \tag{4.7}$$

Defining $\Delta T = T_G^o - T_G$, equation 4.7 can be further expressed as

$$\ln x_{PL}^{*} = \frac{\Delta_{F\to G}\bar{H}^o|_{T_G^o}}{k}\frac{\Delta T}{T_G^o(T_G^o - \Delta T)} . \tag{4.8}$$

Equation 4.8 is well justified for ideal solutions for $\Delta T \ll T_G^o$, assuming no partitioning into the gel phase.

To connect equation 4.8 to the DSC experiments, we first need to evaluate x_{PL}^* from the overall composition in these samples. Since limonene partitions between the water, lipid and vapor phases, the limonene is not entirely in the bilayer. The concentration of limonene in the vapor and water phases has often been assumed to be negligible,[44,84] and the samples treated as though all the limonene added remains in the bilayer. However, due to the volatile nature of limonene, the concentration in the vapor phase may be significant based on equilibration methods. We can determine x_{PL} from the mole ratio of limonene to lipid in the vesicle bilayer, ρ^{bi}, using

$$x_{PL} = 1 - x_{lim} = 1 - \frac{\rho^{bi}}{1 + \rho^{bi}}, \tag{4.9}$$

where $\rho^{bi} = n_{lim}/n_{PL}$. The exclusion of limonene in the vapor makes ρ^{bi} different from the overall lipid mole ratio $\rho = n_{tot}/n_{PL}$ but the size of the error in assuming $\rho^{bi} = \rho$ can be estimated. We find $C_v = \tilde{C}_v C_v^w$, the vapor phase concentration of limonene, using equations 2.7 and 2.9, after dividing the former by k_p to get C_v^w:

$$C_v = \tilde{C}_v \frac{n_{tot}}{V_v + \frac{V_w}{K_{vw}}} = \tilde{C}_v \frac{C_{tot} K_{vw}}{\hat{V}}. \tag{4.10}$$

The moles of limonene in the lipid phase, n_{lim}, are then determined by subtracting from n_{tot} the moles of limonene present in the vapor and water phases, yielding:

$$n_{lim} = n_{tot} - C_v \left(V_v + \frac{V_w}{K_{vw}} \right) = n_{tot}(1 - \tilde{C}_v). \tag{4.11}$$

To use equation 2.9, we estimate K_{lipw} from measured values obtained from HS–SPME experiments using 0.618 mM limonene at low and high temperatures (Table 4.1). V_v and V_w are estimated as $V_{crucible} - V_w$ and m_{sample}/ρ_{water} respectively, where ρ_{water} is the density of water. On average, x_{PL} is approximately 9% lower when calculated with ρ^{bi}, when compared

to ρ. This includes ~10% of n_{tot} lost to the vapor phase during equilibration in the 20 mL vials at room temperature, followed by a further ~0.26% in the crucibles used to conduct DSC measurements.

Using $\Delta_{F\to G}\overline{H}^{o}$ and T_G^o obtained from DSC experiments, ΔT was predicted from equation 4.8 for a range of $x_{lim} = 1 - x_{PL}^*$ values. The predictions, shown alongside the experimental data in Figure 4.6A–B, are in very good agreement with that data, showing that ideal mixing theory is an appropriate approach to help determine the impact that solutes have on T_G. We note that the theory predicts $T_G = 4.09$°C for $\rho = 1.2$. This temperature is below the DSC scan experimental starting point of 10ºC and explains the absence of a peak in that thermogram. A comparison of T_G predictions using x_{lim} values calculated with ρ^{bi} versus ρ is shown in Figure 4.6B. Although the results are quite similar, the x_{lim} values obtained using ρ agree more closely with the theory. This difference between the x_{lim} values is larger at higher mole fractions, where the theory predicts a higher mole fraction for lowering T_G than what is observed using DSC.

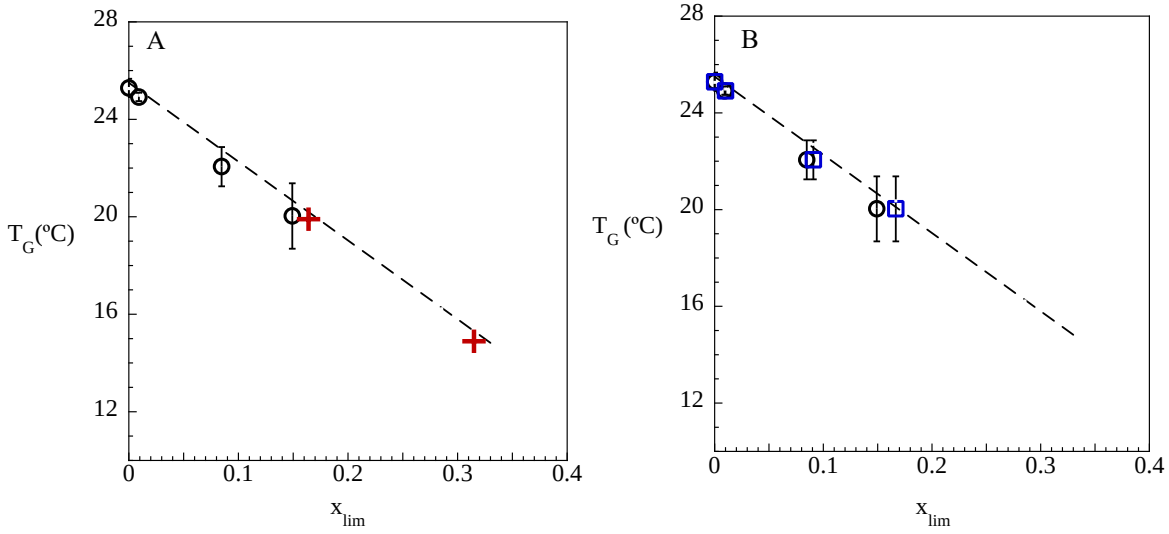

Figure 4.6: Measured phase transition temperatures (○,□) versus limonene mole fraction, x_{lim}; T_G predictions (---) using equation 4.8, with two temperatures marked (+) for compositions relevant to Figures 4.2, 4.8 and 4.9. In (A) mole fractions are calculated with an estimated ρ^{bi} (○) and in (B) a comparison between mole fractions calculated with ρ^{bi} (○) and with ρ (□) is shown.

Duelund et al.[44] and Sarpietro et al.[84] also measured T_G for DMPC bilayers mixed with limonene, for limonene mole fractions in the bilayer up to 0.15. Figure 4.7 provides a comparison of their measurements with our results. Except for an anomalously large ΔT reported by Duelund et al. at the largest limonene concentration, results are in good agreement with these literature values. Duelund and coworkers also compared their results with predictions for ideal mixing in the fluid phase, assuming no limonene in the gel phase. Specifically, they used a simplified version of equation 4.8, obtained by assuming $x_{lim} \ll 1$ and $\Delta T \ll T_G$, which would tend to underestimate ΔT as x_{lim} increases. For two other terpenes, Duelund et al.[44] also found that the theory closely matched the experimental results.

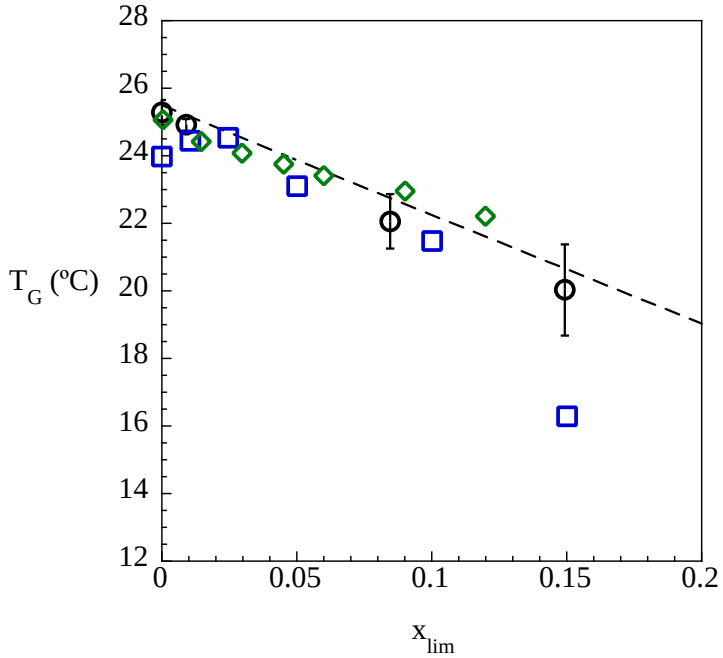

Figure 4.7: DSC phase transition temperatures of DMPC with limonene in the bilayer. Data from this work (○), Duelund et al.[44] (□), and Sarpietro et al.[84] (◇). Dashed line represents prediction using equation 4.8 with $T_G^o = 25.26°C$ and $\Delta_{F\to G}\bar{H}^o = 27550\, J/mol$, and x_{lim} estimated from $\rho^{bi}/(1+\rho^{bi})$.

There are differences in preparation and equilibration methods between our experiments and those in Duelund et al.[44] In the latter, samples were made with vesicles dispersed in buffer with an additional 154 mM NaCl. It is unclear what equilibration procedure

was used for their method, but we have found that, although limonene readily partitions into the bilayer, at least 2 hours of mixing are needed to ensure equilibrium. Finally, we note that, in the work of Duelund et al.[44], information on replicate numbers and error estimates were not given. T_G values reported by Sarpietro et al.,[84] like ours (Figure 4.7), decreased with limonene mole fractions in an approximately linear fashion, matching the predictions of equation 4.8 more closely than values from Duelund et al.[44]

4.3.4 Predicting Solubilization Behavior at Lower Temperatures

4.3.4.1 Estimating Solubilization Behavior with Gel Formation

From equation 4.8, we can find x_{PL}^* for some defined value of ΔT. This procedure was used to help interpret results for $\tilde{C}_v$ as a function of composition for $T < 25$℃, when both gel and fluid phases may be present. For $T = 15$℃ and $\Delta T = 10$℃, equation 4.8 yields $x_{PL}^* = 0.67$, which corresponds to a DMPC concentration of 1.27 mM for samples with 0.618 mM of limonene, assuming $x_{lim} \approx \rho/(1+\rho)$. This composition could thus involve contributions from a gel phase. Since this phospholipid concentration falls in the middle of our data range in Figures 4.2 and 4.3, measured $\tilde{C}_v$ values in these data sets could show a clear influence on partitioning behavior of the presence of fluid and gel phases. In fact, 15ºC data presented in Figure 4.3 shows a strongly decreasing curve at lower phospholipid concentrations, similar to what was seen at 20 and 28ºC, but for $C_{PL} \geq 1.27$ mM there appears to be a plateau which was not observed at higher temperatures. The data below 1.27 mM DMPC can be fit using equation 2.9 to obtain a partition coefficient of 9.668 mM^{-1}. This fit matches the low C_{PL} data more closely than does the fit of a single K_{lipw} to the entire curve, because of the flat shape of the data above 1.27 mM DMPC. These results indicate deviation from constant partitioning behavior at low temperature.

For C_{PL} below 1.27 mM with $x_{PL} < 0.67$, results in Figure 4.8 indicate that we have a fluid phase, with a partition coefficient that is independent of composition. When $x_{PL} \gtrsim 0.67$, a gel phase should form within the DMPC bilayer. The vesicles enter a coexistence region between the fluid and gel phases where the mole fractions of limonene in both, x_{lim}^{G} and x_{lim}^{F} become fixed, as the chemical potential of the fluid and gel phases are equal. As x_{PL} increases overall, we form more of the gel phase, which, according to the freezing point depression model, excludes the solute limonene, and coexists with a decreasing amount of the more concentrated fluid phase fixed at x_{PL}^{*}.

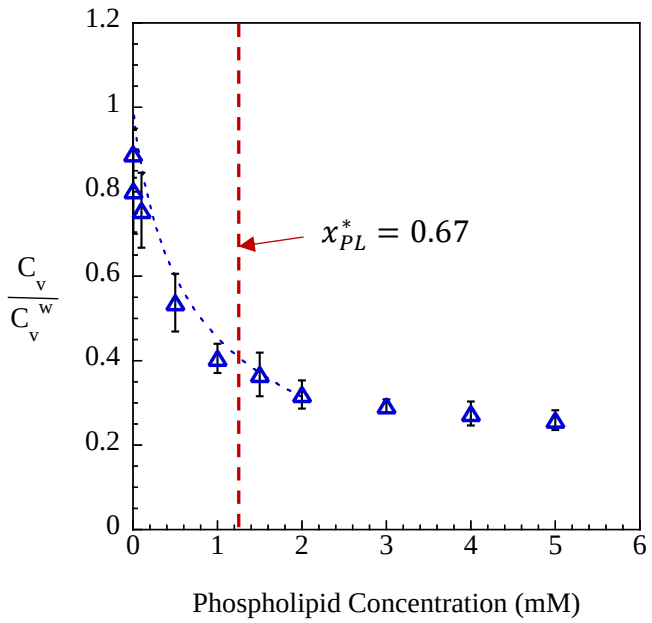

Figure 4.8: Vapor phase concentrations, $\tilde{C}_v$, versus phospholipid concentration for 0.618 mM limonene and DMPC vesicles at 15ºC. Curve (---) represents nonlinear regression fit of K_{lipw} for data in the fluid phase.

4.3.4.2 Using Low C_{tot} to Improve Estimates for Transition

HS–SPME experiments were also performed at 15ºC with a lower total concentration of limonene, 0.204 mM. At this concentration, the approximate DMPC concentration corresponding to $x_{PL}^{*} = 0.67$ is 0.4 mM. In the experiment, as results show in Figure 4.9A, we

observed a plateau or a small bridge between C_{PL} values of ~0.05 and 0.5 mM, over which range the vapor concentration and thus the limonene solubilized remained constant. The three values in this plateau region average to $\tilde{C}_v = 0.82$. For $C_{PL} > 0.5$ mM there was a decrease in limonene vapor phase concentration with increased phospholipid. These features indicate the presence of a coexistence region, followed by a one-phase gel for $C_{PL} > 0.5$ mM. The decreasing values of $\tilde{C}_v$ in the gel–only region indicate non-zero partitioning of limonene. Within the coexistence region fluid and gel phases are present, with their extents reflecting the lever rule.[94] In Figure 4.9B, data from Figure 4.9A is replotted versus $\rho/(1+\rho)$, which equals $n_{tot}/(n_{tot}+n_{PL})$. In this figure, it can more easily be seen that the phase of the phospholipid bilayer changes from fluid → fluid + gel → gel as x_{PL} increases, or as x_{lim} decreases.

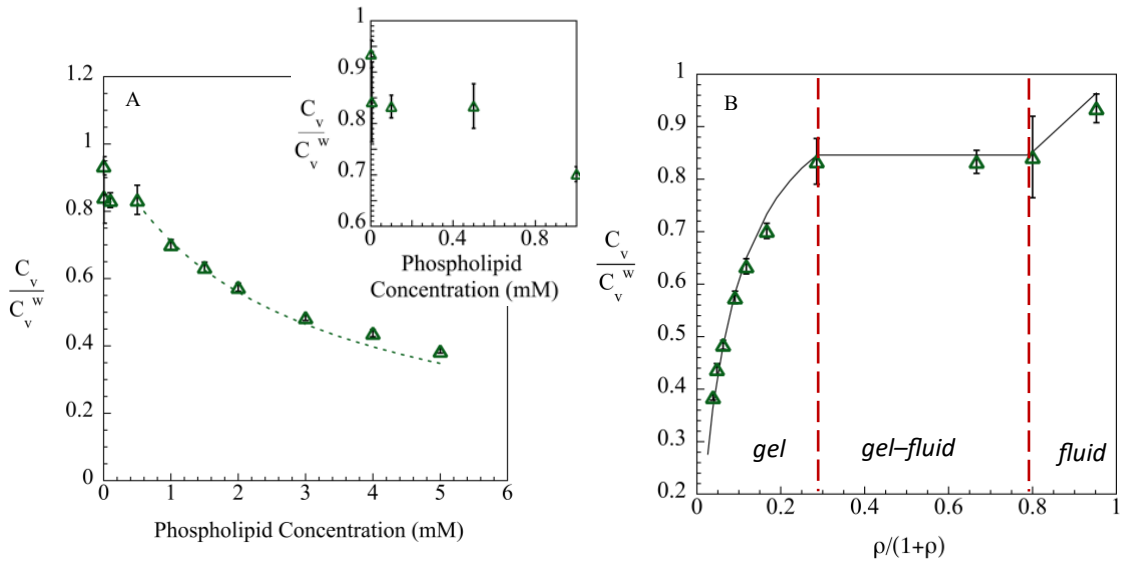

Figure 4.9: Vapor phase concentrations, $\tilde{C}_v$, versus (A) phospholipid concentration, and (B) mole ratio of limonene to phospholipid, for 0.204 mM limonene and DMPC vesicles at 15ºC. Black line in B represents prediction of the partitioning and phase behavior using equation 4.20.

From Figure 4.9A, $\tilde{C}_v = 0.82$ in the coexistence region, and $C_{PL} \geq 0.5$ mM marks the onset of a one-phase gel. Using these values and those in Table 2.2 with equations 4.10 and 4.11, we estimate that $x_{lim} \approx \rho/(1+\rho) = 0.06$ marks the boundary between gel and gel/fluid

coexistence. We see from Figure 4.9A that taking low limonene measurements with C_{tot}= 0.204 mM limonene allowed us to capture partitioning behavior that was unseen at higher C_{tot}. This concentration leads to low enough limonene mole fractions in the bilayer that the phospholipid is able to form the gel phase completely over a significant range of compositions. As can be seen in Figure 4.7A, the region where partitioning into the gel phase estimated to is occur at mole fractions $x_{lim} \leq 0.06$.

To identify x_{lim} at the onset of the fluid region, equation 4.5, which assumes no solutes are present in the gel phase, requires adjustment. In the coexistence region and assuming ideal mixing, the chemical potentials of phospholipid in the gel and fluid phases may be written as

$$\mu_{PL}^{F}|_T = \mu_{PL}^{Fo}|_T + kT \ln x_{PL}^{F} \tag{4.14}$$

and

$$\mu_{PL}^{G}|_T = \mu_{PL}^{Go}|_T + kT \ln x_{PL}^{G}\,, \tag{4.15}$$

respectively. Here, μ_{PL}^{Fo} and μ_{PL}^{Go} are the pure phospholipid reference potentials for the fluid and gel phases, respectively. The chemical potentials in the two phases are equivalent, so that

$$\mu_{PL}^{Fo}|_T + kT \ln x_{PL}^{F} = \mu_{PL}^{Go}|_T + kT \ln x_{PL}^{G}\,. \tag{4.16}$$

This equation can be rearranged to produce a ratio of the mole fractions:

$$\ln \frac{x_{PL}^{F}}{x_{PL}^{G}} = \frac{[\mu_{PL}^{Go}|_T - \mu_{PL}^{Fo}|_T]}{kT}. \tag{4.17}$$

We define x_{PL}^{F}/x_{PL}^{G} as a phospholipid fluid-gel partition coefficient, $K_{F,G}$, yielding

$$K_{F,G} = \frac{x_{PL}^{F}}{x_{PL}^{G}} = \frac{1 - x_{\mathrm{lim}}^{F}}{1 - x_{\mathrm{lim}}^{G}}\,. \tag{4.18}$$

In the above equations, x_i^k is the mole fraction of the component *i* (limonene (lim) or phospholipid (PL)) in the *k* bilayer phase (fluid (F) or gel(G)). Then, following a derivation similar to that used to obtain equation 4.8, the right-side of equation 4.17 can be expressed in terms of enthalpy changes and gel transition temperatures for pure phospholipid, so that

$$\ln K_{F,G} = \frac{\Delta_{F\to G}\bar{H}^o|_{T_g^o}}{k}\frac{\Delta T}{T_G^o(T_G^o - \Delta T)}. \quad (4.19)$$

At $15^{\circ}C$ and with the values in Table 2.2, we obtain a value $K_{F,G} = 0.67$. This value helps to identify the limits of the fluid–gel coexistence region. Values for $K_{F,G}$ for this and higher temperatures are given in Table 4.4.

Table 4.4: Predicted Fluid-Gel Partition Coefficients $K_{F,G}$ from Equations 4.18, 4.19, and Limonene Mole Fraction in Fluid Phase at Coexistence

T (°C)	$K_{F,G}$	x_{lim}^{F*}
15	0.67	0.33
20	0.82	0.18
25	1	0
28	1	0

4.3.4.3 Comparison of Theory and Experiment for $T \leq 20$°C

4.3.4.3.1 Low $C_{tot} = 0.2$ mM at 15°C

The value of $K_{F,G}$ given in equation 4.19 can be used in a prediction of the vapor concentration as a function of ρ for the bilayer in a one-phase gel, one-phase fluid, or two-phase fluid–gel coexistence. Unlike our estimate based on equation 4.8, we here add information on the partitioning of limonene into the gel phase, by fitting equation 2.9 to data points for $C_{PL} \geq 0.5$ mM in the one-phase gel domain in Figure 4.9A, to obtain the gel–phase partition coefficient $K_{lipw}^{G} = 3.7$ mM^{-1}. In this fitting procedure v in equation 2.9 is defined as $v = K_{vw}/(K_{lipw}^{G}C_v^w)$ (*cf.* equation 2.10). Next, $\tilde{C}_v$ at $C_{PL} = 0.5$ mM is calculated from equation 2.9, using this value of K_{lipw} and $\rho = C_{tot}/C_{PL} = 0.4$, to yield the constant vapor concentration $\tilde{C}_v^* = 0.85$ and $C_v^* = 0.014$ mM for limonene in the fluid/gel coexistence region. This coexistence region starts at a mole fraction $x_{lim}^{G*} = K_{lipw}^{G}C_v^*/K_{vw} = 0.058$. Inside the two-

phase region, $\tilde{C}_v^*$ and x_{lim}^{G*} remain constant, since limonene's chemical potential is not changing as the bilayer transitions between the two packings. The coexisting fluid phase is also at a fixed mole fraction x_{lim}^{F*}. This transition to the one-phase fluid is now predicted to occur for $C_{PL} \leq 0.06$ mM, corresponding to $x_{lim} \geq x_{lim}^{F*} = 1 - K_{F,G}\left(1 - x_{lim}^{G*}\right) = 0.37$ from equation 4.18 (Table 4.4).

In Figure 4.9B, we compare these predictions to values for $\tilde{C}_v$ measured by HS–SPME, for samples with $C_{tot} = 0.204$ mM at 15˚C. On the horizontal axis are values for the total system mole fraction, $\rho/(1+\rho)$, as set independently in our experiments. The theoretical predictions as a function of $\rho/(1+\rho)$ are shown with the solid line in Figure 4.9B, and may be represented by the equations

$$\tilde{C}_v = \begin{cases} \dfrac{K_{vw}}{K_{lipw}^{G} C_v^{w}} x_{lim} & \text{for } \rho/(1+\rho) \leq 0.29\ (gel); \\ 0.85 & \text{for } 0.29 \leq \rho/(1+\rho) \leq 0.77\ (2\text{–}phase); \\ \dfrac{K_{vw}}{K_{lipw}^{F} C_v^{w}} x_{lim} & \text{for } \rho/(1+\rho) \geq 0.77\ (fluid). \end{cases} \tag{4.20}$$

Parameters used for this prediction are given in Table 4.1. In equation 4.20, x_{lim} can be related to ρ by equations 2.9 and 2.10, with $x_{lim} = \tilde{C}_v/v$ and the appropriate partition coefficient for gel (K_{lipw}^{G}) and fluid (K_{lipw}^{F}) phases substituted into v and to obtain $\tilde{C}_v$. The resulting solid line prediction in Figure 4.9B shows very good agreement with our measured values for $\tilde{C}_v$ at various values of $\rho/(1+\rho)$, over fluid, gel, and coexistence regions. The width of the coexistence region is also reasonably consistent with the experimental observations across the measured binary compositions of phospholipid and solute.

The value $K_{lipw}^{G} = 3.7$ mM^{-1} for the gel phase at 15˚C (Table 4.1) is significantly lower than values we obtained in fluid bilayers at higher temperatures. The gel phase is promoted by the favorable potential energy interactions between phospholipid chains in a more ordered state. The limonene solute would interfere with those interactions, and its incorporation into

the gel is therefore less favorable than that into a more disordered fluid bilayer, despite benefits due to mixing entropy. However, the limonene incorporated into the gel does significantly shift the onset of gel formation within the bilayer. In section 4.3.4.1, the bilayer composition for the gel to start forming from the fluid phase was estimated as $x_{lim} = 1 - x_{PL}^{*} = 0.33$, where in this estimate any limonene partitioning into the gel phase was neglected. By including limonene partitioning into the gel phase, a lower phospholipid mole fraction ($x_{PL}^{F*} = 0.63$) and a higher limonene mole fraction of $x_{lim}^{F*} = 0.37$ is instead obtained for this transition.

The large difference in K_{lipw} for the gel versus fluid phase of DMPC is consistent with reported literature. For anaesthetics, which partition into the gel phase of DPPC, Kaminoh et al.[95] used a similar analysis to that used to derive equation 4.19 and extended it to calculate partition coefficients in the gel and fluid phases based on the measured decrease in the phase transition temperature. They calculated lower partition coefficients in the gel phase, (approximately a two-fold decrease) in agreement with low solubilization observed experimentally. Simon et al.,[55] and de Young and Dill[81] both observed that the K_{lipw} values of benzene decreased by a factor of three or more below T_G for DMPC.

Our gel K_{lipw} values for limonene represent partitioning into the P_β ripple gel phase. At low enough temperatures, there should be another transition into the L_β gel phase which was not analysed in our experiments. van Wezel et al.[80] shows that for most of the chlorinated benzenes partitioning into DPPC vesicles, not only does K_{lipw} decrease 1–2 orders of magnitude from the L_α fluid phase to P_β, but also decreases a further order of magnitude from the P_β to L_β, where the bilayer is most ordered. Thus, it is possible that even lower temperatures will lead to further decreases in K_{lipw} for limonene in the bilayer.

Using K_{lipw}^{G}, $K_{F,G}$, and equations 4.18 and 4.19, a value of $K_{lipw}^{F} = 23.5\ \mathrm{mM}^{-1}$ was calculated for the partitioning into the fluid phase of the bilayer. This partition coefficient is

significantly higher than that measured for DMPC at higher temperatures, perhaps reflecting enthalpic contributions from the bilayer gel–to–fluid transition, which are captured in $K_{F,G}$. As discussed in Chapter 1, the partition coefficients K_{lipw} represent the Gibbs energy change between a solute in the bilayer and that in the aqueous solvent, in both cases at infinite dilution (equation 2.9). Since here the bilayer exists in different phases depending on its binary composition, the partition coefficients K_{lipw}^{F} and K_{lipw}^{G} reflect effects relative to different reference chemical potentials, namely at infinite dilution of solute within the fluid or gel bilayer, respectively. Physically, one can think of a solute molecule moving from water to the gel bilayer at infinite dilution, then experiencing a change in state from gel to fluid bilayer to create a lower reference chemical potential compared to that associated with higher temperatures.

4.3.4.3.2 High $C_{tot} = 0.6$ mM at 15ºC

Equilibrium experimental measurements on vials with a total $C_{tot} = 0.618$ mM should follow the same thermodynamic predictions at 15˚C, as reflected by the vapor concentration as a function of mole fraction of limonene within the bilayer. In Figure 4.10 data from vials with low (0.204 mM) and high (0.618 mM) limonene concentrations are compared with the theory discussed above. To make this comparison, the vapor concentration is now normalized by the same reference, namely the vapor concentration C_v^o above pure limonene, yielding the ratio $\hat{C}_v = C_v/C_v^o$. This reference concentration was measured in the same vial sets as our sample vials, and was predicted theoretically from the solubility of limonene in water (assumed unchanged from 23˚C), and K_{vw} (Table 2.2).

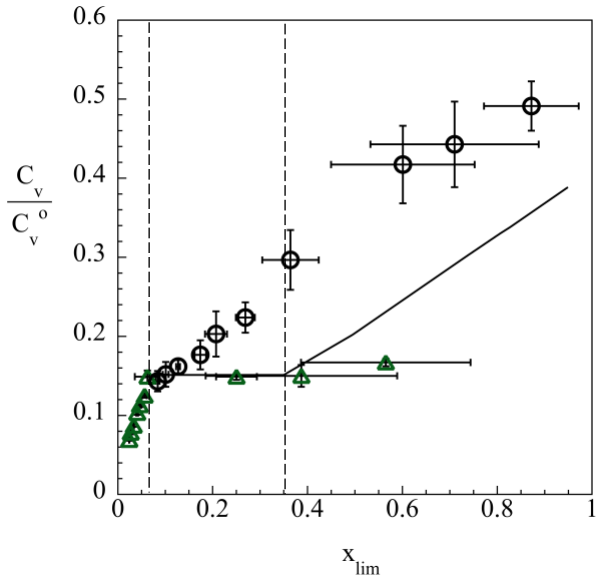

Figure 4.10: Vapor phase concentrations, $\hat{C}_v$, versus mole fraction x_{lim} for 0.204 mM (△) or 0.618 mM (○) limonene and DMPC vesicles at 15˚C. Vertical dashed lines represent transitions from the gel → gel/fluid → fluid phases and the solid black line represents theoretical prediction of $\hat{C}_v$.

On the x-axis of Figure 4.10 is plotted mole fractions within the bilayer, obtained from a solute mole balance: the limonene amount in the vapor phase (measured or predicted) and dissolved directly in water was subtracted from the total amount added to the vial to obtain the moles in the bilayer. The latter is combined with the known phospholipid moles in the vial to determine the mole fraction x_{lim}.

Given the finite limonene solubilized in the gel, here we do not make the assumption that $x_{lim} = \rho/(1+\rho)$, in order to make a more accurate estimate for x_{lim} than that used to find x_{PL}^* in equation 4.5. n_{lim} is calculated with equation 4.11, using the measured value for $\tilde{C}_v$. x_{lim} is then calculated using $n_{lim}/(n_{lim}+n_{PL})$, where $n_{PL} = C_{PL}V_w$ is the moles of phospholipid in the sample. The error, $\sigma_{x_{lim}}$, in x_{lim} is determined by propagating the error in $\tilde{C}_v$. The error in n_{tot} and n_{PL} (from syringe volumes in microliters) are small relative to the error in $\tilde{C}_v$ and therefore we calculate $\sigma_{x_{lim}}$ as the error, $\sigma_{\tilde{C}_v}$, in $\tilde{C}_v$, multiplied by the derivative of the equation used for x_{lim},

$$\sigma_{x_{lim}} = \sigma_{\tilde{C}_v} \left| \frac{d}{d\tilde{C}_v} x_{lim} \right|, \tag{4.12}$$

with the derivative being

$$\frac{d}{d\tilde{C}_v} x_{lim} = \frac{-n_{tot} n_{PL}}{\left(n_{tot} - n_{tot}\tilde{C}_v + n_{PL}\right)^2}. \tag{4.13}$$

For low concentrations of phospholipid, when there is more limonene in the vapor phase, the error in $\tilde{C}_v$ is typically larger, magnifying the uncertainty in x_{lim}.

It is observed from the comparison in Figure 4.10 that $\hat{C}_v$ data for 0.618 mM vials at the three lowest mole fractions compare reasonably well with the theory, which would indicate that these compositions are near the onset of the gel–fluid coexistence. However, data at higher mole fractions are not constant as expected for the two-phase region, but increase nearly linearly with x_{lim}. $\sigma_{x_{lim}}$ is also significantly larger for higher mole fractions, showing an increase in variability. We can make a more robust comparison between the theory and the experimental data when $\tilde{C}_v$ is plotted versus $\rho/(1+\rho)$ rather than the calculated x_{lim}, due to the dependence of x_{lim} on the measured peak areas. This discrepancy seems likely to be an effect of hysteresis, suggesting that the samples have not reached equilibrium within the time available. This explanation is supported by the poor reproducibility for these 0.618 mM samples, both within the sample set on a single run, and between multiple replicate sample sets. Typically, relative standard deviations (RSD) for both replicate sets and triplicates are <12%. However, for these 0.6 mM samples, the RSD was much higher, often >20%. Data from three replicate sets are shown in Figure 4.11.

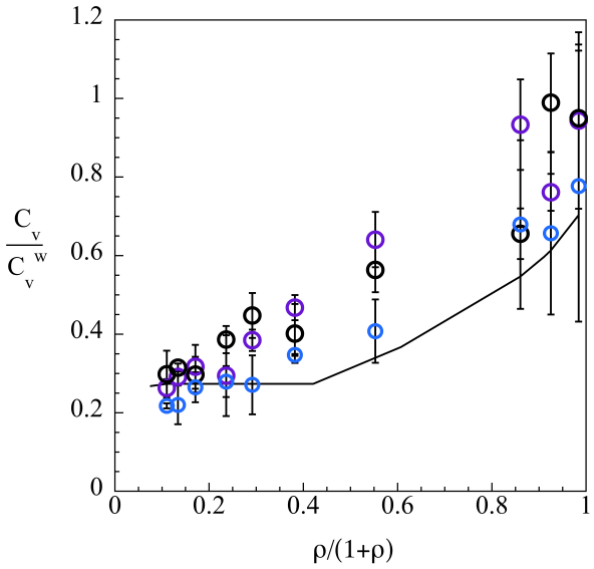

Figure 4.11: Unusually high variability, likely due to hysteresis, in measured vapor phase concentrations of limonene with DMPC vesicles at 15ºC, when $C_{tot} = 0.618$ mM. Different colors (○,○,○) represent different replicate sets, and black line represents prediction of equation 4.20.

Replicates exhibited lower standard deviations at the lowest mole ratios of limonene, where results fell close to the lower end of the coexistence region. Interestingly, the third replicate (blue) showed behavior that was more consistent with the predicted coexistence region, but was not reproduced in the other data sets. If limonene is not at equilibrium at higher mole ratios, in what should be the gel/fluid coexistence and fluid only regions, the apparent partitioning behavior will deviate strongly from theoretical predictions. Because the HS–SPME measurements are conducted over several hours within a sample set, with randomized sample order, it would seem plausible that the poor reproducibility shows the effect of varied time on the limonene distribution—an indication that equilibrium has not been reached. It is possible that much longer equilibration times are needed due to the ordered structure of the gel phase.

To test this hypothesis, we made 1 mM DMPC samples with 0.618 mM limonene, and changed the equilibration method. For one set of samples, limonene was added and the vial was shaken for 3 h at 15ºC. The other set followed our standard procedure: limonene was added

and shaken at room temperature. In both protocols, samples sat for >1 h at 15ºC before sampling. The differences in the vapor phase concentrations are reported in Table 4.5.

Table 4.5: Effects of Preparation Temperature on Vapor Phase Concentration Ratio of 0.6 mM Limonene in 0.1 mM DMPC

Sample preparation	$\tilde{C}_v$
limonene added at room temp	0.514±0.03
limonene added at 15ºC	0.574±0.028

The samples prepared entirely at 15ºC had a higher vapor phase concentration and therefore less limonene in the bilayer. Although both sets of samples spent at least 4 hours sitting at 15ºC before sampling, they did not end up with the same vapor phase concentration of limonene. The ambient temperatures used in the shaking process and the randomized sample order does not appear to have had an impact on the results for low mole ratios of limonene, or for vesicles entirely in the fluid phase. However, for higher mole ratios of limonene, at low temperatures, there are differences in the amount of limonene partitioning into the bilayer. Longer equilibration times for vesicles in the gel phase has been reported by van Wezel et al.[80] who studied the partitioning of chlorobenzenes between DPPC vesicles and water, using separated compartments of water and vesicle dispersions. The typical equilibration time for vesicles in the fluid phase, above $T_G = 41.5$ºC, was 7 days or less. However, for lower temperatures, longer equilibration times were needed. At 30ºC ($\Delta T = 12.5$ºC), the equilibration time was 10 days.[80]

4.3.4.3.3 Results at 20ºC

A comparison between the theory and the data was also made for experiments done at 20ºC, using 0.093 and 0.618 mM limonene. For the data at 0.093 mM limonene, by fitting the data points for $C_{PL} \geq 0.5$ mM, we obtained $K_{lipw}^{G} = 3.6\ \text{mM}^{-1}$ (Figure 4.12A). The constant

vapor concentration for limonene in the fluid/gel coexistence region, $\tilde{C}_v^*$, was found to be 0.95 using equation 2.9 ($C_v^* = 0.0075$ mM). The coexistence region starts from $x_{lim}^{G*} = 0.024$ and the transition to the fluid phase was predicted to occur for $C_{PL} \leq 0.05$ mM, corresponding to $x_{lim} \geq x_{lim}^{F*} = 0.20$. This transition was obtained using $K_{F,G}$= 0.82 and equation 4.18 (Table 4.4).

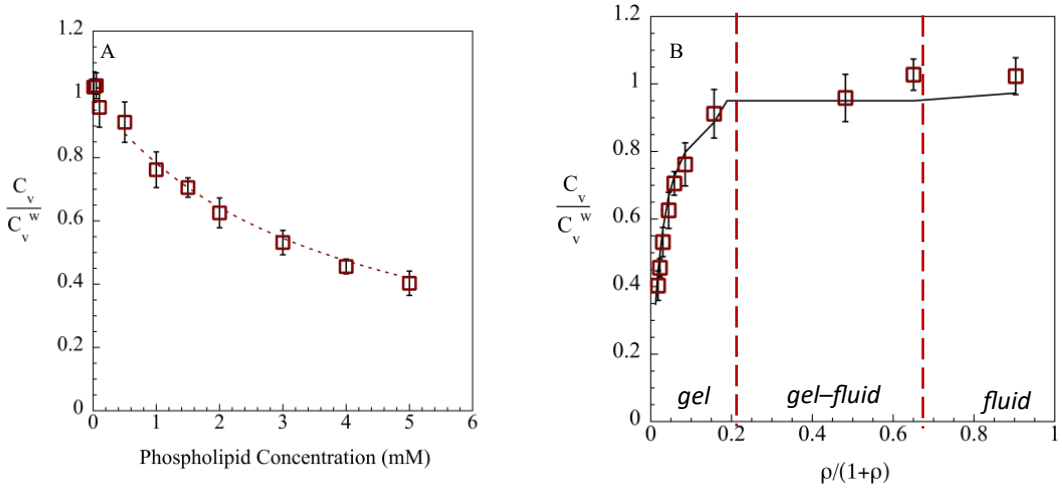

Figure 4.12: Vapor phase concentrations, $\tilde{C}_v$, with respect to (A) phospholipid concentration, and (B) mole ratio of limonene to phospholipid, for 0.093 mM limonene and DMPC vesicles at 20ºC. Lines represent (A) nonlinear regression fit for K_{lipw} and (B) prediction of equation 4.21.

Figure 4.12B shows comparisons of the predictions and measured $\tilde{C}_v$ values with the theoretical predictions represented by the equations

$$\tilde{C}_v = \begin{cases} \dfrac{K_{vw}}{K_{lipw}^{G} C_v^{w}} x_{lim} & \text{for } \rho/(1+\rho) \leq 0.19\ (gel); \\ 0.95 & \text{for } 0.19 \leq \rho/(1+\rho) \leq 0.65\ (2\text{–}phase); \\ \dfrac{K_{vw}}{K_{lipw}^{F} C_v^{w}} x_{lim} & \text{for } \rho/(1+\rho) \geq 0.65\ (fluid). \end{cases} \quad (4.21)$$

As with the data at 15ºC for 0.204 mM limonene, the solid line prediction is in very good agreement with measured values for $\tilde{C}_v$.

A comparison of these low limonene results to experiments done using 0.618 mM limonene at 20ºC is shown in Figure 4.13, here normalized by the vapor phase concentration of pure limonene, C_v^o. The data for 0.093 mM limonene agrees very well with the prediction, showing partitioning into the gel phase. Although the entire data set for 0.618 mM could be fit to obtain a constant partition coefficient, based on the theory of equation 4.21, the four vials with the lowest mole fractions should in fact be in the gel/fluid coexistence region.

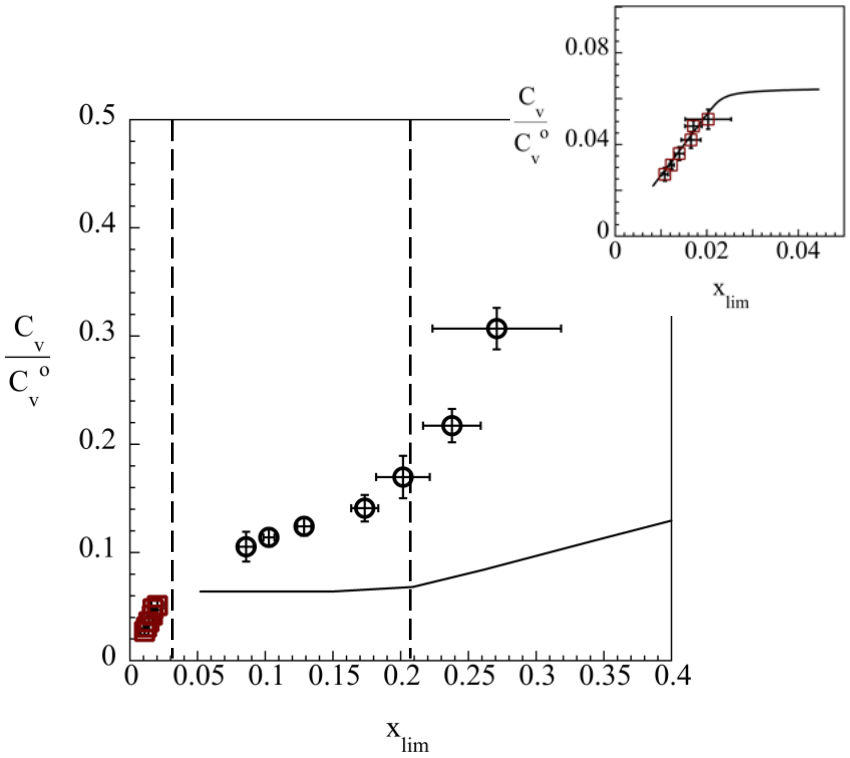

Figure 4.13: Vapor phase concentration, $\hat{C}_v$, versus mole fraction in DMPC vesicles with 0.093 mM (□) or 0.618 mM limonene (○) at 20˚C. Vertical dashed lines represent transitions from the gel → gel/fluid → fluid phases and the solid line represents prediction of C_v^o from equation 4.21.

Note that in Figure 4.13, the data point at the highest mole fractions in each data set was excluded. The ρ ranges of excluded points were 6–61.8 for 0.6 mM limonene and 0.2–9.3 for 0.093 mM limonene. For these points, phospholipid concentrations were very low, and variability in the vapor measurements led to some values of $\tilde{C}_v > 1$, causing aphysical results for our calculated x_{lim}. $\hat{C}_v$ values for the 0.618 mM limonene data in the coexistence region

are observed in Figure 4.13 to be higher than predicted from equation 4.21. However, the range of mole fractions in the coexistence region corresponds to $\hat{C}_v$ values that only weakly increase with x_{lim}, showing a break to a steeper increase as the fluid phase region is entered. These observations are consistent with an effect of hysteresis at lower temperature and higher total limonene conditions where equilibration might take longer.

As with the data at 15ºC, the theoretical prediction for K_{lipw}, in the fluid phase at 20ºC, 30 mM^{-1}, obtained using K_{lipw}^{G}, $K_{F,G}$, and equations 4.18–4.19, is higher than what is experimentally observed at temperatures $\geq$ 25ºC. Interestingly, excluding data points above $C_{PL} = 0.204$ mM, where the coexistence region begins in Figure 4.2, leads to $K_{lipw} = 10.571 \pm 1.17$ mM^{-1} (Table 4.1), which is closer to the K_{lipw} calculated for the fluid phase at higher temperatures where no gel phase forms. However, these values are likely affected by hysteresis and should eventually evolve to a higher K_{lipw}^{F} value. These observations might suggest that the observed large K_{lipw}^{F} value at low temperatures result from slow organizational rearrangements upon cooling. An understanding of the phase behavior is thus important to understand in designing experiments to calculate partition coefficients accurately.

With improved theory for the changes in the phase transition temperature, we can map out the phase behavior of DMPC with added limonene using the predictions for x_{lim} in the gel and fluid phases at 15 and 20ºC. These predictions are based on K_{lipw} values calculated using HS–SPME and capture partitioning into the gel phase that was neglected when using freezing point depression theory. The resulting phase diagram is presented in Figure 4.14, which shows the mole fraction ranges associated with gel, fluid, and gel/fluid coexistence regions. The coexistence region widens as the temperature is lowered from 25 to 15ºC. There is also an increase in the range of x_{lim} where partitioning is observed into the gel phase. The predictions based on freezing point depression are presented as squares and represent the transition from the fluid phase to the gel/fluid coexistence region. For this transition, the values of x_{lim} are

similar for both theories. However, the graph is shifted to the left when freezing point depression is used, as the mole fractions in the gel phase are assumed to be zero.

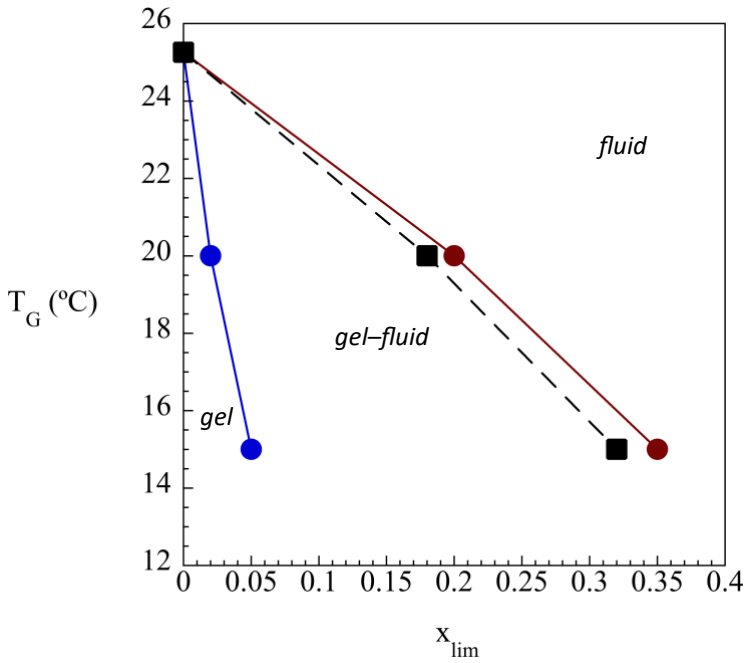

Figure 4.14: Effects of limonene mole fraction in the bilayer on the phase behavior of DMPC from 15 to 25ºC. Calculations are done with (■) and without (●) partitioning into the gel phase.

4.3.5 Temperature vs Fluidity Effects on Solubilization Behavior

Given that concentrations of limonene need to be low to observe solubilization in the gel phase beyond the coexistence region, a concentration of 0.093 mM limonene was chosen for fluid and gel partitioning comparisons. Experiments at 20 and 28ºC and higher limonene concentrations, described in section 4.3.2, were repeated with this lower concentration. Results from these experiments are showed in Figure 4.15. At 28ºC, the lipid–water partition coefficient found using 0.093 mM limonene is 8.396±0.574 mM^{-1}, consistent with expectations for partitioning into the fluid phase. However, at 20ºC, there is a clear difference in solubilization behavior for the 0.093 mM limonene data, with a curve that is much less steep. The higher vapor phase limonene concentrations here indicate decreased partitioning between

the lipid and water phases. For this 20ºC data, the K_{lipw} obtained is 3.642±0.331 mM^{-1}, less than half of the value determined for 28ºC results.

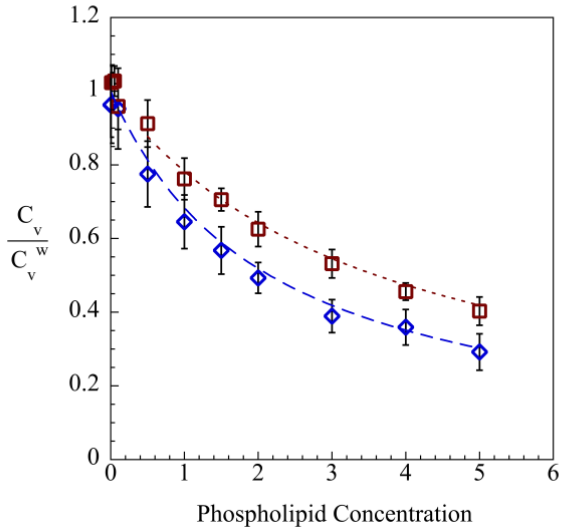

Figure 4.15: Vapor phase concentrations, $\tilde{C}_v$, with respect to phospholipid concentration for 0.093 mM limonene in DMPC vesicles at 28ºC (◇) and 20ºC (□). Curves represent nonlinear regression fits of K_{lipw}.

In contrast, for 0.618 mM limonene at those same temperatures, the difference in K_{lipw} values was much smaller: from 13.19 mM^{-1} at 28ºC to 10.57 mM^{-1} at 20ºC. Due to hysteresis in cooled samples, at 20ºC, it is likely that the system is still not at equilibrium, and the actual K_{lipw} value is higher. It is interesting to compare results for DMPC with the experiments done with lecithin at 20–28ºC. As lecithin is made up of almost entirely (~85%) unsaturated fatty acid tails, its resulting phase transition temperature is below 0ºC.[96] Figure 4.16 shows the vapor phase concentrations for 0.618 mM limonene at 20, 25 and 28ºC. The partitioning behavior is very similar to what we see for fluid phase DMPC, with a steep decrease in $\tilde{C}_v$, and associated K_{lipw} values that are on the order of 10^4 M^{-1} (Table 4.6). Figure 4.17 shows how K_{lipw} changes with temperature for DMPC and lecithin with 0.618 mM limonene. For these samples, above the gel transition temperature, there is some enhanced partitioning with temperature, as the

K_{lipw} values increase by ~25% from 20 to 28ºC for DMPC and ~10% from 20 to 28ºC for lecithin. In contrast, when comparing vesicles in the gel and fluid phases over similar temperature ranges, K_{lipw} increased by ~140%. This increase is in line with observations from de Young and Dill,[56] and Simon et al.,[55] where the gel phase has a much higher impact on solubilization than does the temperature within a single-phase region.

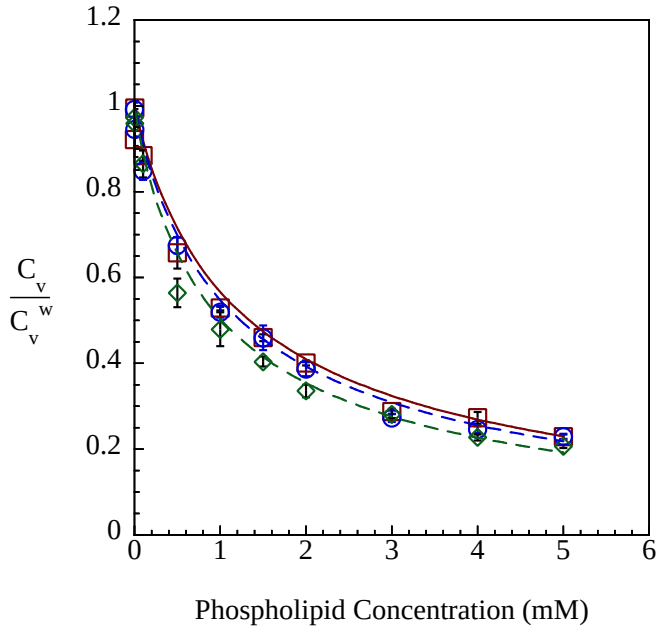

Figure 4.16: Vapor phase concentrations, $\tilde{C}_v$, with respect to phospholipid concentration for 0.618 mM limonene above lecithin dispersions at 20ºC (◇), 25ºC (○) and 28ºC (□). Curves represent nonlinear regression fits of K_{lipw}.

Table 4.6: Partition Coefficients (K_{lipw}) of 0.618 mM Limonene in Sunlipon™ 90 Lecithin Vesicles at Different Temperatures

Size (nm)	<Size> (nm)[a]	T (°C)	K_{lipw}	R^2	$<K_{lipw}>$	$<\widehat{K}_{lipw}> \times 10^5$
234±1.7			11.34±0.76	0.9749		
234.6±1.1	231.7±2.6	20	8.076±6.882	0.9688	10.13±0.46	5.614±0.254
226.4±2.6			10.45±0.76	0.9745		
229.5±2.3			10.55±0.53	0.9834		
221.9±2.4	231±5.8	25	10.29±0.86	0.9839	10.66±0.43	5.905±0.236
241.7±6.1			12.01±1.24	0.9901		
231.9±4.4			11.15±0.10	0.9787		
238.7±5.5	234.3±2.2	28	10.82±0.54	0.9767	11.25±0.45	6.236±0.249
232.3±1.8			14.12±1.35	0.9399		

[a]Errors are standard error of the mean

[b]Nonlinear regression weighted by $1/\sigma^2$, where σ represents the standard deviation of the replicates

[c]$<\widehat{K}_{lipw}>$ values are of order 10^5

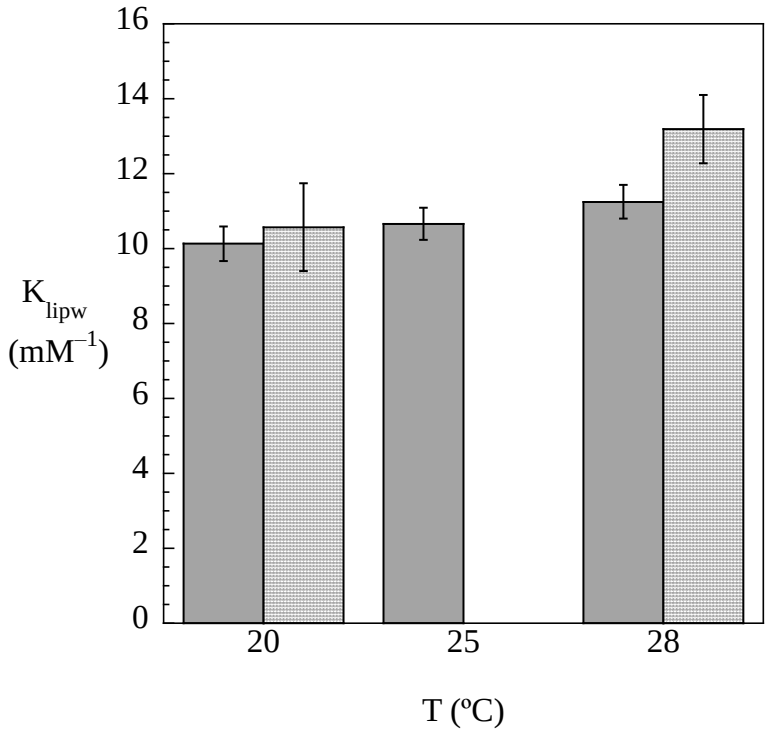

Figure 4.17: Lipid–water partition coefficients of lecithin (dark grey) and DMPC (light grey) for different temperatures.

4.4 Conclusion

Through DSC experiments, limonene has been shown to lower the phase transition temperature of DMPC vesicles. The decrease in T_G occurs linearly with an increase in limonene mole fraction, in a manner consistent with freezing point depression theory. This decrease reflects increased disorder in the gel phase of the bilayer with the incorporation of limonene. As a result, solubilization of limonene by the bilayer results in a range of phases; a gel phase at very small x_{lim}, a gel/fluid coexistence phase, and a fluid phase at high x_{lim}. The coexistence region is characterized by constant limonene vapor phase concentrations, where the chemical potentials of limonene in both phases are equivalent. K_{lipw} for limonene in the gel phase of the bilayer is decreased more than two-fold in comparison to K_{lipw} in the fluid phase. This difference is much more drastic than effects of temperature above T_G. With evidence of partitioning in the gel phase, the freezing point depression model, which assumes the gel phase is pure, can be modified to predict the solubilization behavior of limonene. At low total limonene concentrations the experimental data agrees with the theory quite well, but there are deviations at higher concentrations, likely due to effects of hysteresis.

4.5 Nomenclature

C_p	heat capacity at constant pressure
C_{PL}	phospholipid concentration in water
C_{tot}	n_{tot}/V_w, total moles of limonene in sample, divided by volume of water
C_v^o	vapor phase concentration of limonene above pure reference
C_v^w	vapor phase concentration of limonene above water
C_v	vapor phase concentration of limonene above vesicle dispersion
$\tilde{C}_v^*$	vapor phase concentration of limonene in coexistence region

$\tilde{C}_v$	$\frac{C_v}{C_v^w}$
$\hat{C}_v$	C_v/C_v^o
dq_p	change in heat at constant pressure
ΔG	Gibbs free energy
ΔH	enthalpy change or excess enthalpy
$\Delta_{F\to G}\overline{H}^o$	enthalpy change of pure phospholipid in the direction of cooling
$\Delta\overline{H}_{DMPC}$	molar enthalpy change of DMPC
$\Delta H_{m,dispersion}$	specific enthalpy change of the dispersion
$\Delta\overline{H}^o_{DMPC}$	molar enthalpy change of pure DMPC
ΔH_m	specific enthalpy change, i.e. enthalpy change per mass
$K_{F,G}$	x_{PL}^F/x_{PL}^G in the coexistence region
K_{lipw}	vesicle phospholipid–water partition coefficients
k	Boltzmann's constant
k_p	proportionality constant of limonene in the GC column
K_{vw}	vapor–water partition coefficient
m_f	mass fraction of DMPC in water
m_{water}	mass of water in DSC samples
MW_{PL}	molecular weight of DMPC
n_{lim}	moles of limonene inside the fluid bilayer
n_{PL}	moles of phospholipid in sample
n_{tot}	total moles of limonene in sample
$\Delta_{F\to G}\bar{S}^o$	entropy change of pure phospholipid in the direction of cooling
$\Delta\bar{S}_{DMPC}$	molar entropy change of DMPC

$\Delta\bar{S}^{o}_{DMPC}$	molar entropy change of pure DMPC
T^{o}_{G}	phase transition temperature of pure phospholipid
T_G	phase transition temperature
ΔT	change in T^{o}_{G} with addition of solute, $T^{o}_{G} - T_G$
V_v	vapor volume
V_w	water volume
$\hat{V}$	$1 + \frac{K_{vw}V_v}{V_w}$
x^{F}_{lim}	mole fraction of limonene inside the fluid phase of the bilayer
x^{F*}_{lim}	x^{F}_{lim} at the end of the coexistence region
x^{G}_{lim}	mole fraction of limonene inside the gel phase of the bilayer
x^{G*}_{lim}	x^{G}_{lim} at the start of the coexistence region
x_{lim}	mole fraction of limonene inside the fluid bilayer
x^{*}_{PL}	critical mole fraction of phospholipid inside the bilayer at the phase transition
x^{F}_{PL}	mole fraction of phospholipid inside the fluid phase of the bilayer
x^{F*}_{PL}	x^{F}_{PL} at the end of the coexistence region
x^{G}_{PL}	mole fraction of phospholipid inside the gel phase of the bilayer
x_{PL}	mole fraction of phospholipid inside the bilayer
μ^{F}_{PL}	chemical potential of the phospholipid in the fluid phase
μ^{Fo}_{PL}	chemical potential of pure phospholipid in the fluid phase
μ^{G}_{PL}	chemical potential of the phospholipid in the gel phase
μ^{Go}_{PL}	chemical potential of pure phospholipid in the gel phase
μ_{PL}	chemical potential of the phospholipid
ν	$\frac{K_{vw}V_v + V_w}{V_w K_{lipw} C_{tot}}$

ρ	total limonene to phospholipid mole ratio in sample
ρ^{bi}	mole ratio of limonene to phospholipid in the bilayer
$\sigma_{\tilde{C}_v}$	error in the measured $\tilde{C}_v$ ratio
$\sigma_{x_{lim}}$	error associated with x_{lim}

References

(1) Livney, Y. D. Nanostructured Delivery Systems in Food: Latest Developments and Potential Future Directions. *Curr Opin Food Sci* **2015**, *3*, 125–135. https://doi.org/10.1016/j.cofs.2015.06.010.

(2) Domingo, C.; Saurina, J. An Overview of the Analytical Characterization of Nanostructured Drug Delivery Systems: Towards Green and Sustainable Pharmaceuticals: A Review. *Anal Chim Acta* **2012**, *744*, 8–22. https://doi.org/10.1016/J.ACA.2012.07.010.

(3) Weel, K. G. C.; Boelrijk, A. E. M.; Burger, J. J.; Jacobs, M. A.; Gruppen, H.; Voragen, A. G. J.; Smit, G. Effect of Emulsion Properties on Release of Esters under Static Headspace, in Vivo, and Artificial Throat Conditions in Relation to Sensory Intensity. *J Agric Food Chem* **2004**, *52* (21), 6572–6577. https://doi.org/10.1021/jf0494985.

(4) Van Ruth S.M.; King, C.; Giannouli, P. Influence of Lipid Fraction, Emulsifier Fraction, and Mean Particle Diameter of Oil-in-Water Emulsions on the Release of 20 Aroma Compounds. *J Agric Food Chem* **2002**, *50* (8), 2365–2371. https://doi.org/10.1021/jf011072s.

(5) Ubbink, J.; Schoonman, A. Flavor Delivery Systems. In *Kirk-Othmer Encyclopedia of Chemical Technology*; John Wiley & Sons, 2003; pp 527–563. https://doi.org/10.1002/0471238961.0612012221020209.a01.

(6) Modi, S.; Anderson, B. D. Determination of Drug Release Kinetics from Nanoparticles: Overcoming Pitfalls of the Dynamic Dialysis Method. *Mol Pharm* **2013**, *10* (8), 3076–3089. https://doi.org/10.1021/mp400154a.

(7) Duclairoir, C.; Orecchioni, A. M.; Depraetere, P.; Osterstock, F.; Nakache, E. Evaluation of Gliadins Nanoparticles as Drug Delivery Systems: A Study of Three

Different Drugs. *Int J Pharm* **2003**, *253* (1–2), 133–144. https://doi.org/10.1016/S0378-5173(02)00701-9.

(8) Bueno, V.; Gao, X.; Abdul Rahim, A.; Wang, P.; Bayen, S.; Ghoshal, S. Uptake and Translocation of a Silica Nanocarrier and an Encapsulated Organic Pesticide Following Foliar Application in Tomato Plants. *Environ Sci Technol* **2021**, *2022*, 6722–6732. https://doi.org/10.1021/acs.est.1c08185.

(9) Bisset, N. B.; Webster, G. R.; Dong, Y. D.; Boyd, B. J. Understanding the Kinetic Mixing between Liquid Crystalline Nanoparticles and Agrochemical Actives. *Colloids Surf B Biointerfaces* **2019**, *175*, 324–332. https://doi.org/10.1016/J.COLSURFB.2018.11.063.

(10) Fathi, M.; Mozafari, M. R.; Mohebbi, M. Nanoencapsulation of Food Ingredients Using Lipid Based Delivery Systems. *Trends Food Sci Technol* **2012**, *23* (1), 13–27. https://doi.org/10.1016/j.tifs.2011.08.003.

(11) Nakagawa, K. Nano- and Microencapsulation of Flavor in Food Systems. In *Nano- and Microencapsulation for Foods*; Kwak, H.-S., Ed.; John Wiley & Sons, 2014; pp 249–271. https://doi.org/10.1002/9781118292327.ch10.

(12) Small, D. M.; Prescott, J. Odor/Taste Integration and the Perception of Flavor. *Exp Brain Res* **2005**, *166* (3–4), 345–357. https://doi.org/10.1007/s00221-005-2376-9.

(13) Saini, A.; Panwar, D.; Panesar, P. S.; Bera, M. B. Encapsulation of Functional Ingredients in Lipidic Nanocarriers and Antimicrobial Applications: A Review. *Environ Chem Lett* **2021**, *19* (2), 1107–1134. https://doi.org/10.1007/s10311-020-01109-3.

(14) Premjit, Y.; Pandhi, S.; Kumar, A.; Rai, D. C.; Duary, R. K.; Mahato, D. K. Current Trends in Flavor Encapsulation: A Comprehensive Review of Emerging Encapsulation

Techniques, Flavour Release, and Mathematical Modelling. *Food Res Int* **2022**, *151*, 110879. https://doi.org/10.1016/j.foodres.2021.110879.

(15) Ammari, A.; Schroen, K. Flavor Retention and Release from Beverages: A Kinetic and Thermodynamic Perspective. *J Agric Food Chem*. **2018**, *66*, 9869–9881. https://doi.org/10.1021/acs.jafc.8b04459.

(16) Ollivon, M. Lipid–Flavour Interactions. In *Flavour in Food*; Voilley, A., Etiévant, P., Eds.; Woodhead Publishing Limited, 2006; pp 133–155. https://doi.org/10.1533/9781845691400.2.133.

(17) *Title 21–Food and Drugs Chapter I–Food and Drug Administration, Department of Health and Human Services Subchapter B–Food for Human Consumption*. https://www.ecfr.gov/current/title-21/chapter-I/subchapter-B/part-184 (accessed 2023-11-16).

(18) Assadpour, E.; Jafari, S. M. An Overview of Lipid-Based Nanostructures for Encapsulation of Food Ingredients. In *Lipid-Based Nanostructures for Food Encapsulation Purposes*; Jafari, S. M., Ed.; Academic Press, 2019; pp 1–34. https://doi.org/10.1016/B978-0-12-815673-5.00001-5.

(19) Guichard, E. Interactions between Flavor Compounds and Food Ingredients and Their Influence on Flavor Perception. *Food Rev Int* **2002**, *18* (1), 49–70. https://doi.org/10.1081/FRI-120003417.

(20) Guiotto, E. N.; Tomás, M. C.; Diehl, B. W. K. Sunflower Lecithin; In *Polar Lipids;* Moghis, U. A., Xu, X., Eds.; AOCS Press, 2015, pp 57–75. https://doi.org/10.1016/B978-1-63067-044-3.50007-8.

(21) Cui, L.; Decker, E. A. Phospholipids in Foods: Prooxidants or Antioxidants? *J Sci Food Agric* **2016**, *96* (1), 18–31. https://doi.org/10.1002/JSFA.7320.

(22) Israelachvili, J. N. *Intermolecular and Surface Forces*; Elsevier Science, 2015, pp 538–547.

(23) Aguilar, L. F.; Sotomayor, C. P.; Lissi, E. A. Main Phase Transition Depression by Incorporation of Alkanols in DPPC Vesicles in the Gel State: Influence of the Solute Topology. *Colloids Surf A* **1996**, *108*, 287–293. https://doi.org/10.1016/0927-7757(95)03424-2.

(24) El Maghraby, G. M. M.; Williams, A. C.; Barry, B. W. Interactions of Surfactants (Edge Activators) and Skin Penetration Enhancers with Liposomes. *Int J Pharm* **2004**, *276* (1–2), 143–161. https://doi.org/10.1016/j.ijpharm.2004.02.024.

(25) Mendanha, S. A.; Alonso, A. Effects of Terpenes on Fluidity and Lipid Extraction in Phospholipid Membranes. *Biophys Chem* **2015**, *198*, 45–54. https://doi.org/10.1016/j.bpc.2015.02.001.

(26) Kwon, J. H.; Liljestrand, H. M.; Katz, L. E.; Yamamoto, H. Partitioning Thermodynamics of Selected Endocrine Disruptors between Water and Synthetic Membrane Vesicles: Effects of Membrane Compositions. *Environ Sci Technol* **2007**, *41* (11), 4011–4018. https://doi.org/10.1021/es0618200.

(27) Dulfer, W. J.; Covers, H. A. J. Membrane–Water Partitioning of Polychlorinated Biphenyls in Small Unilamellar Vesicles of Four Saturated Phosphatidylcholines. *Environ Sci Technol* **1995**, *29*, 2548–2554.

(28) Pawliszyn, J.; Pawliszyn, B.; Pawliszyn, M. Solid Phase Microextraction (SPME). *Chem Educator* **1997**, *2* (4), 1–7. https://doi.org/10.1007/s00897970137a.

(29) Dean, J. R. *Extraction Techniques in Analytical Sciences*; Analytical Techniques in the Sciences; Wiley, 2010, 85–116. https://doi.org/10.1002/9780470682494.ch4.

(30) *Solid Phase Microextraction Fundamentals*; 2023. https://www.agilent.com/cs/library/technicaloverviews/public/te-solid-phase-microextraction-fundamentals-spme-arrow-5994-5775en-agilent.pdf

(31) Yang, S.-C. Kinetic Study of Limonene Extraction from Water Using Solid Phase Microextraction, MS Thesis, University of California, Davis, 2014.

(32) Lloyd, N. W. Partitioning and Transport In Complex Nano-Structured Systems: Gradient Diffusion of Ionic Micelles In Gels and Partitioning of Hydrophobic Aroma Compounds, PhD Dissertation, University of California, Davis, 2010.

(33) Pino, V.; Ayala, J. H.; González, V.; Alfonso, A. M. Solid-Phase Microextraction Coupled to Gas Chromatography/Mass Spectrometry for Determining Polycyclic Aromatic Hydrocarbon–Micelle Partition Coefficients. *Anal Chem* **2004**, *76* (15), 4572–4578. https://doi.org/10.1021/ac049915c.

(34) Escher, B. I.; Berg, M.; Mühlemann, J.; Schwarz, M. A. A.; Hermens, J. L. M.; Vaes, W. H. J.; Schwarzenbach, R. P. Determination of Liposome/Water Partition Coefficients of Organic Acids and Bases by Solid-Phase Microextraction. *Analyst* **2002**, *127* (1), 42–48. https://doi.org/10.1039/b109355j.

(35) Karman, A. P. Solubilization and Partitioning of Aroma Compounds into Short-Chain Lecithin and Nonionic Micelles Measured by Headspace Solid-Phase Microextraction, PhD Dissertation, University of California, Davis, 2022.

(36) Skoog, D. A.; Holler, F. J.; Crouch, S. R. *Principles of Instrumental Analysis*, 6th ed.; Brooks Cole, 2006, 788–811.

(37) Evans, D. F.; Wennerström, H. *The Colloidal Domain: Where Physics, Chemistry, Biology, and Technology Meet,* 2nd ed.; Wiley, 1999, 295–350.

(38) McClements, D. J.; Gumus, C. E. Natural Emulsifiers — Biosurfactants, Phospholipids, Biopolymers, and Colloidal Particles: Molecular and Physicochemical

Basis of Functional Performance. *Adv Colloid Interface Sci* **2016**, *234*, 3–26. https://doi.org/10.1016/j.cis.2016.03.002.

(39) Patel, N.; Schmid, U.; Lawrence, M. J. Phospholipid-Based Microemulsions Suitable for Use in Foods. *J Agric Food Chem* **2006**, *54* (20), 7817–7824. https://doi.org/10.1021/jf051288k.

(40) Taylor, T. M.; Gaysinsky, S.; Davidson, P. M.; Bruce, B. D.; Weiss, J. Characterization of Antimicrobial-Bearing Liposomes by ζ-Potential, Vesicle Size, and Encapsulation Efficiency. *Food Biophys* **2007**, *2* (1), 1–9. https://doi.org/10.1007/s11483-007-9023-x.

(41) Fan, L.; Chen, Q.; Mairiyangu, Y.; Wang, Y.; Liu, X. Stable Vesicle Self-Assembled from Phospholipid and Mannosylerythritol Lipid and Its Application in Encapsulating Anthocyanins. *Food Chem* **2021**, *344*, 128649. https://doi.org/10.1016/j.foodchem.2020.128649.

(42) de Jong, O. G.; Kooijmans, S. A. A.; Murphy, D. E.; Jiang, L.; Evers, M. J. W.; Sluijter, J. P. G.; Vader, P.; Schiffelers, R. M. Drug Delivery with Extracellular Vesicles: From Imagination to Innovation. *Acc Chem Res* **2019**, *52* (7), 1761–1770. https://doi.org/10.1021/acs.accounts.9b00109.

(43) Elsharkasy, O. M.; Nordin, J. Z.; Hagey, D. W.; de Jong, O. G.; Schiffelers, R. M.; Andaloussi, S. EL; Vader, P. Extracellular Vesicles as Drug Delivery Systems: Why and How? *Adv Drug Deliv Rev* **2020**, *159*, 332–343. https://doi.org/10.1016/j.addr.2020.04.004.

(44) Duelund, L.; Amiot, A.; Fillon, A.; Mouritsen, O. G. Influence of the Active Compounds of Perilla Frutescens Leaves on Lipid Membranes. *J Nat Prod* **2012**, *75* (2), 160–166. https://doi.org/10.1021/np200713q.

(45) Matos, C.; Lima, J. L. C.; Reis, S.; Nio Lopes, A.; Bastos, M. Interaction of Antiinflammatory Drugs with EPC Liposomes: Calorimetric Study in a Broad

Concentration Range. *Biophys J* **2004**, *86*, 946–954. https://doi.org/10.1016/S0006-3495(04)74170-3.

(46) Kwon, J. H.; Wuethrich, T.; Mayer, P.; Escher, B. I. Development of a Dynamic Delivery Method for in Vitro Bioassays. *Chemosphere* **2009**, *76* (1), 83–90. https://doi.org/10.1016/j.chemosphere.2009.02.023.

(47) Yamamoto, H.; Liljestrand, H. M. Partitioning of Selected Estrogenic Compounds between Synthetic Membrane Vesicles and Water: Effects of Lipid Components. *Environ Sci Technol* **2004**, *38* (4), 1139–1147. https://doi.org/10.1021/es034311w.

(48) Liu, X.-Y.; Yang, Q.; Kamo, N.; Miyake, J. Effect of Liposome Type and Membrane Fluidity on Drug–Membrane Partitioning Analyzed by Immobilized Liposome Chromatography. *J Chromatogr A* **2001**, *913* (1), 123–131. https://doi.org/10.1016/S0021-9673(00)01266-8.

(49) De Paula, E.; Schreier, S. Use of a Novel Method for Determination of Partition Coefficients to Compare the Effect of Local Anesthetics on Membrane Structure. *Biochim Biophys Acta* **1995**, *1240*, 25–33. https://doi.org/10.1016/0005-2736(95)00155-6.

(50) de Castro, B.; Gameiro, P.; Lima, J. L. F. C.; Matos, C.; Reis, S. Location and Partition Coefficients of Anti-Inflammatory Drugs in EPC Liposomes. A Fluorescence Quenching Study Using n-(9-Anthroyloxy)-Stearic Probes. *Colloids Surf A Physicochem Eng Asp* **2001**, *190* (1), 205–212. https://doi.org/10.1016/S0927-7757(01)00680-X.

(51) Pino, V.; Conde, F. J.; Ayala, J. H.; Afonso, A. M.; González, V. Study of the Interactions between Phenolic Compounds and Micellar Media Using Micellar Solid-Phase Microextraction/Gas Chromatography. *J Chromatogr A* **2005**, *1099* (1–2), 64–74. https://doi.org/10.1016/j.chroma.2005.08.080.

(52) Pino, V.; Afonso, A. M.; Ayala, J. H.; González, V. Micellar Solid-Phase Microextraction for Determining Partition Coefficients of Substituted Polycyclic Aromatic Hydrocarbons in Micellar Media: Possible Prediction of Hydrocarbon–Micelle Behaviour. *Anal Bioanal Chem* **2007**, *387* (6), 2271–2281. https://doi.org/10.1007/s00216-006-1029-6.

(53) van der Heijden, S. A.; Jonker, M. T. O. Evaluation of Liposome–Water Partitioning for Predicting Bioaccumulation Potential of Hydrophobic Organic Chemicals. *Environ Sci Technol* **2009**, *43* (23), 8854–8859. https://doi.org/10.1021/es902278x.

(54) Wishnia, A.; Pinder, T. W. Hydrophobic Interactions in Proteins. The Alkane Binding Site of β-Lactoglobulins A and B. *Biochemistry* **1996**, *5*, 1534–1542.

(55) Simon, S. A.; McDaniel, R. V; McIntosh, T. J. Interaction of Benzene with Micelles and Bilayers. *J Phys Chem* **1982**, *86* (7), 1449–1456.

(56) De Young, L. R.; Dill, K. A. Partitioning of Nonpolar Solutes into Bilayers and Amorphous n-Alkanes. *J Phys Chem* **1990**, *94* (2), 801–809. https://doi.org/10.1021/j100365a054.

(57) Lloyd, N. W.; Kardaras, E.; Ebeler, S. E.; Dungan, S. R. Measuring Local Equilibrium Flavor Distributions in SDS Solution Using Headspace Solid-Phase Microextraction. *J Phys Chem B* **2011**, *115* (49), 14484–14492. https://doi.org/10.1021/jp206984q.

(58) Eleni Kardaras. Partitioning Behavior of Limonene in a Sodium Dodecyl Sulfate Surfactant System, MS Thesis, University of California, Davis, 2006.

(59) Karman, A. P.; Ebeler, S. E.; Nitin, N.; Dungan, S. R. Partitioning, Solubility and Solubilization of Limonene into Water or Short-Chain Phosphatidylcholine Solutions. *J Am Oil Chem Soc* **2021**, *98* (10), 979–992. https://doi.org/10.1002/aocs.12535.

(60) Berger, N.; Sachse, A.; Bender, J.; Schubert, R.; Brandl, M. Filter Extrusion of Liposomes Using Different Devices: Comparison of Liposome Size, Encapsulation

Efficiency, and Process Characteristics. *Int J Pharm* **2001**, *223* (1), 55–68. https://doi.org/10.1016/S0378-5173(01)00721-9.

(61) Hope, M. J.; Bally, M. B.; Webb, G.; Cullis, P. R. Production of Large Unilamellar Vesicles by a Rapid Extrusion Procedure. Characterization of Size Distribution, Trapped Volume and Ability to Maintain a Membrane Potential. *Biochim Biophys Acta* **1985**, *812* (1), 55–65. https://doi.org/10.1016/0005-2736(85)90521-8.

(62) *CRC Handbook of Chemistry and Physics*, 95th ed.; Haynes W. M., Ed.; CRC Press, 2014. https://doi.org/10.1201/b17118.

(63) Lloyd, N. W.; Dungan, S. R.; Ebeler, S. E. Measuring Gas–Liquid Partition Coefficients of Aroma Compounds by Solid Phase Microextraction, Sampling Either Headspace or Liquid. *Analyst* **2011**, *136* (16), 3375–3383. https://doi.org/10.1039/c1an15270j.

(64) Gugliotti, M.; Politi, M. J.; Chaimovich, H. Phase Transition Temperature of Vesicles Determined by Surface Tension Measurements: A Fast Method. *J Colloid Interface Sci* **1998**, *198* (1), 1–5. https://doi.org/10.1006/jcis.1997.5253.

(65) Witzke, S.; Duelund, L.; Kongsted, J.; Petersen, M.; Mouritsen, O. G.; Khandelia, H. Inclusion of Terpenoid Plant Extracts in Lipid Bilayers Investigated by Molecular Dynamics Simulations. *J Phys Chem B* **2010**, *114* (48), 15825–15831. https://doi.org/10.1021/JP108675B.

(66) Duelund, L.; Amiot, A.; Fillon, A.; Mouritsen, O. G. Influence of the Active Compounds of Perilla Frutescens Leaves on Lipid Membranes. *J Nat Prod* **2012**, *75* (2), 160–166. https://doi.org/10.1021/np200713q.

(67) Keller, M.; Kerth, A.; Blume, A. Thermodynamics of Interaction of Octyl Glucoside with Phosphatidylcholine Vesicles: Partitioning and Solubilization as Studied by High

Sensitivity Titration Calorimetry. *Biochim Biophys Acta* **1997**, *1326*, 178–192. https://doi.org/10.1016/S0005-2736(97)00022-9.

(68) Schmid, C.; Steinbrecher, R.; Ziegler, H. Partition Coefficients of Plant Cuticles for Monoterpenes. *Trees* **1992**, *6* (1), 32–36. https://doi.org/10.1007/BF00224496.

(69) Dill, K.; Bromberg, S. *Molecular Driving Forces: Statistical Thermodynamics in Biology, Chemistry, Physics, and Nanoscience*, 2nd ed.; Garland Science, 2010, 283–303.

(70) Yalkowsky, S. H. *Solubility and Solubilization in Aqueous Media*; American Chemical Society, 1999, 236–279.

(71) Niu, S. L.; Litman, B. J. Determination of Membrane Cholesterol Partition Coefficient Using a Lipid Vesicle–Cyclodextrin Binary System: Effect of Phospholipid Acyl Chain Unsaturation and Headgroup Composition. *Biophys J* **2002**, *83* (6), 3408–3415. https://doi.org/10.1016/S0006-3495(02)75340-X.

(72) Takegami, S.; Kitamura, K.; Kitade, T.; Hasegawa, K.; Nishihira, A. Effects of Particle Size and Cholesterol Content on the Partition Coefficients of Chlorpromazine and Triflupromazine between Phosphatidylcholine–Cholesterol Bilayers of Unilamellar Vesicles and Water Studied by Second-Derivative Spectrophotometry. *J Colloid Interface Sci* **1999**, *220*, 81–87. https://doi.org/10.1006/jcis.1999.6505.

(73) Berg, D. P.; Rankin, S. A. Partitioning Behavior of Alkan-1-ols between Milkfat and Aqueous Phases as Influenced by Temperature. *J Agric Food Chem* **2005**, *53* (7), 2646–2651. https://doi.org/10.1021/jf048263q.

(74) Heerklotz, H.; Seelig, J. Correlation of Membrane/Water Partition Coefficients of Detergents with the Critical Micelle Concentration. *Biophys J* **2000**, *78* (5), 2435–2440. https://doi.org/10.1016/S0006-3495(00)76787-7.

(75) Heerklotz, H.; Lantzsch, G.; Binder, H.; Klose, G.; Blume, A. Thermodynamic Characterization of Dilute Aqueous Lipid/Detergent Mixtures of POPC and $C_{12}EO_8$ by Means of Isothermal Titration Calorimetry. *J Phys Chem* **1996**, *100*, 6764–6774. https://doi.org/10.1021/jp9523534.

(76) Hawker, D. W. Application of Regular Solution Theory to Solubility in Lipids and Partitioning Involving Lipids. *Toxicol Environ Chem* **1995**, *50* (1–4), 39–49. https://doi.org/10.1080/02772249509358203.

(77) Chu, S. C.; Hung, C. H.; Wang, S. C.; Tsao, H. K. Partition Thermodynamics of Ionic Surfactants between Phosphatidylcholine Vesicle and Water Phases. *J Chem Phys* **2003**, *119* (6), 3441–3452. https://doi.org/10.1063/1.1590312.

(78) Massaldi, H. A.; King, C. J. Simple Technique to Determine Solubilities of Sparingly Soluble Organics: Solubility and Activity Coefficients of *d*-Limonene, *n*-Butylbenzene, and *n*-Hexyl Acetate in Water and Sucrose Solutions. *J Chem Eng Data* **1973**, *18* (4), 393–397. https://doi.org/10.1021/je60059a024.

(79) Picas, L.; Rico, F.; Scheuring, S. Direct Measurement of the Mechanical Properties of Lipid Phases in Supported Bilayers. *Biophys J* **2012**, *102* (1), L01–L03. https://doi.org/10.1016/j.bpj.2011.11.4001.

(80) van Wezel, A. P.; Cornelissen, G.; van Miltenburg, J. K.; Opperhuizen, A. Membrane Burdens of Chlorinated Benzenes Lower the Main Phase Transition Temperature in Dipalmitoyl-Phosphatidylcholine Vesicles: Implications for Toxicity by Narcotic Chemicals. *Environ Toxicol Chem* **1996**, *15* (2), 203–212. https://doi.org/https://doi.org/10.1002/etc.5620150219.

(81) De Young, L. R.; Dill, K. A. Solute Partitioning into Lipid Bilayer Membranes. *Biochemistry* **1988**, *27* (14), 5281–5289. https://doi.org/10.1021/bi00414a050.

(82) Redondo-Morata, L.; Giannotti, M. I.; Sanz, F. Influence of Cholesterol on the Phase Transition of Lipid Bilayers: A Temperature-Controlled Force Spectroscopy Study. *Langmuir* **2012**, *28* (35), 12851–12860. https://doi.org/10.1021/la302620t.

(83) Hill, M. W. The Effect of Anaesthetic-like Molecules on the Phase Transition in Smectic Mesophases of Dipalmitoyllecithin I. The Normal Alcohol up to C = 9 and Three Inhalation Anaesthetics. *Biochim Biophys Acta* **1974**, *356* (1), 117–124. https://doi.org/10.1016/0005-2736(74)90299-5.

(84) Sarpietro, M. G.; Torrisi, C.; Di Sotto, A.; Castelli, F. Interaction of Limonene, Terpineol, and 1,8 Cineol with a Model of Biomembrane: A DSC Study. *Thermochim Acta* **2021**, *700*, 178938. https://doi.org/10.1016/j.tca.2021.178938.

(85) Cornwell, P. A.; Barry, B. W.; Bouwstra, J. A.; Gooris, G. S. Modes of Action of Terpene Penetration Enhancers in Human Skin; Differential Scanning Calorimetry, Small-Angle X-Ray Diffraction and Enhancer Uptake Studies. *Int J Pharm* **1996**, *127* (1), 9–26. https://doi.org/10.1016/0378-5173(95)04108-7.

(86) Atkins, P.; de Paula, J. *Atkins' Physical Chemistry*, 8th ed.; W.H. Freeman and Company, 2006, 46–47.

(87) Di Foggia, M.; Bonora, S.; Tinti, A.; Tugnoli, V. DSC and Raman Study of DMPC Liposomes in Presence of Ibuprofen at Different pH. *J Therm Anal Calorim* **2017**, *127* (2), 1407–1417. https://doi.org/10.1007/s10973-016-5408-8.

(88) Bayerl, T. M.; Köchy, T.; Brückner, S. On the Modulation of a High-Enthalpy Pretransition in Binary Mixtures of DMPC and DMPG by Polar Headgroup Interaction. *Biophys J* **1990**, *57* (3), 675–680. https://doi.org/10.1016/S0006-3495(90)82587-X.

(89) Caffrey, M.; Hogan, J. *LIPIDAT: A Database of Lipid Phase Transition Temperatures and Enthalpy Changes. DMPC Data Subset Analysis*; 1992.

(90) Hill, T. L. *An Introduction to Statistical Thermodynamics*; Dover, 1986, 255–256.

(91) Sugár, I. P. Cooperativity and Classification of Phase Transitions. Applications to One- and Two-Component Phospholipid Membranes. *J Phys Chem* **1987**, *91*, 95–101. https://doi.org/10.1021/j100285a023.

(92) Mendanha, S. A.; Alonso, A. Effects of Terpenes on Fluidity and Lipid Extraction in Phospholipid Membranes. *Biophys Chem* **2015**, *198*, 45–54. https://doi.org/10.1016/j.bpc.2015.02.001.

(93) Vanderkooi, J. M.; Landesberg, R.; Selick II, H.; McDonald, G. G. Interaction of General Anesthetics with Phospholipid Vesicles and Biological Membranes. *Biochem Biophys Acta* **1977**, *464*, 1–16. https://doi.org/10.1016/0005-2736(77)90366-2.

(94) Gershfeld, N. L. Spontaneous Assembly of a Phospholipid Bilayer as a Critical Phenomenon: Influence of Temperature, Composition, and Physical State. *J Phys Chem* **1989**, *93*, 5256–5261. https://doi.org/10.1021/j100350a043.

(95) Kaminoh, Y.; Tashiro, C.; Kamaya, H.; Ueda, I. Depression of Phase Transition Temperature by Anesthetics: Nonzero Solid-Membrane Binding. *Biochem Biophys Acta* **1988**, *946*, 215–220. https://doi.org/10.1016/0005-2736(88)90395-1.

(96) Rigolle, A.; Gheysen, L.; Depypere, F.; Landuyt, A.; Van Den Abeele, K.; Foubert, I. Lecithin Influences Cocoa Butter Crystallization Depending on Concentration and Matrix. *Eur J Lipid Sci Technol* **2015**, *117* (11), 1722–1732. https://doi.org/10.1002/ejlt.201400555.

Appendix 1: Typical Composition on Sunlipon™ 90

Table A1.1: Information Supplied by Perimondo on Composition of Sunlipon™ 90 Samples

Content	Amount	Acyl tails	Mass (g)	Weight %
Phosphatidylcholine	90 %	Total Acyl tails	62.6	
Lysophosphatidylcholine	1.6 %	14:0 Myristic	0.1	0.16
Moisture	0.9 %	15:0 Pentadecanoic	0.2	0.32
Ethanol	0.1 %	16:0 Palmitic	6.1	9.74
Peroxide Value	<10 meq O_2/kg Max	16:1 Palmitoleic	0.1	0.16
Heavy Metals	≤10 ppm	17:0 Heptadecanoic	0.04	0.06
Arsenic	≤2 mg/kg	18:0 Stearic	1.5	2.40
		18:1 Oleic	11.1	17.73
		18:2 Linoleic	43.3	69.17
		18:3 alpha Linolenic	0.1	0.16
		20:0 Arachidic	0.1	0.16
		20:1 Gadoleic	0.1	0.16
		22:0 Behenic	0.1	0.16
		24:0 Lignoceric	0.03	0.05

Appendix 2: Comparison of Averaging Procedures for Evaluating Partition Coefficients

Table A2.1: Comparison of Partition Coefficients of Limonene in Lecithin Vesicle Dispersions Found by Fitting Individual Replicates (<K_{lipw}>) Versus Fitting the Average of all the Data (<K_{lipw}> fit)

<Size> (nm)	T (°C)	C_{tot} (mM)	K_{lipw} (mM^{-1})	R^2	<K_{lipw}> (mM^{-1})[a]	<K_{lipw}> fit (mM^{-1})	R^2
230.3±4.6	25	0.093	7.393±0.851 5.773±0.146 4.965±0.179	0.9864 0.9290 0.9632	5.484±0.112	5.506±0.306	0.9800
203.8±1.5	25	0.618	10.39±1.12 11.42±1.23 9.507±0.839	0.9376 0.9700 0.9668	10.19±0.59	11.10±0.63	0.9927
231±5.8	25	0.618	10.55±0.53 10.29±0.86 12.01±1.24	0.9834 0.9839 0.9901	10.66±0.43	11.21±0.77	0.9949
134.7±7.4	25	0.618	12.77±1.74 13.28±1.78 13.08±1.45	0.9644 0.9548 0.9572	13.04±0.94	13.82±2.95	0.9742
234.3±2.2	28	0.618	11.15±1.0 10.81±0.54 14.12±1.35	0.9787 0.9767 0.9399	11.25±0.45	11.83±0.65	0.9903
205.8±2.7	20	0.093	8.303±0.591 10.56±0.36 9.492±0.266	0.9961 0.9948 0.9968	9.688±0.201	9.711±0.375	0.9962
208±9.3	20	0.297	10.36±0.29 12.00±0.53 11.41±0.45	0.9965 0.9949 0.996	10.90±0.22	11.39±0.05	0.9993
231.7±2.6	20	0.618	11.34±0.76 8.076±6.882 10.45±0.761	0.9749 0.9688 0.9745	10.13±0.46	9.920±0.544	0.9918
210.9±10.3	20	0.803	11.44±0.606 10.34±0.13 11.81±0.45	0.9874 0.9898 0.9648	10.48±0.119	10.45±0.83	0.9940
207.9±15.3	20	1.24	7.393±0.783 6.025±2.791 6.461±0.943	0.9817 0.8918 0.9429	6.969±0.589	7.006±0.792	0.9876

Table A2.2: Comparison of Partition Coefficients of Limonene in DMPC Vesicle Dispersions Found by Fitting Individual Replicates (<K_{lipw}>) Versus Fitting the Average of all the Data (<K_{lipw}> fit)

<Size> (nm)	T (°C)	C_{tot} (mM)	K_{lipw} (mM^{-1})	R^2	<K_{lipw}> (mM^{-1})	<K_{lipw}> fit (mM^{-1})	R^2
203.3±2.5	20	0.618	13.41±1.93 10.87±3.22 8.415±1.653	0.9571 0.9649 0.9737	10.57±1.17	9.812±2.429	0.9641
203.3±2.5	20	0.618	12.80±1.51 10.15±1.92 7.712±0.965	0.9567 0.9715 0.9652	9.336±0.749	9.577±1.435	0.9849
200.6±5.7	28	0.618	12.68±2.95 13.92±1.13 11.41±1.85	0.9588 0.9868 0.9735	13.19±0.91	11.58±0.92	0.9812
138.1±1.2	28	0.618	10.76±0.90 11.14±0.94 11.73±1.04	0.8967 0.9717 0.9586	11.17±0.55	11.62±1.49	0.959
63.5±1.4	28	0.618	10.02±2.01 12.05±1.46 10.40±1.47	0.9137 0.963 0.9422	10.98±0.92	10.689±1.53	0.9765
208.9±10.1	28	0.093	9.956±0.959 11.17±2.132 7.063±0.76	0.9926 0.9578 0.9873	8.396±0.574	9.107±0.469	0.9973
189.3±4	20	0.093	3.263±0.594 3.834±0.506 3.731±0.525	0.9729 0.9844 0.9772	3.642±0.311	3.808±0.337	0.9907
220.3±13.5	15	0.618	9.444±2.962 10.04±3.821	0.9162 0.845	9.668±2.341	9.894±1.605	0.9738
200.6±5.7	15	0.204	4.018±0.257 3.483±0.281 3.463±0.496	0.9713 0.9729 0.8924	3.735±0.177	3.735±0.19	0.9823

Appendix 3: Data for Limonene in Sunlipon 90™ Lecithin Vesicles at 20ºC

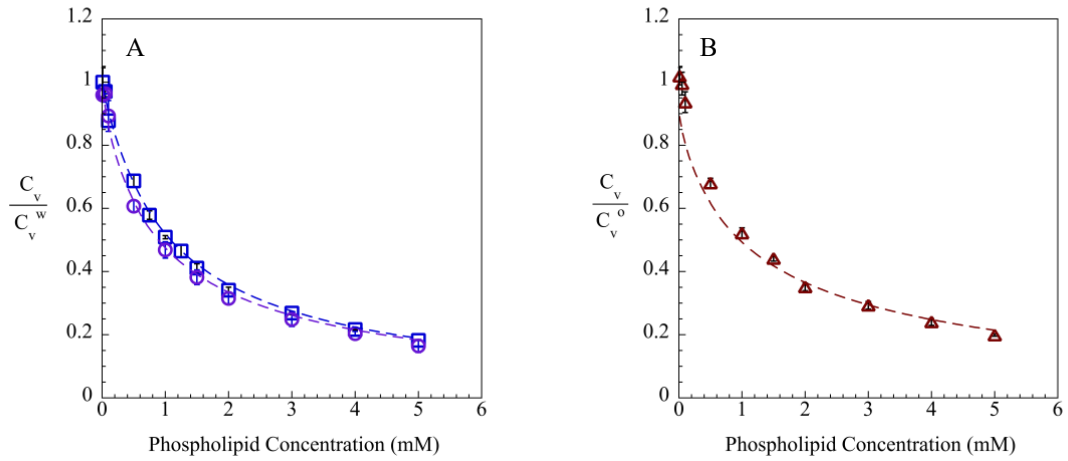

Figure A3.1: Vapor phase concentration above dispersions of Sunlipon™ 90 lecithin vesicles at 20ºC, for (A) 0.297 mM (□), 0.803 mM (○), and (B) 1.24 mM (△) total limonene. Curved lines represent nonlinear regression fits for K_{lipw}.